Identification and characterization of RomX and RomY, two novel motility regulators in *Myxococcus xanthus*

Disseration

zur Erlangung des akademischen Grades
des Doktors der Naturwissenschaften
(Dr. rer. nat.)

dem Fachbereich Biologie
der Philipps-Universität Marburg
vorgelegt

von

Dobromir Szadkowski

aus Nowy Dwor Mazowiecki, Polen

Marburg an der Lahn, 2018

Die Untersuchungen zur vorliegenden Arbeit wurden von August 2013 bis April 2018 am Max-Planck-Institut für terrestrische Mikrobiologie in Marburg unter der Leitung von Prof. Dr. MD Lotte Søgaard-Andersen durchgeführt.

Vom Fachbereich Biologie der Philipps Universität Marburg
als Dissertation angenommen am ___.___.___

Erstgutachter: Prof. Dr. MD Lotte Søgaard-Andersen

Zweitgutachter: Prof. Dr. Martin Thanbichler

Weitere Mitglieder der Prüfungskommission:

Prof. Dr. Victor Sourjik

Prof. Dr. Gert Bange

Tag der mündlichen Prüfung: ___.___.___

Die während der Promotion erzielten Ergebnisse sind zum Teil in folgenden Originalpublikationen veröffentlicht worden:

MglC, a Paralog of *Myxococcus xanthus* GTPase-Activating Protein MglB, Plays a Divergent Role in Motility Regulation,
McLoon AL, Wuichet K, Hasler M, Keilberg D, **Szadkowski D,** Søgaard-Andersen L. J Bacteriol 2015 Nov;198(3):510-20

The RomX/RomR MglA GEF complex establishes front-rear polarity for efficient motility in *M. xanthus*
Szadkowski D, Carreira L, Harms A, Wuichet K, Wigbers M, Potapova A, Keilberg D, Gerland U & Søgaard-Andersen L. (in preparation)

Dla Rodzicow

Table of contents

Abstract

Well-defined front-rear cell polarity is essential for directional cell movement. The rod-shaped *Myxococcus xanthus* cells move using two motility systems and with defined front-rear polarity. Both systems are polarized, i.e. type IV pili assemble at the leading pole while the Agl/Glt gliding motility complexes assemble at the leading, translocate rearward to propel the cell, and disassemble at the lagging pole. During cellular reversals, which are induced by the Frz chemosensory system, polarity of the motility systems is inverted. The Ras-like GTPase MglA together with MglB, the cognate MglA GTPase activating protein (GAP) and the RomR response regulator constitute a module that determine front-rear polarity. MglA-GTP and MglB localize to and define the leading and lagging pole, respectively. MglA-GTP and MglB depend on polarly localized RomR for correct polar targeting. During the Frz system-induced reversals, MglA, MglB and RomR switch poles.

Here, using a comparative genomics approach together with experimental work, we identify RomX and RomY as integral components of the polarity module. RomX localizes asymmetrically to the poles with a large cluster at the lagging pole. *In vitro* data analyses demonstrated that RomX not only interacts directly with RomR alone and MglA-GTP alone but that RomR, RomX and MglA together form a heteromeric RomR/RomX/MglA-GTP complex. In this complex, RomX is sandwiched between RomR and MglA-GTP. Moreover, our data provide evidence that the RomR/RomX complex has MglA GEF activity. *In vivo*, polarly localized RomR recruits RomX and, in turn, the RomR/RomX complex recruits MglA-GTP to the leading cell pole. Thus, the RomR/RomX complex has dual functions in establishing front-rear polarity for motility in *M. xanthus*, it is a GEF that stimulates the accumulation of MglA-GTP, the active form of MglA, and it is a polar recruitment factor that recruits MglA-GTP to the leading cell pole. Both activities contribute to a high local concentration of MglA-GTP at this pole. At the leading pole, the RomR/RomX/MglA-GTP complex stimulates the assembly of Agl/Glt gliding motility complexes and is also incorporated into these complexes. However, in the absence of MglB, RomR/RomX is not essential for assembly of these complexes. Importantly, the Agl/Glt complexes assembled in the absence of RomR/RomX are less stable and transfer less directionally towards the lagging pole. These results suggest that RomR/RomX at the leading and MglB at the lagging cell pole establish leading lagging polarity axis for efficient gliding motility.

RomY localizes unipolarly with a cluster at the lagging cell pole. *In vivo* experiments demonstrated, that RomY regulates reversals and cell polarity similarly to MglB. Moreover, RomY localization depends on MglB suggestíng a functional connection between these two proteins. Protein-protein interaction analyses suggested that RomY directly interacts with MglA and RomX. Moreover, RomX and RomR are not essential for gliding motility in the absence of RomY. Based on these data we suggests that RomY either stimulates MglB GAP activity or MglA GTPase activity.

Zusammenfassung

Eine klar definierte Polarität des vorderen und hinteren Zellpols ist für eine gerichtete Zellbewegung essentiell. Die stäbchenförmigen Zellen von Myxococcus xanthus benötigen für ihre Bewegung zwei Motilitätssysteme und eine klar definierte Polarität der Zellpole. Dabei sind beide Motilitätssysteme polarisiert: die Typ IV Pili sind am vorderen Pol angeordnet, dagegen werden die Komplexe, die für die Gleitbewewegung benötigt werden, zwar am vorderen Pol zusammengebaut, wandern aber im Zuge der Gleitbewegung zum hinteren Zellpol, wo sie anschließend abgebaut werden.

M. xanthus Zellen wechseln regelmäßig die Richtung ihrer Bewegung, wobei der alte vordere Pol zum neuen hinteren Zellpol wird. Während eines Richtungswechsels müssen die beiden Motilitätssysteme synchron ihre Polarität innerhalb der Zelle ändern, um eine erneute Vorwärtsbewegung in die entgegengesetzte Richtung zu garantieren. Die Ras-ähnliche GTPase MglA bildet zusammen mit MglB, dem verwandten MglA GTPase aktivierenden Protein (GAP) und dem RomR Response-Regulator ein Modul, das die Polarität des vorderen und hinteren Zellpols bestimmt. Die polare Lokalisation von MglA-GTP und MglB definiert den vorderen und hinteren Zellpol und ist abhängig von dem polar lokalisierten RomR. Während des durch das Frz-System induzierten Richtungswechsels wechseln MglA-, MglB- und RomR von dem einen zum anderen Pol.

In Rahmen einer großen vergleichenden Genomanalyse konnten wir RomX und RomY als weitere integrale Komponenten dieses Polaritätsmoduls identifizieren. RomX lokalisiert asymmetrisch an den Polen mit einem großen Cluster am hinteren Pol. In-vivo- und in-vitro-Experimente zeigten, dass das polare RomX zwischen seinem polaren Rekrutierungsfaktor RomR und MglA-GTP liegt. Der RomR / RomX / MglA-GTP-Komplex stimuliert den Aufbau von Gleitmotilitätskomplexen am vorderen Pol und wird dabei selbst Teil des Komplexes. Überraschenderweise sind RomX und RomR nur dann für die Gleitbewegung notwendig, wenn MglB abwesend ist. In Abwesenheit von MglB translozieren die Gleitmotilitätskomplexe weniger gerichtet zum hinteren Zellpol und die von den Zellen zurückgelegte Nettodistanz ist stark reduziert. Unsere Daten legen übereinstimmend nahe, dass ein RomX / RomR Komplex als Guanin-Nukleotid-Faktor (GEF) auf MglA-GDP wirkt und somit die gerichtete Zellbewegung reguliert. Am vorderen Zellpol bindet der RomX / RomR Komplex MglA-GTP und stimuliert dadurch den Aufbau der Gleitmotilitätskomplexe. Am hinteren Pol stimuliert der RomX / RomR Komplex dagegen den Abbau der Gleitmotilitätskomplexe.

RomY lokalisiert unipolar mit einem Cluster am hinteren Zellpol. In vivo Experimente zeigten, dass RomY Richtungswechsel und Zellpolarität ähnlich wie MglB reguliert. Darüber hinaus hängt die RomY-Lokalisierung von MglB ab, was eine funktionelle Verbindung zwischen den Proteinen vermuten läßt. Proteininteraktionsstudien haben gezeigt, dass RomY direkt mit MglA und RomX interagiert. Bemerkenswerterweise sind RomX und RomR in Abwesenheit von RomY für die Gleitmotilität entbehrlich. Basierend auf diesen Daten schlagen wir vor, dass RomY die MglB GAP oder MglA GTPase Aktivität reguliert.

Abbreviations

ATP/ADP	adenosin tri-/diphosphate
BACTH	bacterial Adenylate Cyclase-based Two Hybrid
bp	base pair
BSA	bovine serum albumin
cAMP	3’,5′-cyclic monophosphate
cDNA	single-stranded complementaty DNA
CTT	casitone Tris medium
CR	congo red
DNA	deoxyribonucleic acid
DMSO	dimethyl sulfoxide
DTT	dithiothreitol
EDTA	ethylenediaminetetraacetic acid
EPS	exopolysaccharides
GAP	GTPase activating proteins
GEF	guanine nucleotide exchange factor
GFP	green fluorescent protein
GTP/GDP	guanosine tri-/diphosphate
h	hours
HPK	histidine protein kinase
IM	innermembrane
IPTG	isopropyl β-D-1-thiogalaktopyranoside
kDa	kilodalton
LPS	lipopolysaccharides
MBP	maltose binding protein
mGTP/mGDP	(2'-(or-3')-O-(N-Methylanthraniloyl) Guanosine Tri-/diphosphate
min	minutes
MOPS	3-(N-morpholino) propanesulfonic acid
OD	optical density
OM	outermembrane
PMF	proton motive force
pN	piconewton
SD	standard deviation
SDS-page	sodium dodecyl sulfate polyacrylamide gel electrophoresis
T4P	type IV pili
TB	trypan blue
TEMED	N,N,N′,N′-Tetramethylethane-1,2-diamine
TIRF	total internal reflection fluorescence microscope
YFP	yellow fluorescent protein
WT	wild type
X-gal	5-Brom-4-chlor-3-indoxyl-β-D-galactopyranosid

1. Introduction

1.1 Spatial organization of bacterial cells

Until recently, bacterial cells were thought of as compartmented sacks of proteins localizing diffusely in the cytoplasm, inner membrane, periplasm or outer membrane. Development of microscopy techniques such as electron and fluorescence microscopy allowed studying in more details not only the morphology of bacterial cells but also the spatial organization of their content. The observation that bacterial chemoreceptors localize to the cell poles and that the division protein FtsZ localizes to the division site changed our thinking about bacteria, from unorganized sacks of proteins to highly spatially organized cells with proteins localizing to specific subcellular regions (Bi & Lutkenhaus, 1991, Alley *et al.*, 1992, Maddock & Shapiro, 1993). Since then, many studies of the spatial organization of bacterial cells have shown that protein localization can be highly dynamic and change in response to external or internal signals or, alternatively, this localization is cell cycle dependent. Cell polarity with proteins localizing asymmetrically within a cell is important for many processes in bacteria including growth, division, cell cycle regulation, motility and signal transduction (Shapiro *et al.*, 2009). Major questions in bacterial cell biology are how proteins find their correct localization and in some cases change this localization over time.

Eukaryotic cells have developed sorting machineries based on vesicle transport that deliver protein cargo to the proper destinations. Bacterial cells lack vesicle sorting- and transport systems. Instead, protein localization in bacteria is typically mediated by a diffusion and capture mechanism. In this mechanism, proteins diffuse rapidly throughout the three dimensions of the cytoplasm or in the two dimensions of the membranes. These diffusing proteins can then recognize and bind to a cellular cue or specific landmark proteins.

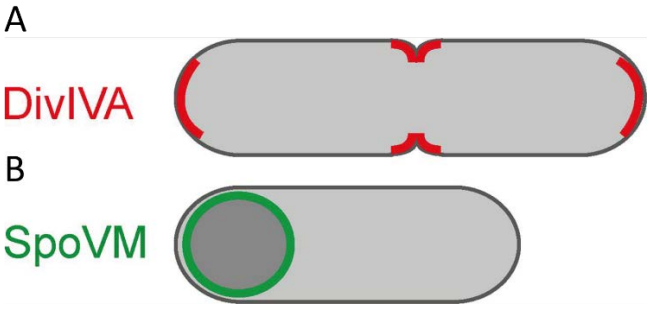

Figure 1. Curvature as a geometrical cue for protein localization.
(A) DivIVA from *B. subtilis* localizes to membranes with negative curvature.
(B) SpoVM of *B. subtilis* localizes to membranes with positive curvature. Figure reproduced from Treuner-Lange &Søgaard-Andersen, 2014.

Well studied examples of cellular cues for protein localization include geometrical cues and membrane lipids. An example of a protein that binds to a geometrical cue is DivIVA from *Bacillus subtilis*. The DivIVA protein localizes at bacterial cell poles and division sites by directly recognizing high negative curvature of a membrane (Lenarcic *et al.*, 2009, Ramamurthi & Losick, 2009) (Figure 1, A). Proteins can also recognize positive curvature of the membrane. For instance, SpoVM recognizes and binds to membranes with positive curvature created during endospore formation in *B. subtilis* (Ramamurthi *et al.*, 2009) (Figure 1, B). It has also been proposed that not only membrane curvature but also certain membrane lipids can serve as a spatial cue for protein localization in bacteria. Cardiolipin-rich domains have been identified at the poles and division sites of *B. subtilis* (Kawai *et al.*, 2004) and *Escherichia coli* (Mileykovskaya & Dowhan, 2000). Localization of the mechanosensitive channel MscC and transporter ProP in *E. coli* correlates with subcellular cardiolipin composition (Romantsov *et al.*, 2010). These observations suggest that cardiolipins may act as a recognition cue for certain proteins. However, it remains unknown whether this is due to direct interactions between a protein and cardiolipin.

Protein localization involving a landmark protein recruiting another protein is the best-studied mechanism leading to specific cellular protein localization. These landmark proteins can be divided into polymer-forming proteins and non-polymer-forming proteins. DivIVA is a well-studied example of a polymer-forming landmark protein. As mentioned, DivIVA binds to membrane regions with negative curvature. At the division site, DivIVA binds and directly interacts and recruits MinJ, that recruits the cell division inhibitory MinCD complex (Bramkamp *et al.*, 2008, Patrick & Kearns, 2008, Gregory *et al.*, 2008) (Figure 2, A).

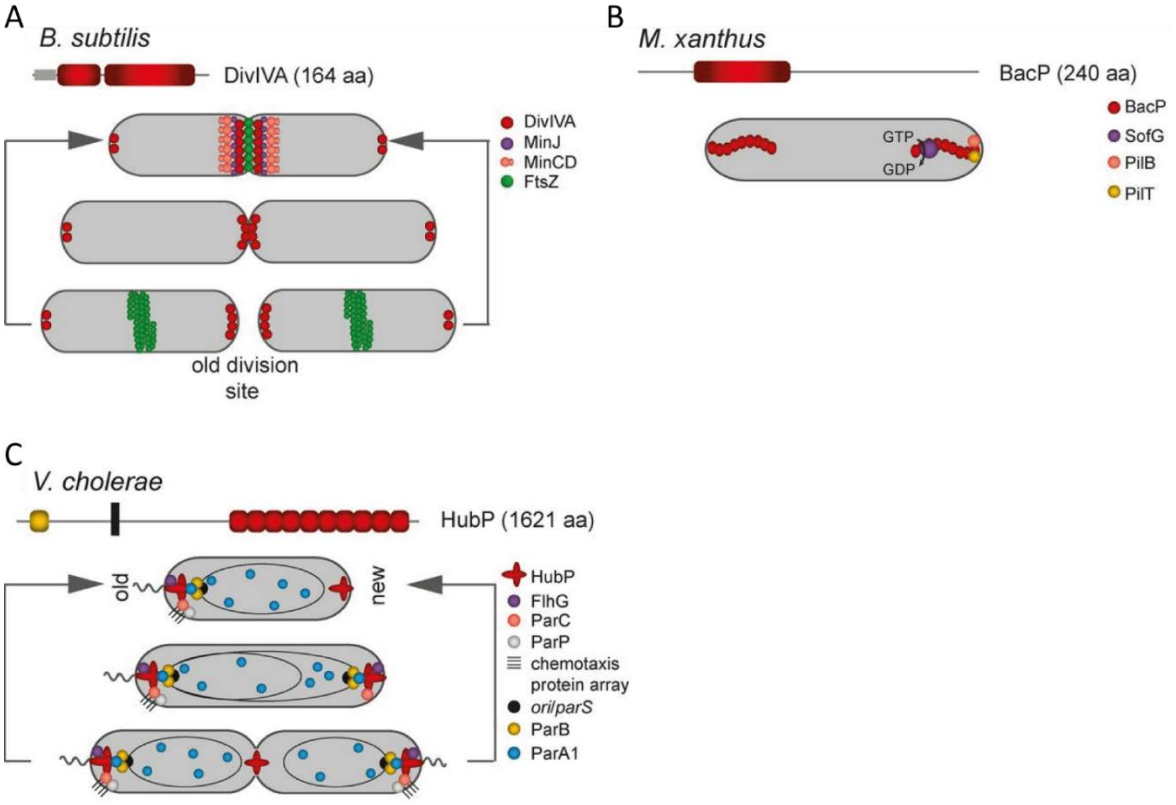

Figure 2. **Polymer and nonpolymer forming landmark proteins.**
(A) The domain structure of the polymer-forming protein DivIVA is indicated in grey and coiled-coil in red. Bottom part shows localization of DivIVA and associated proteins during the cell cycle.
(B) The domain structure of the polymer-forming BacP with bactofilin domain in red. Bottom: Localization on BacP and associated proteins. SofG associates with the BacP landmark only at one pole. GTP hydrolysis by SofG is indicated.
(C) The domain structure of nonpolymer forming HubP with the peptidoglycan binding LysM domain in yellow, black represents transmembrane domain, and the repeat rich region is in red. Bottom part shows localization of HupP and associated proteins during the cell cycle. Figure modified from Treuner-Lange &Søgaard-Andersen, 2014.

Another example of polymer-forming proteins that function as landmarks are the bactofilins (Kuhn *et al.*, 2010). In *Caulobacter crescentus* the bactofilins BacA and BacB in a cofactor independent manner polymerize *in vitro* and recruit the peptidoglycan synthase PbpC to the stalked pole *in vivo* (Kuhn *et al.*, 2010). *Myxococcus xanthus* possesses four bactofilins, which also spontaneously polymerize *in vitro* to form long filaments (Kuhn *et al.*, 2010, Koch *et al.*, 2011, Bulyha *et al.*, 2013). BacP localizes to large patches in the two subpolar regions and functions as a landmark for the small GTPase SofG (Bulyha *et al.*, 2013). SofG, in turn, is important for the polar localization of the ATPases PilB and PilT that are important for type IV pili (T4P) function and motility (Bulyha *et al.*, 2013)(Figure 2, B).

The integral membrane protein HubP from *Vibrio cholerae* is a well-studied example of a non-polymer forming landmark protein that localizes to the cell poles. The N-terminal peptidoglycan binding LysM domain is necessary and sufficient for HubP localization to the cell poles. HubP in turn, recruits and directly interacts with the ParA1 ATPase, which plays a role in chromosome 1 segregation, and with the ParA ATPase FlhG, which is involved in flagella assembly regulation (Yamaichi *et al.*, 2012, Fogel & Waldor, 2006, Correa *et al.*, 2005) (Figure 2, C). While it is relatively well-understood how polymer forming proteins such as DivIVA (Lenarcic *et al.*, 2009, Ramamurthi & Losick, 2009) and PopZ from *C. crescentus* (Bowman *et al.*, 2008, Ebersbach *et al.*, 2008) become localized, much less is known about how non-polymer forming landmarks eventually become localized.

1.2 Characteristics of small eukaryotic GTPases

In eukaryotes, small Ras-like GTPases, also known as small GTP-binding proteins, have important functions in protein localization and regulation of cell polarity (Jaffe & Hall, 2005, Charest & Firtel, 2007, Kortholt & van Haastert, 2008, Chiou *et al.*, 2017). Recently, small Ras-like GTPases have also emerged as being important for protein localization and regulation of cell polarity in bacteria (Schumacher &Søgaard-Andersen, 2017). Small Ras-like GTPases function as molecular switches. The GDP-bound form represents the inactive protein, while the GTP-bound form represents the active form and interacts with downstream effectors to activate downstream pathways. GDP as well as GTP are tightly bound to these GTPases and, moreover, their intrinsic GTPase activity is low (Bourne *et al.*, 1991). Generally, the activity of small GTPases is regulated by guanine nucleotide exchange factors (GEFs) and GTPase activating proteins (GAPs). GEFs promote GDP to GTP exchange in that way stimulating the accumulation of the active form. GAPs promote GTP hydrolysis in that way stimulating accumulation of the inactive form (Bos *et al.*, 2007) (Figure 3). Certain small GTPases are prenylated on their C-terminus, which provides the attachment of their active form to endomembranes. These GTPases can be displaced from the membranes by guanidine dissociation inhibitors (GDIs) that bind to the C-terminal lipid to maintain the small GTPase in an inactive complex (Cherfils & Zeghouf, 2013).

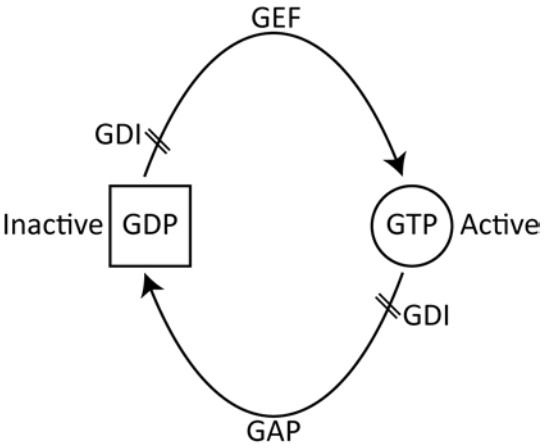

Figure 3. Regulation of small GTPases by GEF, GAP and GDI.
GEF catalyses the exchange of GDP to GTP. GAP activates GTPase activity and hydrolysis of GTP to GDP. GDI proteins affect nucleotide dissociation and inhibit GAP activity.

Structural characterization of GEFs revealed that GEFs share mechanistic hallmarks but they showed a stunning diversity in amino acid sequence and structure (Cherfils & Zeghouf, 2013). Neverthless, GEFs of different families are thought to follow common reaction schemes (Bos *et al.*, 2007). GEFs catalyze the dissociation of the nucleotide from the small GTPase by modifying the nucleotide-binding site leading to a decreased affinity for the nucleotide. In the current model for how GEFs function, the GEF first associates with the GDP-bound small GTPase. GDP dissociates from this complex leaving the GEF bound to the nucleotide-free GTPase. Next, the GTPase binds GTP, promoting GEF dissociation from the complex and leaving the GTPase in the active form (Vetter & Wittinghofer, 2001, Hodgkin & Kaiser, 1979).According to this model, a stable complex only exists between the GEF and the nucleotide-free GTPase. *In vitro* studies have also shown that the affinity of the small GTPase for GTP and GDP is similar and the GEF does not favor rebinding of GDP or GTP (Bos *et al.*, 2007). Because the GTP concentration *in vivo* is higher than the GDP concentration, GTP binding to the nucleotide-free GTPase is favored. However, for some GEFs interactions with cognates GTPases in theGTP bound were shown. Detailed biochemical studies revealed that the interaction is part of a positive feedback loop and activates GEF, what in turn leads to accumulation of GTPase-GTP (Margarit *et al.*, 2003, Menetrey *et al.*, 2007, Richardson *et al.*, 2012, Cohen *et al.*, 2007, Chen *et al.*, 2010, Lin *et al.*, 2006).

Similar to the GEFs of small GTPases, the GAPs of these GTPases are structurally diverse and belong to different subfamilies (Bos *et al.*, 2007). Structural studies of pairs of cognate GTPases and GAPs have revealed that the general mechanism of GTPase

stimulation of a GAP is to complete the GTPase active site by providing the so-called arginine finger into the GTPase active site (Rittinger *et al.*, 1997, Scheffzek *et al.*, 1997).

1.3 *Myxococcus xanthus* as a model organism

M. xanthus is a rod-shaped, Gram-negative soil bacterium. *M. xanthus* has a complex life cycle in which cells grow and divide in the presence of nutrients. If placed on a solid surface, *M. xanthus* cells move to form swarming colonies in the presence of nutrients. In the absence of nutriens, *M. xanthus* cells initiate a developmental program that leads to the formation of multicellular fruiting bodies inside which the rod-shaped motile cells differentiate to spherical spores. Cell motility and its regulation are required for formation of swarming colonies as well as for fruiting body formation (Kroos *et al.*, 1988).

M. xanthus cells do not possess flagella, and thus they are not able to swim. However, they are able move on a solid surface along their long axis. To facilitate motility, *M. xanthus* cells use two genetically independent motility systems, gliding, also referred to as adventurouss (A) motility and type IV pili-dependent motility, also referred to as social (S) motility. The gliding motility system was initially referred to as adventurous because it allows single cell movement, while the type IV pili-dependent system was initially referred to as social because it is generally used by cells to move in groups (Hodgkin & Kaiser, 1979). Inactivation of one motility system, leaves cells motile by means of the second system, while inactivation of both systems leads to non-motile cells (Hodgkin & Kaiser, 1979). Additionally, *M. xanthus* cells change direction of movement on average every 10–15 minutes (Blackhart & Zusman, 1985). During these events, which are referred to as reversals, cells change polarity with the old lagging cell pole becoming the new leading cell pole and *vice versa*

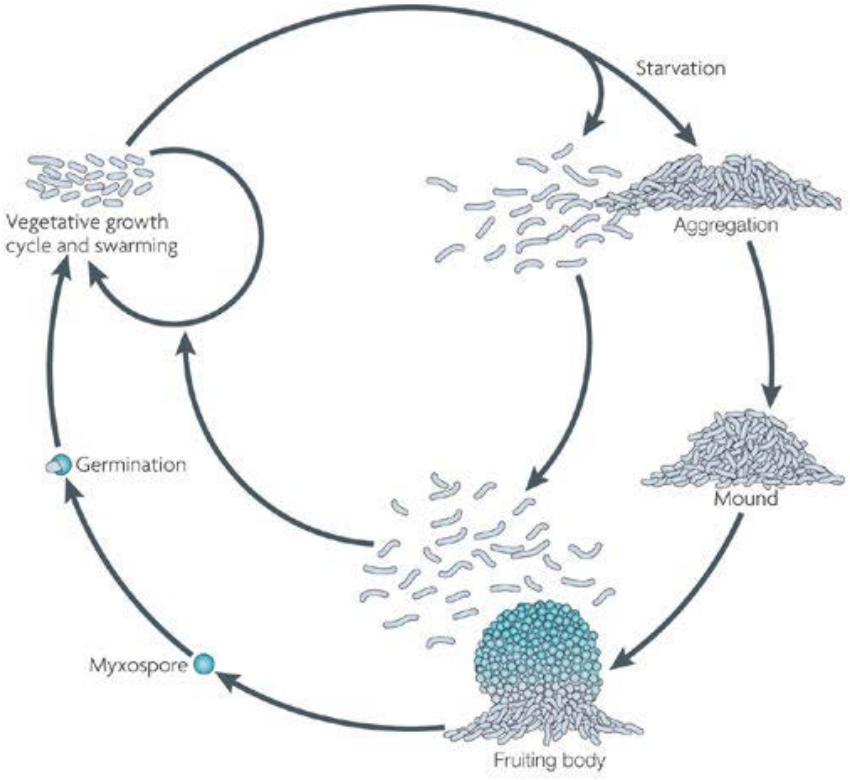

Figure 4. Schematic representation of the *M. xanthus* life cycle.
Figure reproduced from Mauriello *et al.*, 2010a.

1.4 Type IV pili motility

Type IV pili- (T4P) dependent motility in *M. xanthus* is similar to twitching motility in *Pseudomonas aeruginosa*. T4P are widespread among bacteria and play a role in natural transformation (Dubnau, 1999), pathogenesis (Craig & Li, 2008), biofilm formation (O'Toole & Kolter, 1998) and predation (Evans *et al.*, 2007). In *M. xanthus*, T4P-dependent motility is favoured on wet and soft surfaces (Shi & Zusman, 1993) and depends on T4P (Kaiser, 1979) and exopolysaccharides (Yang *et al.*, 2000). T4P extend from the leading cell pole, attach to a surface, and then retract, pulling a cell forward (Kaiser, 1979, Skerker & Berg, 2001, Zhou & Nan, 2017). During retractions, T4P generate a force up to 150 pN (Merz *et al.*, 2000). In *M. xanthus*, retraction of T4P is thought to be stimulated by exopolysaccharides (Li *et al.*, 2003).

T4P function depends on a conserved set of 11 proteins (Wall & Kaiser, 1999) (Figure 5, A). The T4P machinery (T4PM) that supports extension and retraction of T4P is a multi-layered structure that spans from the outer membrane to the cytoplasm (Chang *et al.*, 2016). It consists of the PilQ secretin that forms an outer membrane pore for the pilus; TsaP that forms a periplasmic ring around PilQ; a mid-periplasmic ring formed by the periplasmic domains of PilQ and PilP; a lower periplasmic ring formed by PilO and

PilN that connect across the inner membrane to the PilM protein that forms a cytoplasmic ring. The inner membrane protein PilC form the cytoplasmic dome inside the PilM ring. The pilus is formed by PilA, the major subunit of the pilus (Chang *et al.*, 2016) (Figure 5, B and C). The cytoplasmic ATPases PilB and PilT provide the energy for T4P extension and retraction, respectively (Jakovljevic *et al.*, 2008) and associate and interact directly with PilC and PilM (Bischof *et al.*, 2016, Chang *et al.*, 2016). During T4P extension, PilA subunits are extracted from the outer leaflet of the inner membrane and inserted at the base of the growing pilus in a process that is powered by PilB (Jakovljevic *et al.*, 2008, Chang *et al.*, 2016). During retractions, the PilA subunits are removed from the base and reinserted into the inner membrane in a process powered by PilT (Jakovljevic *et al.*, 2008, Chang *et al.*, 2016).

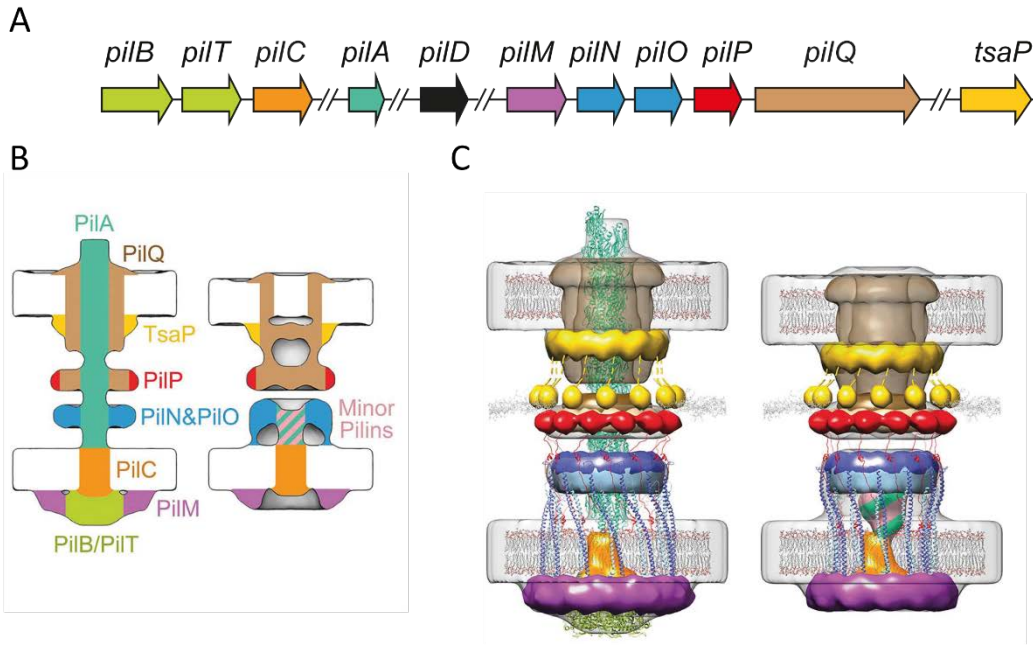

Figure 5. Genetic map of pili locus and architectural model of type IV pili complex.
(A) Genetic map of *pil* locus. All the *pil* genes are clustered at the same locus, but not all *pil* genes are shown, *tsaP* is not a part of *pil* cluster. Figure modified from Friedrich *et al.*, 2014.
(B) Schematic model of piliated (left) and non piliated (right) type IV pili machinery.
(C) Architectural models of piliated (left) and non piliated (right) type IV pili basal bodies. The colour code for the proteins is similar to the one used for the genes. B and C are reproduced from Chang *et al.*, 2016.

Assembly of the T4PM starts from PilQ in the outer membrane (OM) and proceeds inwards (Friedrich *et al.*, 2014). PilQ localization to the outer membrane depends on the Tgl pilotin (Friedrich *et al.*, 2014) Tgl is an OM lipoprotein and in its absence, PilQ does not form oligomeric form. Next, PilP, PilN, PilO and PilM are incorporated into the T4PM and in parallel TsaP is incorporated. Following PilPNOM incorporation, PilC in the inner membrane is incorporated (Figure 6). Finally, PilB and PilT can associate with

the base of this machinery to stimulate extension or retraction of T4P (Friedrich *et al.*, 2014).

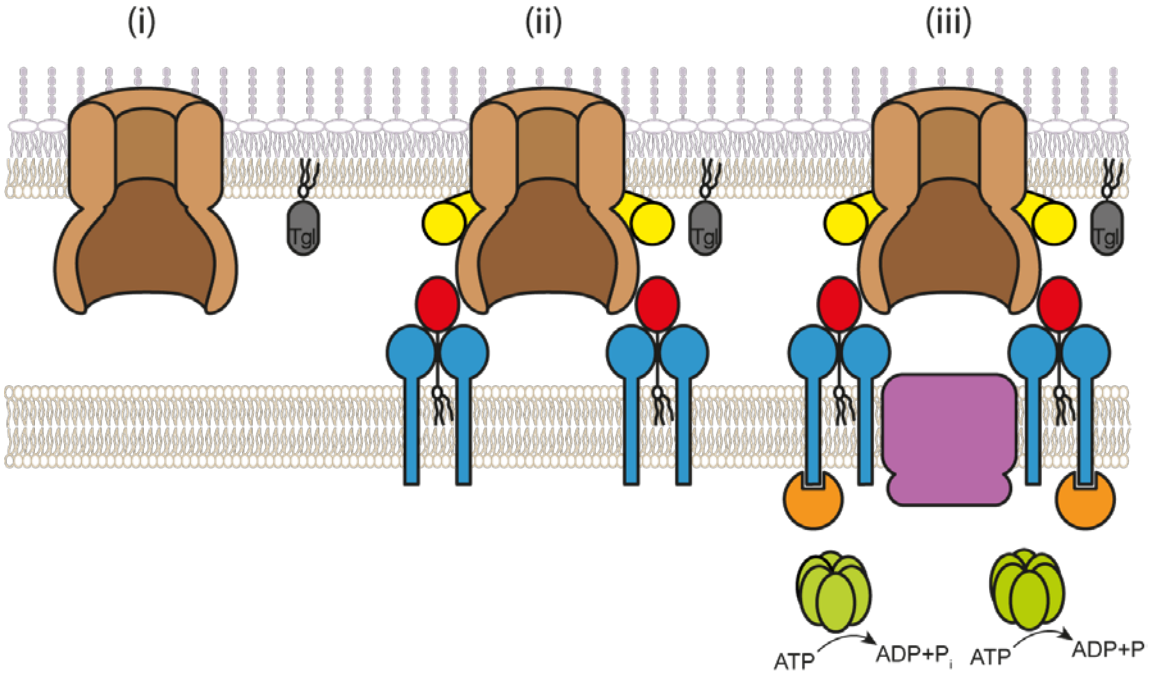

Figure 6. Model of assembly of the *M. xanthus* type IV pili machinery.
Description in text. Colour code for the proteins as in Figure 5. Figure modified from Friedrich *et al.*, 2014.

T4P assemble only at the leading cell pole in *M. xanthus* and during reversals, the pole at which T4P are assembled switches (Kaiser, 1979, Mignot *et al.*, 2005). The mechanism underlying this switch in polarity of T4P depends on dynamic protein localization to the cell poles. T4PM proteins can be divided into two groups. One group includes the proteins that are localized to both cell poles and remain at the cell poles during a reversal (TsaP, PilQPNOCM). The second group is composed of the two ATPases PilB and PilT. PilB primarily localizes to the leading cell pole while PilT primarily localizes to the lagging cell pole (Friedrich *et al.*, 2014, Nudleman *et al.*, 2006, Bulyha *et al.*, 2009). Notably, during a reversal, PilB and PilT are released from the cell poles and then associate with new leading and lagging cell pole, respectively. Therefore, the mechanism underlying T4P polar switching during a reversal involves dynamic localization of PilB and PilT. As described in more details below, the polarity regulation involved in sorting PilB and PilT to the correct cell poles involves the two small GTPases, MglA and SofG (Bulyha *et al.*, 2013).

1.5 Gliding motility

Gliding motility, which is favoured on hard and dry surfaces, is generally used by *M. xanthus* to move as single cells (Shi & Zusman, 1993). The exact mechanism of

gliding motility in *M. xanthus* remains unclear. Bioinformatics together with *in vivo* protein localization and protein–protein interaction studies have revealed that the machinery involved in gliding motility also spans from the outer membrane to the cytoplasm.

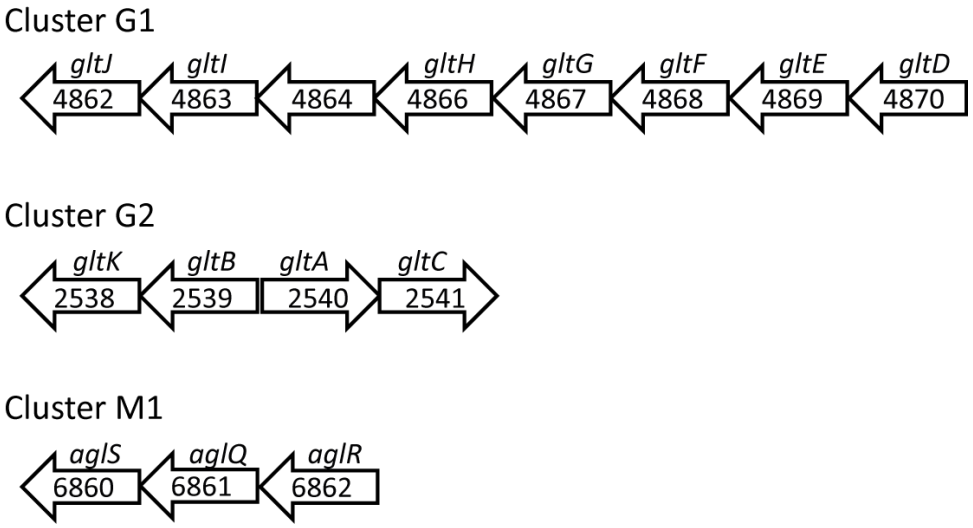

Figure 7. Genetic organisation of clusters carrying gliding motility genes.
Genes of G1, G2 and M1 clusters are depicted as arrows. Arrow orientation indicates coding direction of the genes, numbers in the arrows show MXAN genes numbers.

Luciano *et al.* identified three genomic regions referred as G1, G2 and M1 that encode components of the gliding motility machinery (Figure 7) (Luciano *et al.* 2011). In addition to the proteins encoded in these three clusters, the cytoplasmic protein AglZ (Yang *et al.*, 2004, Mignot *et al.*, 2007) together with the actin-like protein MreB (Mauriello *et al.*, 2010b, Treuner-Lange *et al.*, 2015) and the small GTPase MglA (Leonardy *et al.*, 2010, Zhang *et al.*, 2010) are important for gliding motility. The proteins encoded by the G1 and G2 clusters are thought to make up structural comonents of the gliding machinery (Luciano *et al.*, 2011, Jakobczak *et al.*, 2015, Faure *et al.*, 2016) and localize to the cell envelope and cytoplasm as shown in Figure 8. By contrast, the three proteins encoded by the M1 cluster make up the motor of the machinery and localize to the inner membrane (Sun *et al.*, 2011, Nan *et al.*, 2013) (Figure 8).

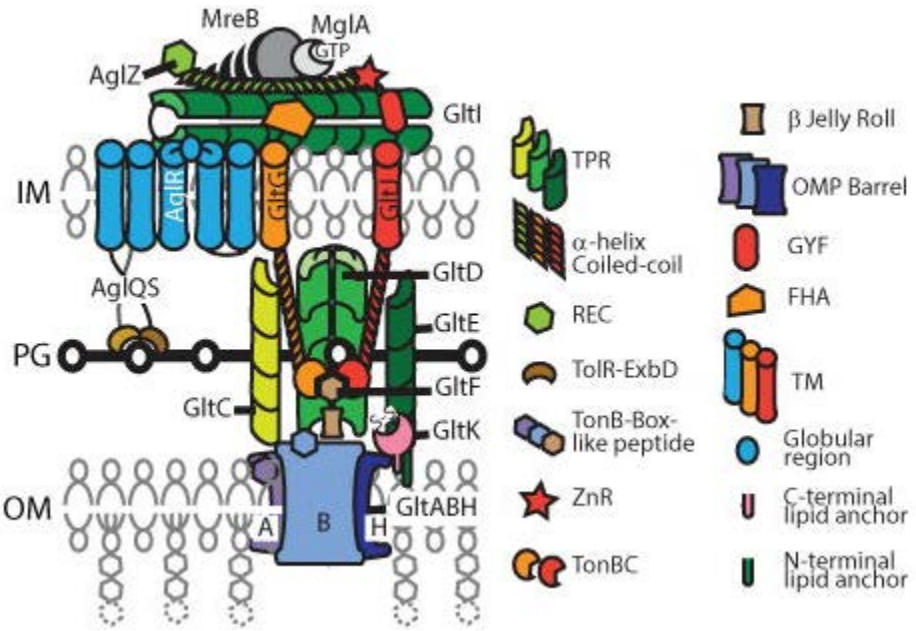

Figure 8. Predicted domain architecture and subcellular localization of proteins required for gliding motility.
Figure reproduced from Faure *et al.*, 2016.

Experiments with carbonyl cyanide-m-chlorophenylhydrazone (CCCP) has shown that the proton motive force (PMF) is the source of energy for gliding motility in *M. xanthus*. The PMF arises from gradients in both the chemical potential energy, in the form of a pH difference across the inner membrane, and electrical potential energy, caused by a voltage difference across the inner membrane. Nigericin that reduces the pH gradient without changing membrane potential abolishes gliding motility whereas, valinomycin that destroys the membrane potential without changing the magnitude of the pH gradient has no effect on the gliding motility. Based on these data, it was concluded that the pH gradient across the membrane is a source of energy for gliding motility.

The M1 cluster encodes the component of a proton conducting channel: AglQ, AglR, AglS. Bioinformatics analysis shows that AglR is a TolQ/ExbB/MotA homolog, whereas AglQ and AglS are TolR/ExbD/MotB homologs. The MotA/MotB proteins build a stator part of the flagellar rotary motor, the TolQ/TolR complex is important for the outer membrane stability (Bernadac *et al.*, 1998) and the ExbB/ExbD proteins are involved in the activation of TonB-dependent transporters in the outer membrane (Postle, 2007). All three protein complexes form a proton channel in the inner membrane. Moreover, in all three systems energy from the proton flux can be converted to a mechanical output with a change in protein conformation.

Assembly and disassembly of the gliding motility machinery depend on the small Ras like GTPase MglA. MglA is absolutely required for both gliding and T4P-dependent

motility (Hodgkin & Kaiser, 1979) and function as a nucleotide-dependent molecular switch to stimulate motility (Mauriello *et al.*, 2010b, Leonardy *et al.*, 2010, Patryn *et al.*, 2010, Zhang *et al.*, 2010, Miertzschke *et al.*, 2011). MglA in its active GTP-bound form is incorporated into the gliding motility complexes (Treuner-Lange *et al.*, 2015). MglA-GTP interacts directly interact with MreB (Mauriello *et al.*, 2010b, Treuner-Lange *et al.*, 2015). MglA also interacts directly with AglZ; however, it is not known whether this interact is nucleotide-dependent (Mauriello *et al.*, 2010b). MglA, MreB and AglZ are thought to form a complex that interacts with GltI in the cytoplasm in that way connecting to the gliding motility machinery (Treuner-Lange *et al.*, 2015, Faure *et al.*, 2016). Also, the MglA, MreB and AglZ complex stimulates formation of the gliding motility complexes at the leading cell pole (Treuner-Lange *et al.*, 2015) and MglA-GTP has also been suggested to regulate directionality of the gliding machinery (Nan *et al.*, 2011).

1.5.5 Two models of gliding motility

Two models have been proposed to explain how the gliding motility complex assembles to generate movement, the motor cargo model and the focal adhesion model (Figure 9).

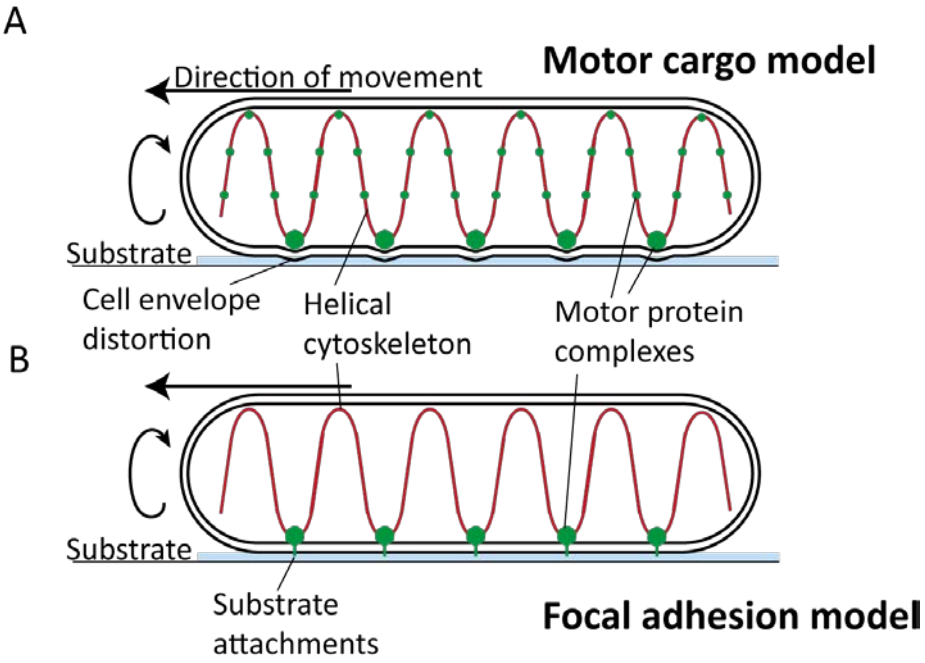

Figure 9. Schematic of the two models of the gliding motility machinery.
(A) Motor cargo model in which motor proteins (green dots) tracking on a helical cytoskeleton deform peptidoglycan and OM in order to create traction.
(B) Model of focal adhesion mechanism in which multi-protein complexes (green dots) span the inner and outer membrane and attach to the substrate.

1.5.5.1 Motor cargo complex

The motor cargo complex model was proposed based on the localization of GltD protein (Nan *et al.*, 2011). GltD was proposed to localize to both the cytoplasm and periplasm (Nan *et al.*, 2010). 3D reconstructions of GltD-mCherry fluorescence showed that GltD-mCherry forms a twisted endless looped helix that spans the length of the cells (Figure 10). Additionally, the distance between adjacent nodes is nearly identical to that of MreB helices, 0.45±0.09 and 0.47±0.1 µm, respectively (Nan *et al.*, 2011, Mauriello *et al.*, 2010b).

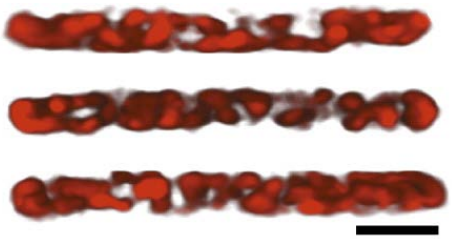

Figure 10. GltD forms a twisted endless looped helix.
3D reconstruction of the GtlD helix from three individual cells. Scale bar: 1 µm. Figure reproduced from Nan *et al.*, 2011.

Moreover, the GltD helix rotates as cells move on a 1.5% agar surface and changes direction of rotation when cells reverse their direction. Furthermore, this helix rotates clockwise when viewed from the lagging cell pole. In addition, rotation depends on the PMF and polymerization of MreB. The calculated linear velocity of the GltD helix (4.4-9.6 µm/min) is in agreement with the maximum velocity of a gliding cell (≈2-4 µm/min) (Sun *et al.*, 1999). GltD localizes with a higher concentration at the leading cell pole and when the cell reverses, GltD relocalizes to the new leading cell pole. AglR also forms a helix that spans the length of the cells (Figure 11) (Nan *et al.*, 2013). The pitch of the AglR helix (1.34±0.51 µm) is similar to that of GltD. Moreover, the velocity of the rotating helices of AglR and GltD is similar. By tracking AglR, Nan *et al.* (2013) discovered that AglR moves along the cell width and cell lengths in zigzag trajectories in two dimensions suggesting that AglR molecules move in helical trajectories in three dimensions (Nan *et al.*, 2013). Additionally, AglR molecules tended to slow down near the ventral side of cells, i.e. the part of the cell surface where a cell is in contact with the substratum during gliding. Slowing down of the motor units depends on the hardness of the surface suggesting that the motor units slow down due to resistance of the underlying surface. Like for GltD, AglR movement depends on PMF and MreB polymerization.

Additionally, helical movement of AglR depends on GltD and in the absence of GltD, helical movement of AglR is replaced by linear motion along the long axis of the cell. By contrast, in the absence of AglZ, AglR moves faster but loses its directionality (Nan *et al.*, 2013). Finally, TIRF images of cells expressing cytoplasmic GFP placed on glass microscope slide revealed intensity variations similar to the periodicity of MreB and GltD with a period of 0.83±0.23 µm (Nan *et al.*, 2011).

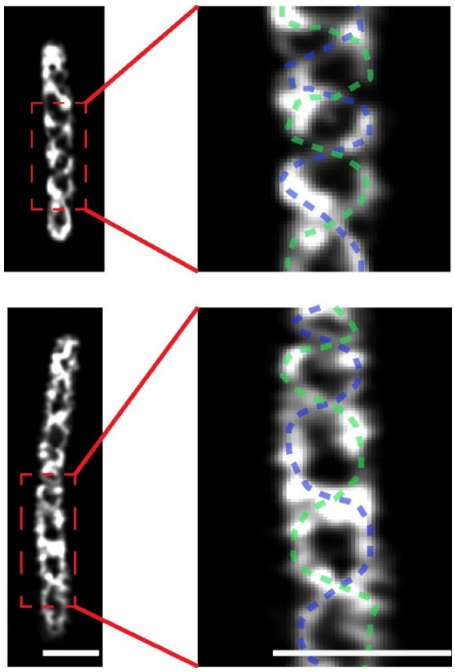

Figure 11. AglR forms a twisted endless helix.
Structured illumination microscopy of AglR-pamCherry in two fixed cells. For each cells, the area in which void fields are covered with helical fluorescence signal. Helical tracks are shown on a magnified section of each cell. Scale bar: 1 µm. Figure reproduced from Nan *et al.*, 2011.

Based on these data the motor cargo model was proposed. In this model, the motor proteins (AglQRS) together with other proteins important for gliding motility are hypothesized to form a complex and move on an endless looped helix that spans the length of cells. When these complexes are at the ventral side of a cell, it is speculated that they slow down because of increased resistance, in that way creating nearly stationary clusters along the cell length. At the positions where these clusters form, they are thought to push on and distort the cell envelope resulting in directed cell movement (Figure 9, A).

1.5.5.2 The focal adhesion complexes model

The focal adhesion model was proposed by Mignot *et al.* and is based on AglZ localization. In fully motile cells, AglZ localizes at the leading cell pole and in ordered

clusters spanning the cell length. As cells move forward, AglZ clusters stay in fixed positions with respect to the substratum. The only clusters that move with a cell are those at the leading cell pole. Moreover, clusters disassembled close to the lagging cell pole (Mignot *et al.*, 2007) (Figure 12).

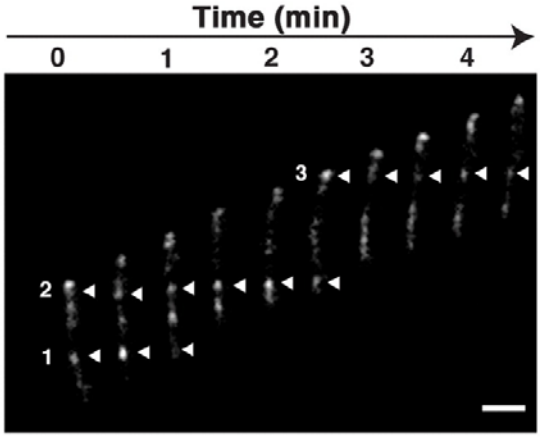

Figure 12. AglZ localizes in clusters along the cell length and stay in fixed position relative to the substratum in moving cells.
AglZ-YFP localization in moving cell. White arrowheads highlight the position of stationary AglZ-YFP clusters. Scale bar: 1 µm. Figure reproduced from Mignot *et al.*, 2007.

The number of AglZ clusters correlates with cell length (Mignot *et al.*, 2007) and the localization of AglZ clusters correlates with the site of force generation (Sun *et al.*, 2011). Importantly, cephalexin treated cells, which elongate up to 10 times of normal length, has almost normal gliding motility suggesting that the force for gliding is distributed along the cell body. Based on these observations, it was suggested that the force for motility is generated at the sites of the AglZ clusters (Mignot *et al.*, 2007). Because the clusters do not move relative to the substratum they were referred to as focal adhesion complexes (Mignot *et al.*, 2007) by analogy to eukaryotic focal adhesion complexes (Hoiczyk & Baumeister, 1998).

Since the initial model was proposed for focal adhesion complexes as the site of force generation for gliding motility, most Glt and Agl proteins have been shown to (co-)localize in focal adhesion complexes (Mignot *et al.*, 2007, Nan *et al.*, 2010, Sun *et al.*, 2011, Jakobczak *et al.*, 2015, Treuner-Lange *et al.*, 2015, Faure *et al.*, 2016). In the current model for assembly of the Agl/Glt complexes for gliding motility, assembly occurs at the leading cell pole leading to formation of the complex that spans from the cytoplasm to the outer membrane (Figure 9, B). The assembly is stimulated by the AglZ/MglA/MreB complex. Upon assembly, the complex adheres to the substratum and generates a force that propels a cell forward. As an Agl/Glt gliding motility complex approaches the lagging cell pole, it disassembles (see details below). Interestingly, recent

data suggest that the Agl/Glt complexes do not only move between poles but also move across the cell width following a helical path. In agreement with counterclockwise rotation of AglZ clusters, Faure *et al.* have found that a moving cell is rotating clockwise during cell propulsion and angular velocity is proportional to the speed of the cell (Faure *et al.*, 2016). These findings suggest that surface adhesion of a focal adhesion complex leads to clockwise rotation and forward drive of the cell.

Finally, Balagam *et al.* simulated a head-to-side collision between two cells moving on crossing paths with parameters fitted to the motor cargo and the focal adhesion complexes model. In the simulation for the motor cargo model both cells changed direction. By contrast, in the focal adhesion model, the new common direction was the same as the direction of the primary cell before collision. To identify which of the two scenarios simulate the behaviour of colliding *M. xanthus* cells, experiments with colliding cells were performed. In the experiments, the direction of the primary cells did not change after collision. This behaviour is similar to the simulations of the focal adhesion model of gliding motility. Thus, comparison of simulations with experimental observation indicates that the focal adhesion complexes model of the gliding motility is correct (Balagam *et al.*, 2014). From hereon, I discuss gliding motility within the framework of the focal adhesion complex model.

1.6 Slime

Gliding *M. xanthus* cells deposit slime. The composition of slime is not known in details; however, it can be stained with fluorescently labelled concavalin A demonstrating that it contains polysaccharide (Ducret *et al.*, 2012). Slime was proposed to be secreted at the focal adhesion sites to promote adhesion of focal adhesion complexes to the substrate. However, cells that lack gliding motility (*aglQ*, *gltD* and *gltE* mutants) still deposit slime underneath the cell body, showing that slime export to the cell surface and deposition do not require an active Agl/Glt machinery. Furthermore, a *wza*^{0} mutant, in which all of putative exopolisacharides (EPS) export machineries are lacking, a *difA* mutant, which is reduced in EPS production, and a *sasA* mutant, which is reduced in LPS O-antigen synthesis, are still moving by gliding motility and deposit slime. Therefore, these results suggest that the polysaccharide component of slime is neither EPS nor LPS (Ducret *et al.*, 2012). Similarly, the mechanism involved in slime synthesis remains unknown.

1.7 Cell polarity and motility regulation – spatial control of motility

Both motility systems in *M. xanthus* are polarized with T4P assembling only at the leading cell pole and focal adhesion complexes assembling at the leading and disassembling at the laggng cell pole. Moreover, this polarity is dynamic and changes during reversals. A protein module consisting of the Ras-like GTPase MglA, its cognate GTPase activating protein (GAP) MglB, and the response regulator RomR establishes polarity of the two motility systems, while signaling by the Frz chemosensory system inverses the polarity (Leonardy *et al.*, 2010, Zhang *et al.*, 2010, Miertzschke *et al.*, 2011, Patryn *et al.*, 2010, Keilberg *et al.*, 2012, Zhang *et al.*, 2012).

1.7.1 Spatial organization of cell polarity by MglA, MglB and RomR

MglA is absolutely essential for movement by both motility system in *M. xanthus* (Hartzell & Kaiser, 1991) and functions as a nucleotide-dependent molecular switch to stimulate motility (Leonardy *et al.*, 2010, Zhang *et al.*, 2010, Miertzschke *et al.*, 2011, Patryn *et al.*, 2010). As other members of the Ras superfamily of small GTPases, MglA is active and stimulates motility in its GTP-bound form and is inactive in the GDP-bound state. Patryn *et al.* reported a K_D of 11.8 µM for GTP and 9.6 µM for GDP (Patryn *et al.*, 2010). Using $MglA_{Tt}$ from *Thermus thermophilus*, which is 62/81% identical/similar to $MglA_{Mx}$ from *M. xanthus*, Leonardy *et al.* reported K_D's of 24.6 nM and 7.3 nM for GTP and GDP, respectively (Leonardy *et al.*, 2010). Moreover, Miertzschke *et al.*) suggested that the affinity of $MglA_{Tt}$ for GTP could be even 100-fold lower than for GDP (Miertzschke *et al.*, 2011). Nevertheless, in the current model for regulation of MglA activity, it is hypothesized that GDP to GTP exchange would be stimulated by a so far unknown guanine nucleotide exchange factor (GEF) (Figure 13).

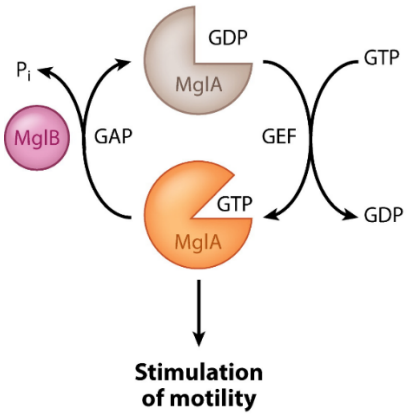

Figure 13. GTPase cycle of MglA.
Figure reproduced from Schumacher &Søgaard-Andersen, 2017.

MglB is not essential for motility *per se* but important for regulation of motility (Leonardy *et al.*, 2010, Zhang *et al.*, 2010). Structural analyses of MglB from *T. thermophilus* demonstrated that MglB is a Roadblock/LC7 protein (Miertzschke *et al.*, 2011). Moreover, the crystal structure of an MglA–MglB complex revealed that they interact with a 1:2 stoichiometry, and in contrast to other Ras-like GTPases and their cognate GAPs, no residues from MglB reach into the active site of MglA, confirming the absence of any conserved potential catalytic residue (Miertzschke *et al.*, 2011) (Figure 14).

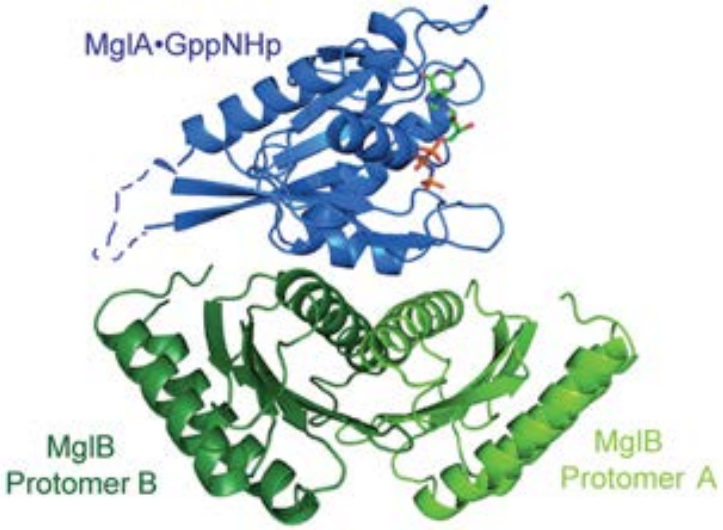

Figure 14. The MglA-MglB complex.
Structure of MglA-GppNHp (blue) bound to the MglB (green). Dotted lines show flexible loops that were not visible in electron density. Figure reproduced from Miertzschke *et al.*, 2011.

RomR is essential for gliding motility and important for T4P-dependent motility (Zhang *et al.*, 2012, Keilberg *et al.*, 2012). Sequence analysis showed that RomR possesses an N-terminal receiver domain and C-terminal output domain. The output domain of RomR contains a conserved C-terminal region (RomR-C) and an unstructured proline-rich region that links the two conserved regions (Keilberg *et al.*, 2012) (Figure 15).

Figure 15. Schematic representation of RomR. RomR contains three distinct regions: N-terminal response regulator domain (REC), an unstructured proline rich linker domain (Linker), and a conserved C-terminal part (RomR-C). Numbers correspond to amino acid sequence of RomR. Figure reproduced from Keilberg *et al.*, 2012.

MglA, MglB as well as RomR localize dynamically to the cell poles (Figure 16). In the active GTP-bound form, MglA localizes to the leading cell pole while the inactive form MglA-GDP is diffusely localized throughout the cytoplasm. MglB localizes primarily at the lagging cell pole. Finally, RomR localizes in a bipolar asymmetric pattern with the bigger cluster at the lagging cell pole (Zhang *et al.*, 2012, Keilberg *et al.*, 2012). RomR has been suggested to have two pole targeting determinants, one is the linker region in the output domain and the second is RomR-C (Figure 15) (Keilberg *et al.*, 2012). Furthermore, both regions are necessary for motility (Keilberg *et al.*, 2012). The RomR receiver domain failed to localize to the poles but has been suggested to be important for cellular reversals (Leonardy *et al.*, 2007).

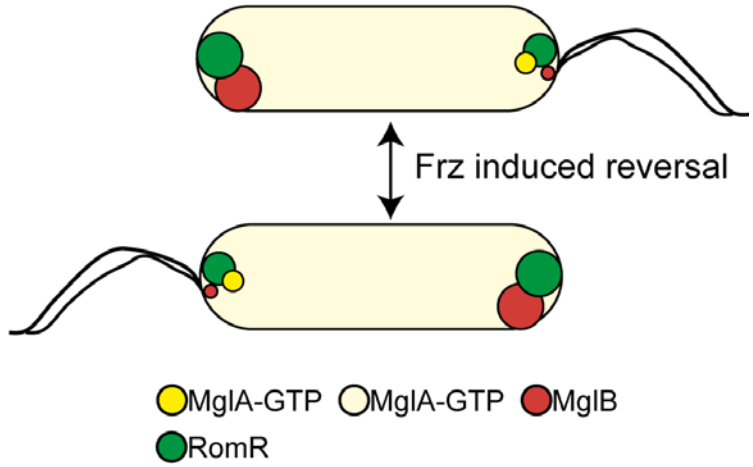

Figure 16. Model for spatial dynamic regulation of motility in *M. xanthus*.
Localization of MglA, MglB and RomR at the leading and lagging cell poles before and after a cellular reversal.

Localization of MglA, MglB are RomR is mutually dependent. In the absence of MglB, MglA as well as RomR localize in bipolar symmetric patterns. Similar bipolar localization was observed for MglA locked in the GTP-bound form. In the absence of MglA, MglB as well as RomR localize unipolarly (Zhang *et al.*, 2010, Keilberg *et al.*, 2012, Zhang *et al.*, 2012, Leonardy *et al.*, 2010). Importantly, localization studies of an MglA variant locked in the GTP-bound form have shown that RomR is polar targeting determinant for MglA-GTP (Keilberg *et al.*, 2012, Zhang *et al.*, 2012). Finally, in the absence of RomR, MglA localizes diffusely to the cytoplasm and MglB becomes more unipolar. MglA, MglB and RomR are not only mutually dependent on each other for localization but also directly interact (Miertzschke *et al.*, 2011, Keilberg *et al.*, 2012). How the three proteins become asymmetrically localized to the cell poles is not well-

understood except that (1) MglB excludes MglA-GTP from the lagging cell pole by stimulating the conversion of MglA-GTP to MglA-GDP at this pole; and, (2) RomR is a polar targeting determinant of MglA-GTP at the leading cell pole (Patryn *et al.*, 2010, Leonardy *et al.*, 2010, Zhang *et al.*, 2010, Miertzschke *et al.*, 2011, Keilberg *et al.*, 2012, Zhang *et al.*, 2012)

During the Frz-induced reversals, MglA-GTP, MglB and RomR are released from their respective poles and rebind to the relevant opposite cell poles (Figure 16) (Leonardy *et al.*, 2007, Keilberg *et al.*, 2012, Zhang *et al.*, 2012, Zhang *et al.*, 2010, Leonardy *et al.*, 2010). Time-lapse microscopy analyses have suggested that MglA is the first protein to be released and rebind to the new leading cell pole (Leonardy *et al.*, 2010, Zhang *et al.*, 2010). These observations were confirmed by colocalization studies in which it was observed that MglA and MglB colocalize at the old lagging cell pole immediately before cells reverse (Zhang *et al.*, 2010).

The output of the MglA/MglB/RomR module is generated by MglA-GTP (Zhang *et al.*, 2012, Keilberg *et al.*, 2012). Moreover, deletion of *mglB* restored gliding in a Δ*romR* strain (Keilberg *et al.*, 2012). Additionally, MglA locked in the GTP form restored gliding in a *romR* mutant (Keilberg *et al.*, 2012). How MglA-GTP stimulates motility at the leading pole is not understood for the T4P-dependent system except that correct polar localization of PilB, PilT and FrzS depends on MglA-GTP (Bulyha *et al.*, 2013, Zhang *et al.*, 2012). In the case of the gliding motility system, MglA-GTP at the leading cell pole interacts with AglZ and MreB to stimulate assembly of the Agl/Glt motility machinery in that way stimulating formation of the focal adhesion complexes (Treuner-Lange *et al.*, 2015). MglA-GTP not only stimulates formation of these compexes but is also incorporated into them. By incorporating MglA-GTP into the gliding motility complexes, these complexes become sensitive to the MglB GAP activity at the lagging pole and disassemble at this cell pole. Consistently, a Δ*mglB* mutant and a strain containing MglA locked in the GTP-bound form hypperreverse because the gliding motility complexes are not disassembled at the lagging cell pole (Leonardy *et al.*, 2010, Zhang *et al.*, 2010, Miertzschke *et al.*, 2011, Treuner-Lange *et al.*, 2015).

1.7.2 Frz chemosensory system

The reversal frequency is regulated by the Frz chemosensory system (Blackhart & Zusman, 1985). The components of this signal transduction system show high similarity to the components of chemosensory systems involved in chemotaxis in other bacteria

(McBride *et al.*, 1989, Trudeau *et al.*, 1996) (Figure 17). In details, the Frz system consists of the following components: FrzCD, a cytoplasmic MCP (methyl-accepting chemotaxis protein) homolog, two CheW homologs, FrzA and FrzB, a methyltransferase FrzF, which methylates FrzCD, a methylesterase FrzG, which demethylases FrzCD, a CheA histidine kinase with a CheY-like receiver domain, FrzE, and a response regulator with two CheY-like receiver domains, FrzZ (Figure 17). The specific signals that induce cellular reversals are not known. It has been proposed that the intercellular C-signal, which is important for development, (Jelsbak &Søgaard-Andersen, 2002,Søgaard-Andersen & Kaiser, 1996) and exopolysaccharide (Zhou & Nan, 2017) may regulate Frz activity. However, it is not know how these extracellular compounds would regulate Frz activity in the cytoplasm. Current data suggests that these signal(s) could be sensed by FrzCD or by FrzF (Scott *et al.*, 2008, Bustamante *et al.*, 2004).

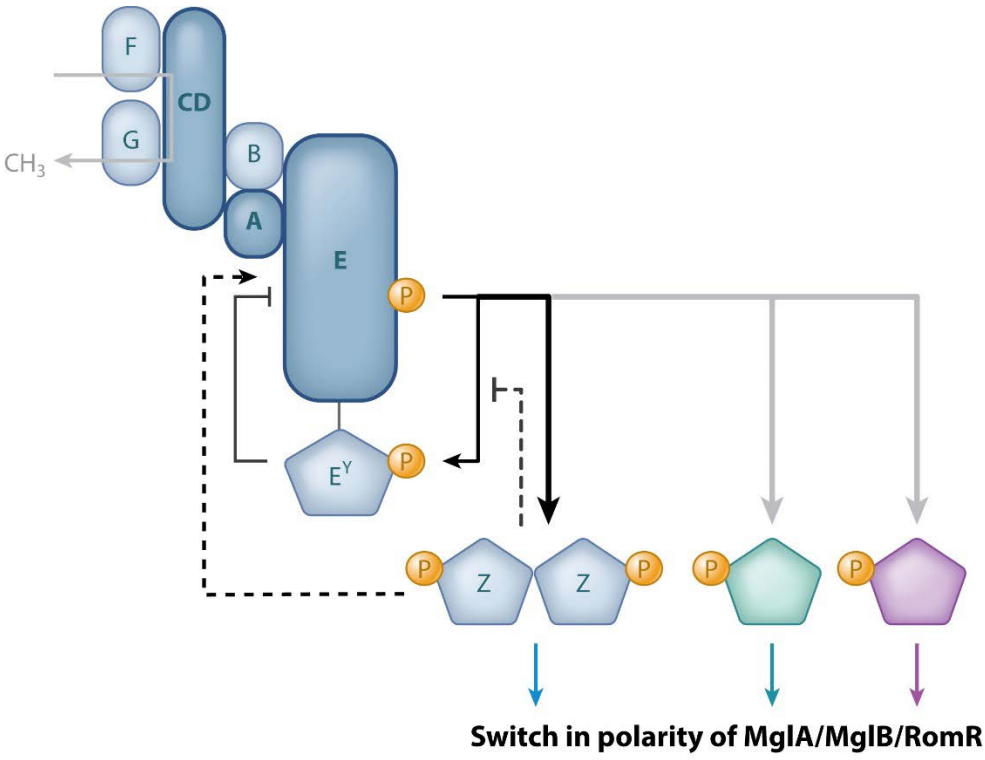

Figure 17.Schematic representation of the Frz pathway from *M. xanthus.*
Frz protein are blue with the core Frz proteins (FrzCD, FrzA and FrzE kinase domain) shown in dark blue. Experimentally confirmed phosphotransfers from FrzE kinase are indicated with black arrows. FrzE is suggested to phosphorylated $FrzE^{CheY}$ at low signalling level (thin line) and FrzZ at high signalling level (thick line) Phosphorylated $FrzE^{CheY}$ inhibits FrzE kinase activity. Phosphorylated FrzZ inhibits phosphotransfer to $FrzE^{CheY}$, stimulates kinase activity or both (dashed lines). FrzE may phosphorylate RomR (green pentagon) or not known response regulator (purple pentagon) at the higher signalling level (thick grey arrows). Coloured arrows at the bottom show the Frz output. Proteins labelled with single letters have the Frz prefix. Figure reproduced from Schumacher &Søgaard-Andersen, 2017.

Upon receiving a signal, FrzE autophosphorylates at a conserved histidine residue in the histidine phosphotransfer (Hpt) domain (Inclan *et al.*, 2007, Inclan *et al.*, 2008). *In vitro* experiments showed direct phosphotransfer from FrzE Hpt domain to both CheY-like domains of the FrzZ (Inclan *et al.*, 2007). Inclan *et al.* suggested that FrzE CheY-like domain inhibits autophosphorylation of the Hpt domain. Alternatively, the FrzE CheY-like domain may act as a phosphosink for the kinase (Inclan *et al.*, 2008). Further studies on FrzZ confirmed *in vitro* phosphorylation of both CheY-like domain, with Asp52 as the preferential site of phosphorylation. Moreover, the reversal frequency is directly correlated with the amount of phosphorylated FrzZ present in a cell with a higher pool of phospho-FrzZ correlating with a higher reversal frequency (Kaimer & Zusman, 2013). Kaimer & Zusman also showed that FrzZ phosphorylation depends on cell-surface contact (Kaimer & Zusman, 2013). Furthermore, FrzZ phosphorylation is independent of cell movement, i.e. cells with defective gliding and T4P-dependentmotility still accumulate phospho-FrzZ. Phospho-FrzZ localizes to the leading cell pole and its localization depends on MglA and FrzE CheY-like domain (Kaimer & Zusman, 2013, Kaimer & Zusman, 2016).

Interestingly, FrzE overexpression resulted in inhibition of FrzZ phosphorylation and reduced reversals (Kaimer & Zusman, 2016). This inhibitory effect of FrzE is mediated by the C-terminal CheY-like domain (Kaimer & Zusman, 2016). Furthermore, substitution of the conserved Asp residue (Asp709) in the FrzE CheY-like domain to a non-phosphorylatable amino acid residue ($FrzE^{D709A}$) resulted in hyper-reversing cells and a high level of FrzZ phosphorylation independent of the $FrzE^{D709A}$ level (Kaimer & Zusman, 2016). This indicates that phosphorylation of the CheY-like domain in FrzE is required for this inhibitory effect (Kaimer & Zusman, 2016). It was suggested that FrzZ transfers the signal from the Frz system to the downstream effectors (Kaimer & Zusman, 2013). Surprisingly, a double mutant *frzZ* $frzE^{D709A}$ showed wild type reversal behaviour (Kaimer & Zusman, 2016). Furthermore, a *frzZ* mutant was still able to respond to isoamyl alcohol, which is an artificial activator of the Frz system, unlike a kinase (*frzE*) or MCP (*frzCD*) mutant, suggesting that FrzZ is not required for signal transduction under these conditions. Observation of cells moving by T4P-dependent motility revealed rare reversals in a *frzZ* mutant, suggesting that FrzZ is important for reversals in the T4P-dependent motility system but not strictly required (Guzzo *et al.*, 2015). In the current model for the Frz system induced reversals, FrzZ acts as a stimulator of reversals. Moreover, the response regulator RomR (see details below) and/or a yet unknown

response regulator would contribute to transducing the reversal signal to the MglA/MglB/RomR module (Figure 17). The output response of the Frz system is a reversal. At the cellular, this involves an inversion of the leading-lagging cell pole with the relocation of MglA, MglB and RomR. How the Frz system connects to the MglA/MglB/RomR polarity module remains unknown. Of note, RomR was proposed as a connector between Frz and the polarity module (Guzzo *et al.*, 2015, Leonardy *et al.*, 2007, Keilberg *et al.*, 2012) because a RomR variant that mimics the phosphorylated form of RomR ($RomR^{D53E}$) caused a hyper-reversing and RomR with blocked phosphorylation ($RomR^{D53N}$) a hypo-reversing phenotype. Moreover, the effect of the $RomR^{D53E}$ variant was observed in cells lacking FrzZ or several components of the Frz system (Leonardy *et al.*, 2007, Keilberg *et al.*, 2012). However, until now a kinase involved in RomR phosphorylation has not been identified.

1.7.3 Regulation of cell polarity by MglC, an MglB homolog

Most *mglA* genes are located next to an *mglB* gene (Wuichet &Søgaard-Andersen, 2014). However, *M. xanthus* encodes an orphan paralog of MglB, named MglC (McLoon *et al.*, 2015). MglB and MglC from *M. xanthus* only share 8%/17% identity/similarity. However, structural prediction of MglC showed that MglC is predicted to have Roadblock/LC7 fold similar to the MglB homolog from *T. thermophilus* (McLoon *et al.*, 2015, Miertzschke *et al.*, 2011). In-frame deletion of *mglC* causes a defect in both motility systems. In the case of the gliding motility system, this defect was traced down to a defect in reversals while it still remains unknown whether the defect in T4P-dependent motility is caused by a reversal defect. Epistasis analysis have shown that MglC acts in the same pathway as MglA, MglB and RomR. MglC localizes predominantly at the lagging cell pole with occasional localization of a smaller cluster at the leading cell pole. Localization of MglC is dynamic and switches pole during a cellular reversal. In the absence of MglA, localization of MglC shows highly asymmetric pattern. In the Δ*mglB* mutant, MglC shows predominantly bipolar symmetric localization. Thus, MglB is not necessary for polar MglC localization but is important for correct polar asymmetry. In contrast, in the absence of RomR, MglC shows diffuse localization. Thus, MglC polar localization completely depends on RomR. Analysis of direct protein-protein interaction have shown that MglC directly interacts with MglB and RomR. Because of the opposite reversal frequencies of Δ*mglB* and Δ*mglC* strains and the direct MglB-MglC interaction, it was hypothesized that MglC could act as an inhibitor of the GAP activity of MglB on MglA.

However, in a GTPase assay no inhibitory effect of MglC on the GAP activity of MglB was observed (McLoon *et al.*, 2015). It remains unknown how MglC regulates reversals. However, it was suggested that by interacting with both, RomR and MglB, MglC could function between Frz system and RomR or between RomR and MglB.

1.7.4 Regulation of motility by the small GTPase SofG

As described, PilB and PilT are polarly localized (Bulyha *et al.*, 2009) and sorted to the opposite cell poles by MglA (Bulyha *et al.*, 2013). However, MglA is not necessary for the PilB and PilT polar localization. PilB and PilT polar localization is also independent of the stationary T4PM components (Friedrich *et al.*, 2014).

Two or more small GTPases often function in parallel or in the same pathway to regulate polarity or motility in eukaryotes (Charest & Firtel, 2007, Heasman & Ridley, 2008). Based on these observations, Bulyha *et al.* identified an orphan small GTPase, named SofG, that regulates T4P-dependent motility. SofG shows 34% identity and 50% similarity to MglA and, similarly to MglA, contains an intrinsic Arg finger, which is important for its function. So far, a GAP and a GEF for SofG have not been identified (Bulyha *et al.*, 2013).

SofG itself localizes in a subpolar cluster and is important for polar PilB and PilT localization (Bulyha *et al.*, 2013). Moreover, SofG localization depends on BacP (Bulyha *et al.*, 2013), a bactofilin cytoskeletal protein that polymerizes *in vitro* independently of any cofactors and *in vivo* localizes to two subpolar patches (Kuhn *et al.*, 2010). The SofG cluster is highly dynamic and shuttles back and forth between the subpolar localization and the cell pole over one of the BacP patches. Importantly, dynamics of the SofG cluster depends on GTP hydrolysis, SofG variant that is impaired in GTP hydrolysis does not show dynamics of the WT protein. Additionally, SofG GTP hydrolysis is important for the polar localization of PilT and PilB (Bulyha *et al.*, 2013).

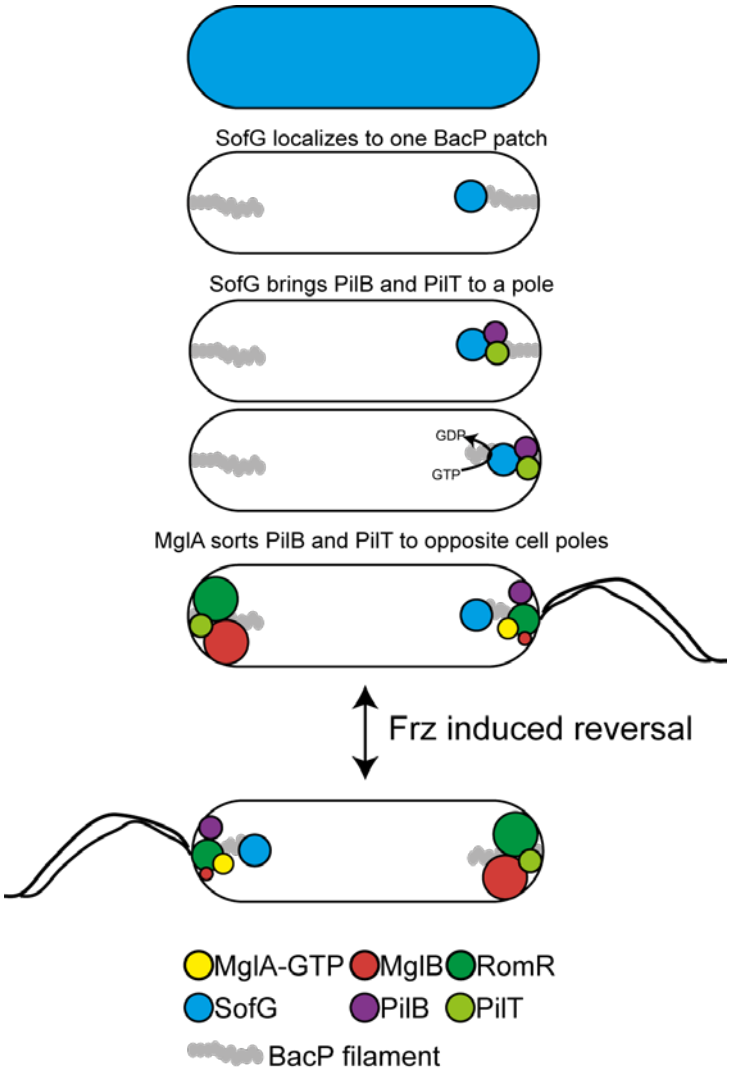

Figure 18. Modelf for polar and dynamic PilB and PilT localization regulated by two small GTPases. Details in text.

Based on these results Bulyha *et al.* (2013) proposed a model in which the dynamic localization of PilB and PilT is regulated by a cascade of two small GTPases. First, SofG localizes to one of the BacP patches. This subpolar SofG cluster shuttles and brings PilT and PilB to the same pole. Next, MglA sorts PilB and PilT to the opposite cell poles and sets up correct T4P asymmetry (Bulyha *et al.*, 2013) (Figure 18).

1.8 Scope of this study

M. xanthus is a model organism for studying bacterial multicellularity, cell-cell communication, development and motility. Regulation of motility combines a typical bacterial chemosensory system (Frz system) with a polarity module (MglA/MglB/RomR) that incorporates typical eukaryotic components for polarity. However, it is not known how the Frz system connects to the MglA/MglB/RomR polarity module. Similarly, we

lack a clear understanding of the importance of the MglA GTPase cycle because an MglA GEF has not been identified so far. In this study, by using a comparative genomic approach, we identified RomX and RomY as candidate components of the polarity module. By using fluorescence live-cell imaging, protein-protein interaction analyses, *in vitro* analyses of proteins, we demonstrate that RomX and RomY are integral components of the polarity module.

2. Results

2.1. Identification of RomX and RomY

romR has a limited genomic distribution and, generally, co-occurs with MglA and MglB (Keilberg *et al.*, 2012). Therefore, in order to identify novel proteins that play a role in regulation of polarity and motility, we searched for proteins with the same genomic distribution as *romR* in 1609 completely sequenced prokaryotic genomes (personal communication, Kristin Wuichet).

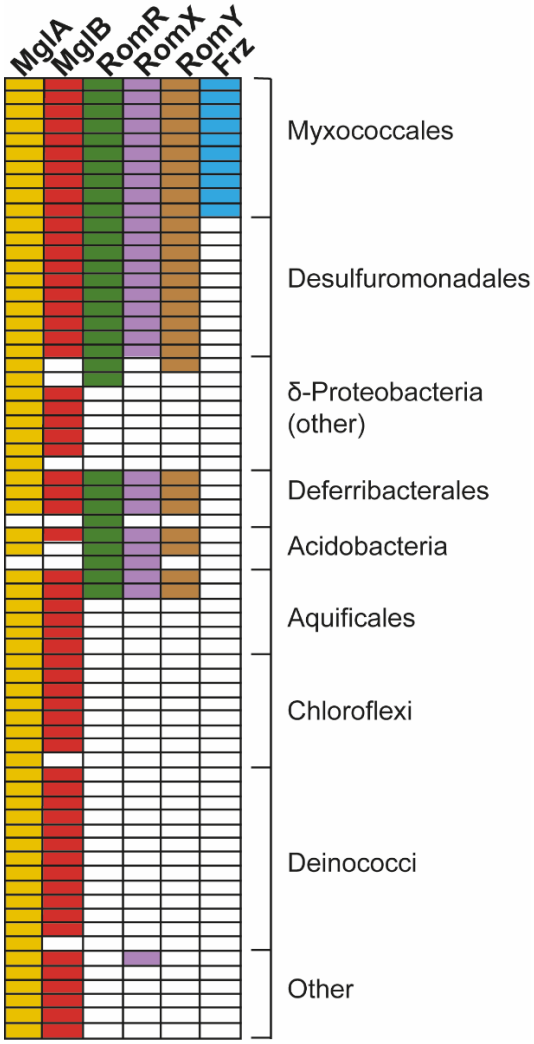

Figure 19. RomX and RomY have the same genomic distribution as RomR.
Each column represents the presence (color) or absence (white) of MglA, MglB, RomR, RomX, RomY and Frz system (Kristin Wuichet, personal communication).

The analysis revealed two proteins, MXAN_3350 (from hereon RomX) and MXAN_5749 (from hereon RomY) that co-occur with RomR. *romX* and *romY* are conserved in 28 out of 31 genomes containing *romR* (Figure 19). RomX is encoded in 28 out of 31 genomes encoding RomR and in one genome that does not encode RomR (Figure 19). Seven genomes encode two RomX homologs. Among the genomes that

encode RomX as well as RomR, one does not encode MglA and MglB and one does not encode MglB. By contrast, *romY* only co-occurs with *romR*. Moreover, all genomes that encode RomR and RomY also encode MglA, indicating a possible connection between RomR, RomY and MglA.

romX and *romY* were not identified in genetic screens to identify regulators of motility or reversals. However, based on the bioinformatic analyses, we hypothesized that RomX and RomY are new motility regulatory proteins.

2.2. Characterization of RomX in *Myxococcus xanthus*

All 36 RomX homologs share a domain that does not match any currently characterized domain models. Seven genomes encode two RomX homologs (Figure 20, A). In the case of these proteins, one of the paralogs contain an N-terminal response regulator receiver domain in addition to the conserved RomX domain.

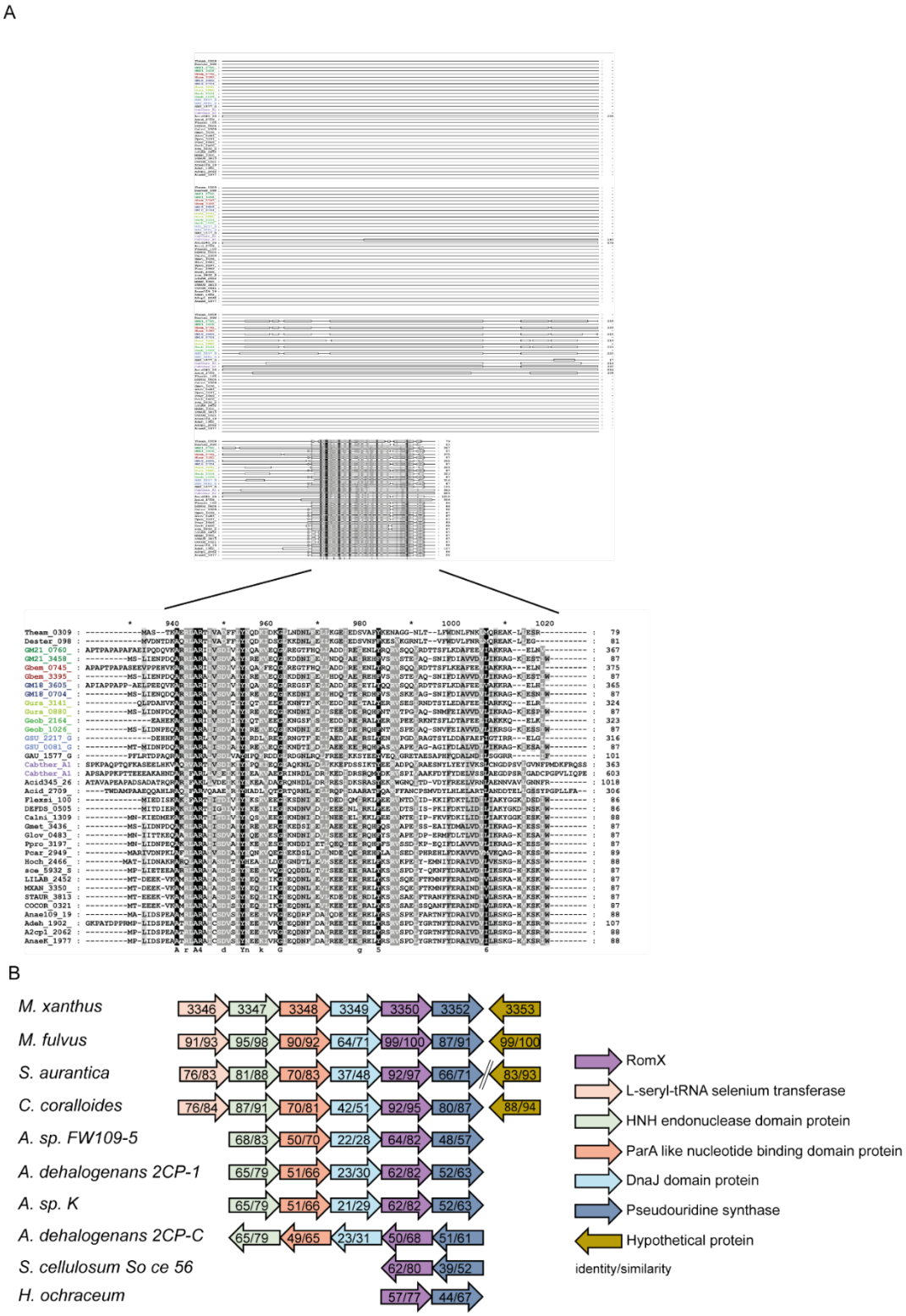

Figure 20. Bioinformatics analysis of RomX

(A) Alignment of identified RomX homologs. Gene accession number showed in the same colour are coming from the same species.

(B) Conservation of *romX* neighbourhood in selected myxobacterial genomes. Genes are depicted as arrows. Arrow orientation indicates coding direction. Homologous proteins are indicated in same colours. Numbers in arrows in *M. xanthus* indicate gene number. Numbers in arrows (outside of *M. xanthus*) indicate identity and similarity of their encoded protein to their *M. xanthus* homolog. Numbers were obtained from Pairwise Sequence Alignement of protein using EMBOSS Needle. Right part shows predicted proteins functions based on the NCBI BLAST and conserved domain analysis (Marchler-Bauer *et al.*, 2017).

The *romX* locus is conserved in myxobacterial genomes (Figure 20, B). *rluA* in *M. xanthus*, which is predicted to encode a pseudouridine synthase, was identified in a transposon mutagenesis screen as potentially important for gliding motility (Youderian *et al.*, 2003); however, none of the remaining genes flanking *romX* have been implicated in motility.

2.2.1 RomX is important for both motility systems

To test the role of *romX* in motility, we generated an in-frame deletion of *romX*. To evaluate T4P-dependent and gliding motility in the *romX* mutant, motility was tested on soft (0.5%) agar, which is favorable to T4P-dependent motility, and hard (1.5%) agar, which is favorable to gliding motility. T4P-dependent motility is evident by the formation of flares at the colony edge. Gliding motility is evident by the presence of single cells at the edge of a colony.

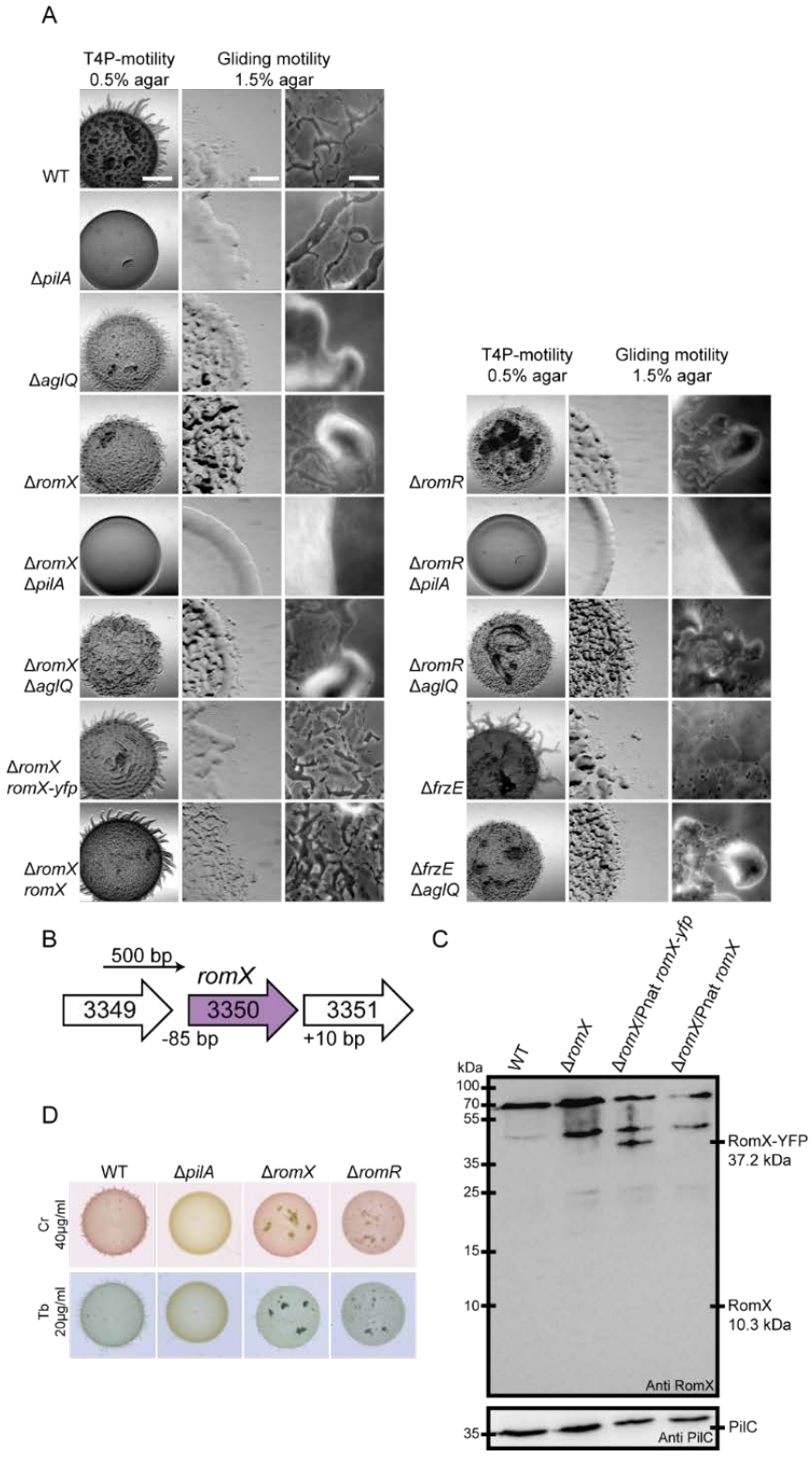

Figure 21. Δ*romX* mutant shows defect in T4P-dependent motility, no gliding motility and normal EPS accumulation.

(A) Motility assays showing colonies of indicated mutants after 24 hours incubation on agar plates favoring T4P-dependent motility (0.5% agar) and gliding motility (1.5% agar), respectively. Bars, 1000 µm (T4P-dependent motility), 500µm (gliding motility – left panel) and 50 µm (gliding motility – right panel).

(B) Genomic neighborhood of *romX*. Genes are depicted as arrows. Arrow orientation indicates coding direction. Numbers below indicate distance between genes. Arrow above shows genomic fragment used as a promoter for the ectopic expression of *romX*.

(C) Immunoblot of RomX accumulation. Cells were grown in liquid culture, harvested, and total protein (1 mg per lane) was separated by SDS–PAGE and analyzed by immunoblot using α-RomX. Calculated molecular masses of RomX and RomX-YFP are indicated. Immunoblot with α-PilC serves as loading control.
(D) EPS accumulation in WT and selected mutants. Aliquots of 20 µl cell suspensions at 7×10^9cells/ml were spotted on 0.5% agar supplemented with 0.5% CTT and 40µg/ml congo red (Cr) or20 µg/ml trypan blue (Tb) and incubated at 32 °C for 24 hours.

WT formed the flares characteristic of T4P-dependent motility on 0.5% agar. The Δ*pilA* mutant that lacks the major pilin and therefore does not display T4P-dependent motility served as a negative control. The Δ*romX* mutant formed less and shorter flares in comparison to WT. In the case of gliding motility, WT showed single cells at the colony edge on hard agar while the Δ*aglQ* mutant, which lacks an essential component of the gliding machinery and served as a negative control, did not. The Δ*romX* mutant only displayed small groups of cells at the colony edge but no single cells. To more carefully test for defects in the two motility systems, we inactivated *pilA* or *aglQ* in the Δ*romX* mutant. The double deletion strain Δ*romX*Δ*aglQ* on 0.5% agar formed short flares that were undistinguishable from the flares of the Δ*romX* mutant. Surprisingly, the Δ*romX*Δ*aglQ* mutant still moved on 1.5% agar in a similar fashion to the Δ*romX* mutant. We hypothesize that this movement is performed by T4P-dependent motility. The Δ*pilA*Δ*romX* double mutant showed a flat colony edge under both conditions (Figure 21, A). Because RomX was identified as co-occurring with RomR, we compared the motility characteristics of the three Δ*romX* mutants to that of the corresponding Δ*romR* mutants. The three Δ*romX* mutants and the three Δ*romR* mutants have similar motility phenotypes (Figure 21, A).

To confirm that the motility defects in the Δ*romX* mutant was caused by lack of RomX, complementation strains in which *romX* and *romX-YFP* were ectopically expressed under the control of the native promoter (Figure 21, B) were generated. α-RomX antibodies failed to detect a protein of the calculated size of RomX (10.3 kDa) in immunoblot analysis of total cell extracts from WT and the complementation strain expressing *romX* ectopically from the Mx8 *attB* site; by contrast, these antibodies detected the ectopically expressed RomX-YFP protein (Figure 21, C) suggesting that this protein is either overexpressed or that native RomX cannot be detected by immunoblotting due to its small size. Both complementation strains displayed WT motility (Figure 21, A). Based on these experiments, we conclude that RomX is important for T4P-dependent motility and necessary for gliding motility.

Defects in T4P-dependent motility can be caused by lack of EPS accumulation (Li *et al.*, 2003, Lu *et al.*, 2005). To test the possibility that the defect in T4P-dependent

motility in the Δ*romX* mutant was caused by lack of EPS, EPS accumulation was checked using colorimetric assays. Cells were inoculated on solid medium containing nutrients and supplemented with congo red or trypan blue. We observed no difference in congo red and trypan blue binding for WT and the Δ*romX* mutant. In this experiment, the Δ*pilA* mutant served as a negative control and no binding of congo red and trypan blue was observed for this strain (Figure 21, D) (Black *et al.*, 2006). Thus, the defect in T4P-dependent motility in the Δ*romX* strain is not caused by lack of EPS accumulation. As expected, the Δ*romR* mutant also bound congo red and trypan blue similarly as WT (Figure 21, D). Thus, the defect in T4P-dependent motility in the Δ*romR* strain is also not caused by lack of EPS accumulation.

To further examine the effect of RomX on T4P-dependent motility, we analysed the motility characteristics of single cells moving by means of T4P using an assay in which single cells are submerged in a 1% methylcellulose solution and moving on a polystyrene surface (Hu *et al.*, 2011). As shown in Figure 22, A, cells of the WT and the Δ*aglQ* strain with inactivated gliding motility moved with similar velocity. Therefore, under these experimental conditions, cells were moving by T4P-dependent motility. Importantly, the velocity of the Δ*romX*Δ*aglQ* and Δ*romR*Δ*aglQ* cells were not statistically significantly different from that of the WT and the Δ*aglQ* cells (Figure 22, A). Moreover, because the Δ*romX* and Δ*romR* mutants accumulate EPS as WT (Figure 21, B), the observed single cell movement on 1% methylcellulose (in this assay) was not due to bypass of a lack of EPS by the methylcellulose. However, under the same conditions, the Δ*romX*Δ*aglQ* and Δ*romR*Δ*aglQ* mutants reversed much less frequently than WT and the Δ*aglQ* strain (Figure 22, B). In total, these data demonstrate that RomX and RomR are not important for T4P-dependent motility *per se* but they are important for reversals in the T4P-dependent motility systems.

Altogether, these observations demonstrate that RomX has two functions in motility. First, RomX is important for reversals in T4P-dependent motility but is not important for T4P-dependent motility *per se* as previously described for RomR (Keilberg *et al.*, 2012, Zhang *et al.*, 2012); and, second, RomX is essential for gliding motility as previously described for RomR (Keilberg *et al.*, 2012, Zhang *et al.*, 2012). Consistently, a Δ*frzE*Δ*aglQ* double mutant had the same motility characteristics as the Δ*romR*Δ*aglQ* and Δ*romX*Δ*aglQ* double mutants on hard and soft agar (Figure 21, A).

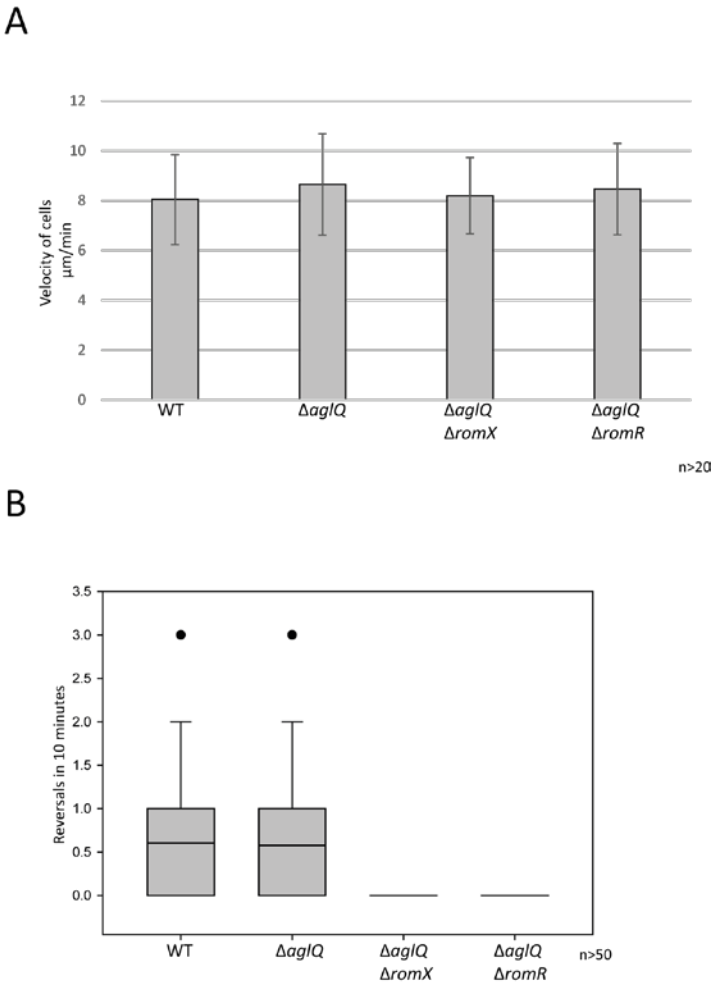

Figure 22. *romX* and *romR* mutants show WT like velocity when moving by T4P, but fail to reverse.
(A) Velocity of WT and selected mutants on 1% methylcellulose. Single moving cells were tracked for 10 min. n>20.
(B) Reversal frequency of WT and selected mutants on 1% methylcellulose. Shown are boxplots of the measured reversals of isolated cells for 10 min, boxes enclose the 25th and 75th percentile, whiskers represent the 10th and 90th percentile, and dots outliers. n>50.

2.2.2 RomX acts in the same pathway as RomR, MglA and MglB

We tested whether RomX acts together with MglA, MglB and RomR in the same pathway. To test the relationship between RomX and MglA, MglB as well as RomR, genetic epistasis experiment in which motility phenotypes were analyzed was performed.

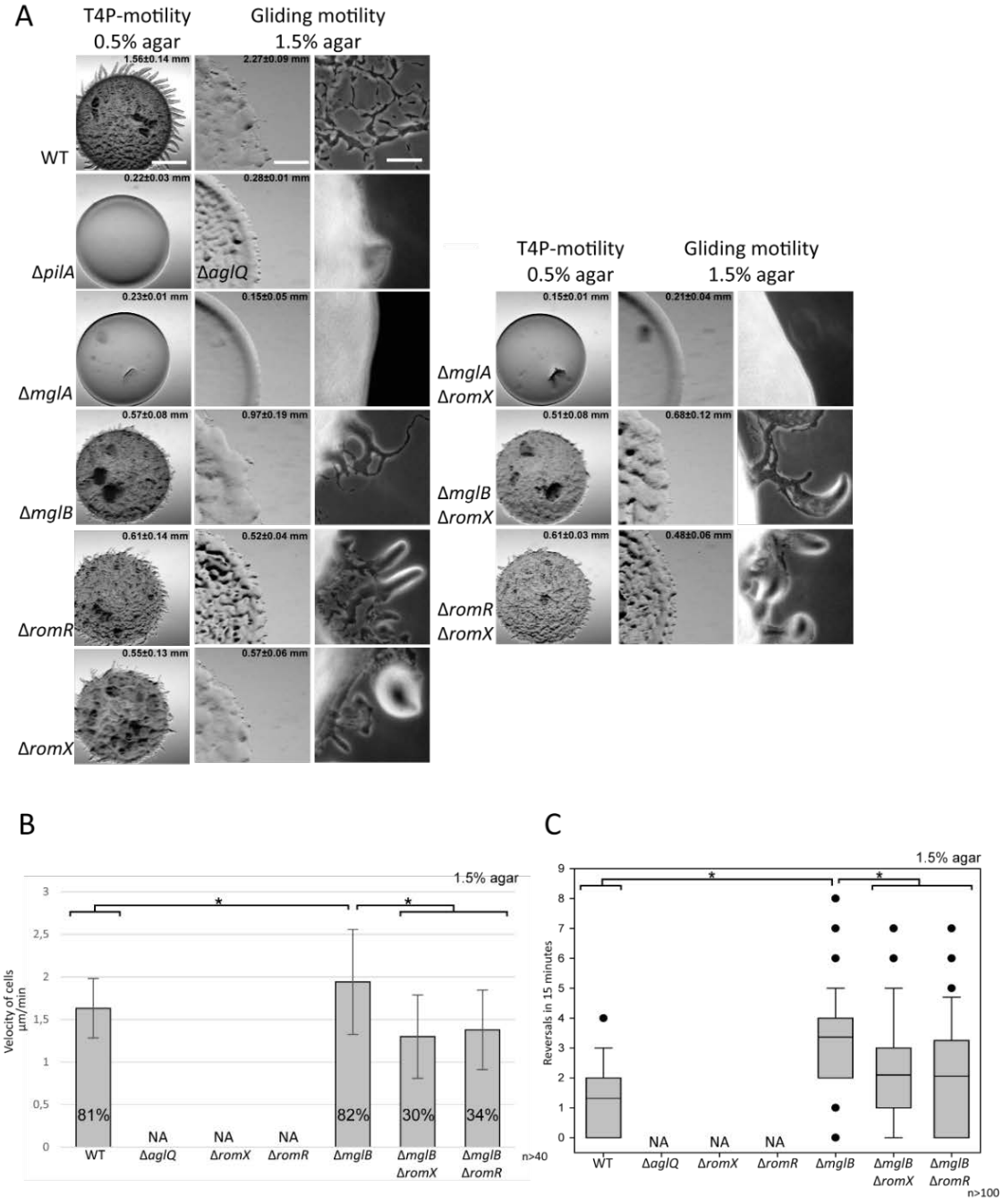

Figure 23. RomX acts in the same pathway as MglA&B and RomR to regulate motility.

(A) Motility assays as described in Figure 21 comparing single and double mutants of *romX*, *mglA*, *mglB* and *romR*. The numbers indicate the increase in colony diameter in mm ± standard deviation after 24h. Scale bars, 1000 µm (T4P-dependent motility), 500µm (gliding motility – left panel) and 50 µm (gliding motility – right panel).

(B) Velocity of WT and selected mutants on 1.5% agar, 0.5% CTT. Single moving cells were tracked for 15 min. Graph presents velocity of the cells in µm/min ± standard deviation. Student's t-test was employed for statistical analysis and * indicates p< 0.001. n>20 for each of two independent experiment. Number in each column represents percent of moving single cells. n>450 for each of two independent experiment. NA – not applicable; Δ*aglQ*, Δ*romX*, Δ*romR* were not moving as single cells in the tested conditions.

(C) Reversal frequency of WT and selected mutants on 1.5% agar, 0.5% CTT. Shown are boxplots of the measured reversals of isolated cells for 15 min, boxes enclose the 25th and 75th percentile, whiskers represent the 10th and 90th percentile, and dots outliers. Student's t-test was employed for statistical analysis and * indicates p< 0.001. n>50 for each of two independent experiment. NA – not applicable; Δ*aglQ*, Δ*romX*, Δ*romR* were not moving as single cells in the tested conditions.

Δ*mglA* and Δ*mglA*Δ*romX* mutants showed flat colony edges under both tested conditions (Figure 23, A). This suggests that MglA acts downstream of RomX. The double Δ*mglB*Δ*romX* mutant showed short, misformed flares similarly to the single Δ*mglB* and Δ*romX* mutants on 0.5% agar. Importantly, no additive effect on T4P-dependent motility of the two single deletions were observed in the double Δ*mglB*Δ*romX* deletion. For gliding motility, we observed that the colony edge of Δ*mglB*Δ*romX* mutant was similar to that of the Δ*mglB* mutant. However, the increase in colony diameter of the Δ*mglB*Δ*romX* mutant was significantly smaller than the increase of the Δ*mglB* mutant (t-test $p<0.05$). Additionally, Δ*mglB*Δ*romX* cells spread significantly more than cells of Δ*romX* mutant (t-test $p<0.05$) (Figure 23, A). Thus, from these data it is not clear whether MglB and RomX act in the same pathway. Single deletions of Δ*romR* and Δ*romX* caused similar motility phenotype on both tested conditions. Moreover, no additive effect of the two single deletions was observed in the double deletion Δ*romR*Δ*romX* (Figure 23, A). These observations suggest that RomR and RomX act in the same pathway.

To better understand the gliding motility defect in the Δ*mglB*Δ*romX* mutant, analysis of single cells movement on 1.5% agar was performed. WT single cells were moving with an average velocity 1.53 μm/min and 79% of observed cells were moving (Figure 23, B). The Δ*aglQ* mutant lacks gliding motility, served as a negative control and did not display single cell movement. 81% of the Δ*mglB* cells moved and they moved faster than WT (Figure 23, B). As mentioned the Δ*romX* and Δ*romR* mutants lack gliding motility (Figure 21, A and Figure 23, B). Importantly, in both the Δ*mglB*Δ*romX* and Δ*mglB*Δ*romR* mutant gliding motility was partially restored. However, these two strains moved significantly slower than single Δ*mglB* mutant. Moreover, only approx. 30% of the Δ*mglB*Δ*romX* and Δ*mglB*Δ*romR* mutants cells displayed single cell gliding (Figure 23, B). Thus, gliding motility of the Δ*romX* and Δ*romR* mutants is partially restored in the absence of *mglB*.

Additionally, reversal frequencies were quantified. Under the tested conditions, WT reversed on average 1.28 times in 15 min. In agreement with previous observations (Leonardy *et al.*, 2010, Zhang *et al.*, 2010), the Δ*mglB* mutant hyperreversed with on average 3.14 reversals in 15 min (Figure 23, C). The Δ*mglB*Δ*romX* mutant as well as the Δ*mglB*Δ*romR* mutant was also hyper-reversing in comparison to WT. However, Δ*mglB*Δ*romX* and Δ*mglB*Δ*romR* reversed significantly less than the Δ*mglB* mutant (t-test $p<0.001$).

In total, the epistasis experiments suggest that *romX* acts in the same pathway as *mglA*, *mglB* and *romR*. Moreover, analysis of single cells moving by gliding motility and reversals revealed that RomX and RomR have antagonistic function to MglB.

2.2.3 RomX localizes dynamically to the cell poles

MglA, MglB, RomR and RomX were localized using active fluorescent fusion proteins expressed as the only copy. First, the stability of the used fusions was investigated by immunoblot analysis on whole cell lysates.

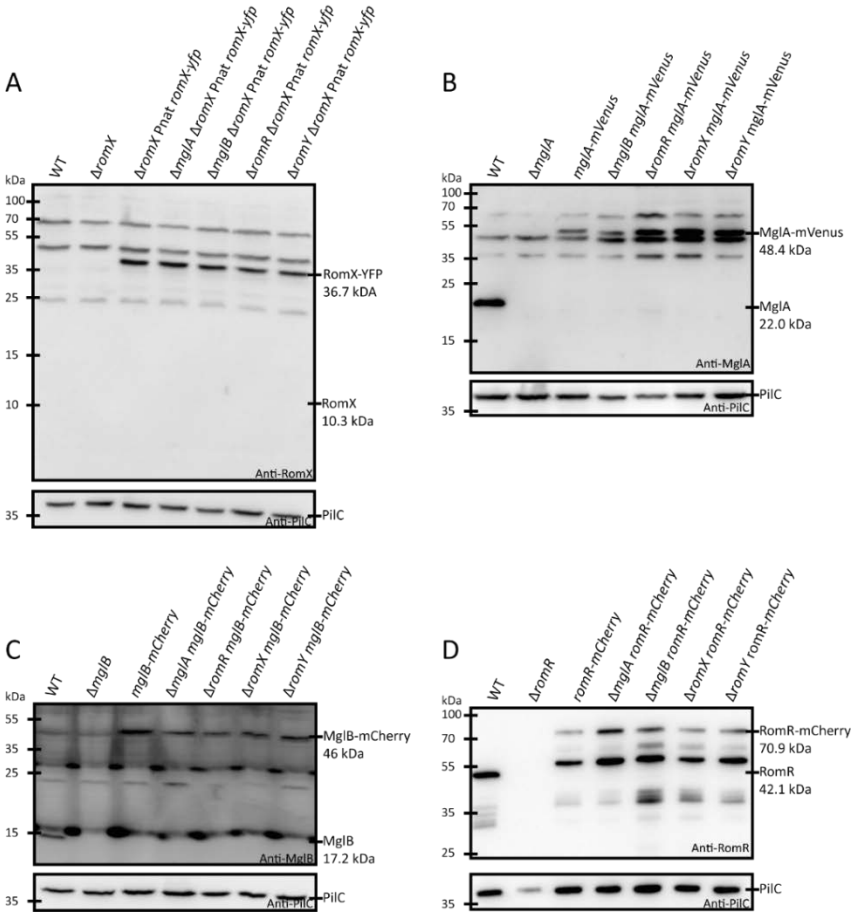

Figure 24. MglA, MglB, RomR and RomX fluorescent fusions are stable.

(A) Immunoblot of RomX-YFP. Cells were grown in liquid culture, harvested, and total protein (1 mg per lane) was separated by SDS–PAGE and analyzed by immunoblot using α-RomX. Calculated molecular masses of RomX and RomX-YFP are indicated. Immunoblot with α-PilC serves as loading control.

(B) Immunoblot of MglA-mVenus. Cells were grown and protein separation as in A. SDS-PAGE analyzed by immunoblot using α-MglA. MglA and MglA-mVenus with calculated molecular masses are indicated. Immunoblot with α-PilC serves as loading control.

(C) Immunoblot of MglB-mCherry. Cells were grown and protein separation as in A. SDS-PAGE analyzed by immunoblot using α-MglB. MglB and MglB-mCherry with calculated molecular masses are indicated. Immunoblot with α-PilC serves as loading control.

(D) Immunoblot of RomR-mCherry. Cells were grown and protein separation as in A. SDS-PAGE analyzed by immunoblot using α-RomR. RomR and RomR-mCherry with calculated molecular masses are indicated. Immunoblot with α-PilC serves as loading control.

We tested whether RomX-YFP is stable in Δ*romX* mutant and in double deletion mutants with Δ*mglA*, Δ*mglB*, Δ*romR* or Δ*romY*. Native RomX protein was not detectable

in the WT strain. RomX-YFP was detected in all investigated mutants. No degradation products were observed in the immunoblot analysis (Figure 24, A). Next, accumulation of the endogenous MglA-mVenus fusion was studied. This fusion accumulated at native level and was stable in all investigated strains (Figure 24, B). Endogenous MglB-mCherry fusion also accumulated at native level and it was stable in the all tested strains (Figure 24, C). Finally, accumulation of the endogenous RomR-mCherry fusion was tested. This fusion also accumulated in all investigated strains. However, its level of accumulation was lower than native RomR in the wild type as well as in the Δ*romX* and Δ*romY* mutants (Figure 24, D).

As mentioned, the RomX-YFP fusion complemented the motility defects of the Δ*romX* mutant (Figure 21, A). MglB-mCherry was previously reported to be fully functional (Keilberg *et al.*, 2012). Strain that expressed *mglA-mVenus* as the only copy of *mglA* showed a minor defect in both T4P-dependent and gliding motility (Figure 25, A). RomR-mCherry was fully functional (Figure 25, B).

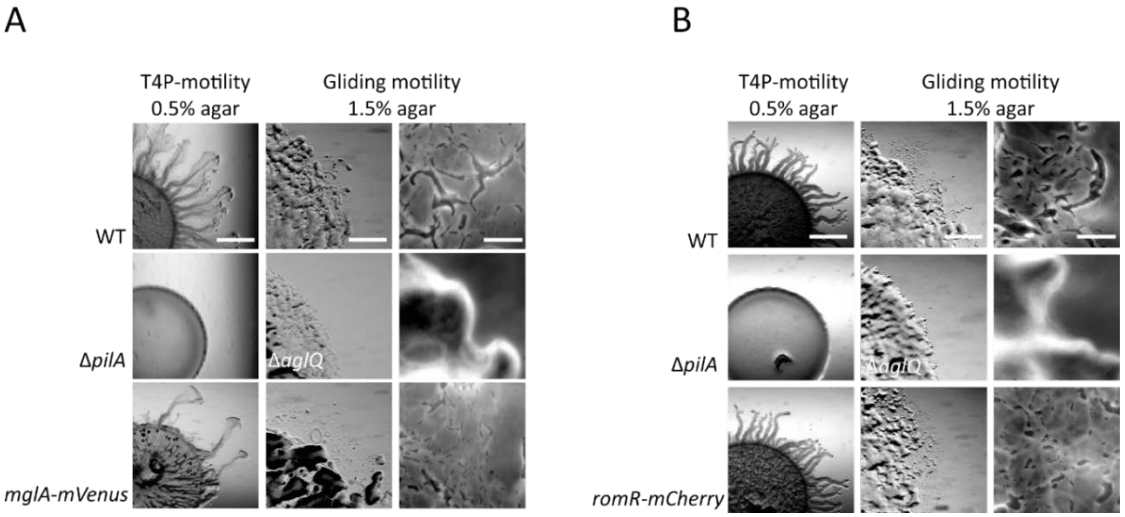

Figure 25. MglA-mVenus and RomR-mCherry are functional fluorescent fusions.
(A) Motility assays of *mglA-mVenus.* Motility assay performed as in Figure 21, A. Scale bars, 1000 μm (T4P-dependent motility), 500 μm (gliding motility – left panel) and 50 μm (gliding motility – right panel).
(B) Motility assay of *romR-mCherry.* Motility assays performed as in Figure 21, A. Scale bars, 1000 μm (T4P-dependent motility), 500 μm (gliding motility – left panel) and 50 μm (gliding motility – right panel).

Using fluorescence microscopy, we found that RomX-YFP predominantly localized in an asymmetric bipolar pattern with a large cluster at the lagging pole and a small cluster at the leading cell pole. Approx. 50% of the fluorescence signal was collected from the cell body. During reversals, the polar clusters switched polarity (Figure 26, A).

Next, we analyzed the localization of RomX in the absence of MglA, MglB and RomR. In the absence of MglA, RomX localized mainly unipolarly. By contrast, in the absence of MglB, RomX localized more bipolar symmetric than in WT. When examining RomX localization in the absence of RomR, we found that RomX localized diffusely throughout the cytoplasm (Figure 26, B). Therefore, polar asymmetry of RomX depends on MglA and MglB, while polar localization depends on the RomR.

Next, we analyzed the localization of MglA, MglB or RomR in the absence of each other or RomX. As previously observed, MglA localized mainly in a unipolar pattern (Leonardy *et al.*, 2010, Zhang *et al.*, 2010, Patryn *et al.*, 2010) (Figure 26, C). As previously observed (Zhang *et al.*, 2010, Leonardy *et al.*, 2010), MglA localization pattern shifted towards bipolar symmetric in the absence of MglB. Finally, we confirmed that MglA in the absence of RomR localized diffusely throughout the cytoplasm (Keilberg *et al.*, 2012, Zhang *et al.*, 2012). Importantly, MglA also localized mainly diffusely throughout the cytoplasm in the absence of RomX (Figure 26, C). Thus, polar localization of MglA depends on both RomX and RomR. As previously observed (Keilberg *et al.*, 2012, Zhang *et al.*, 2012), MglB localized in bipolar asymmetric pattern. As previously reported (Keilberg *et al.*, 2012, Zhang *et al.*, 2012), MglB localization changed to more bipolar asymmetric with a large fraction of cells with unipolar localization in the absence of MglA. Moreover, MglB was more unipolar in the absence of RomR. In the absence of RomX, MglB also localized mainly unipolar. Thus, polar asymmetry of MglB depends on MglA, RomR and RomX. As previously observed (Leonardy *et al.*, 2007, Keilberg *et al.*, 2012, Zhang *et al.*, 2012), RomR localized in a bipolar asymmetric pattern similarly to MglB. As reported earlier (Keilberg *et al.*, 2012, Zhang *et al.*, 2012), RomR in the absence of MglA localized predominantly in a unipolar pattern. Moreover, we confirmed that RomR localized more symmetric in the absence of MglB (Keilberg *et al.*, 2012, Zhang *et al.*, 2012). In the absence of RomX, localization of RomR changed towards unipolar (Figure 26, C). Therefore, RomR polar asymmetry depends on MglA, MglB and RomX.

Altogether, these data suggest that RomX, similarly to RomR, is important for polar localization of MglA-GTP. Because RomR is important for polar localization of RomX but not *vice versa*, these observations strongly suggest that RomR is a polar targeting determinant of RomX, which in turn helps to bring about polar localization of MglA-GTP. Moreover, polar asymmetry of MglB and RomR depends on RomX. We speculate that these latter effects are indirect and caused by the lack of polar localization of MglA-

GTP in the absence of RomX because MglB and RomR are also shifted towards unipolar localization in the absence of MglA (Keilberg *et al.*, 2012, Zhang *et al.*, 2012).

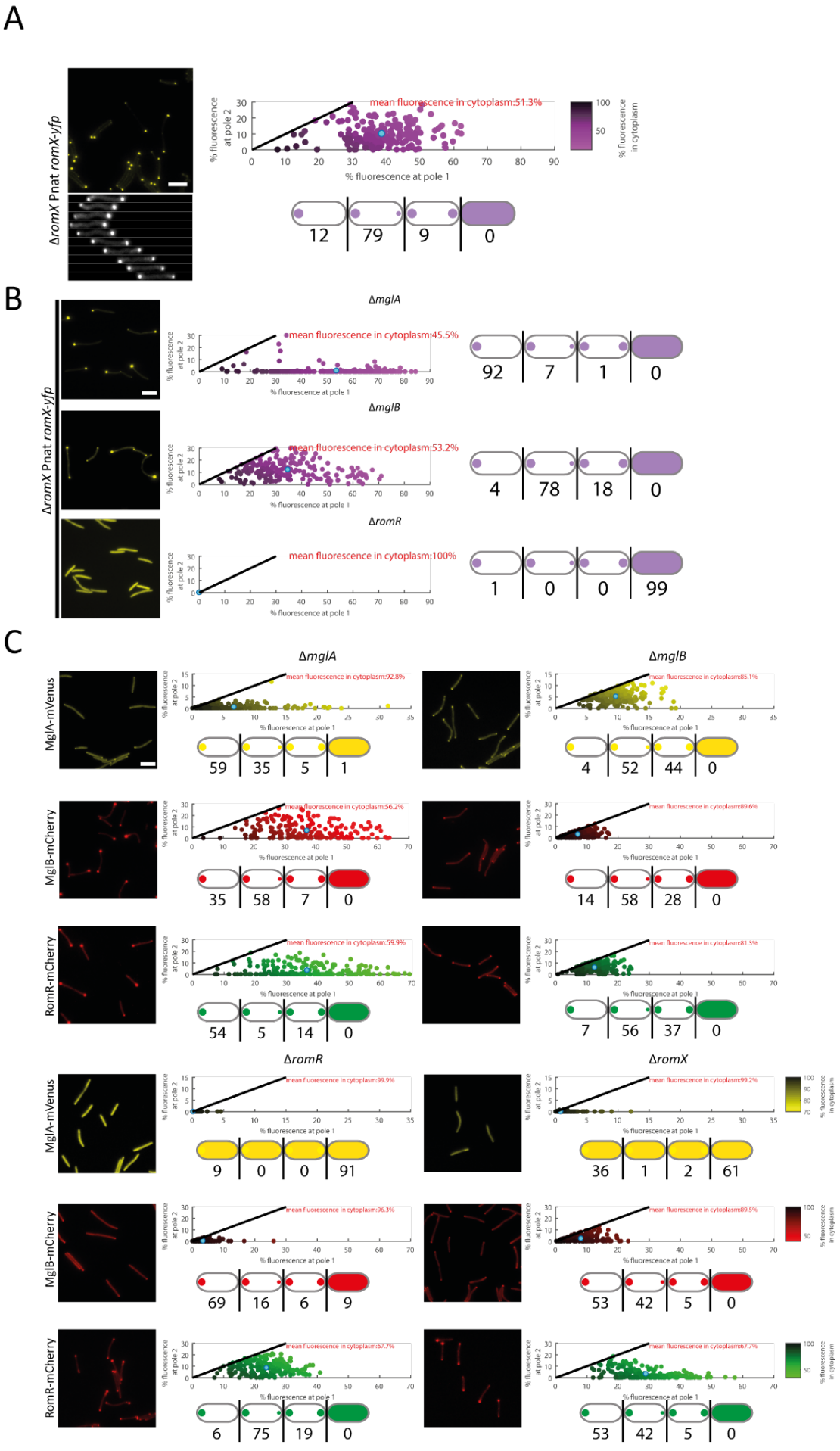
A
ΔromX Pnat romX-yfp
mean fluorescence in cytoplasm:51.3%
% fluorescence at pole 2
% fluorescence at pole 1
% fluorescence in cytoplasm
12 79 9 0
B
ΔromX Pnat romX-yfp
ΔmglA
mean fluorescence in cytoplasm:45.5%
92 7 1 0
ΔmglB
mean fluorescence in cytoplasm:53.2%
4 78 18 0
ΔromR
mean fluorescence in cytoplasm:100%
1 0 0 99
C
ΔmglA
ΔmglB
MglA-mVenus
mean fluorescence in cytoplasm:92.8%
59 35 5 1
mean fluorescence in cytoplasm:85.1%
4 52 44 0
MglB-mCherry
mean fluorescence in cytoplasm:56.2%
35 58 7 0
mean fluorescence in cytoplasm:89.6%
14 58 28 0
RomR-mCherry
mean fluorescence in cytoplasm:59.9%
54 5 14 0
mean fluorescence in cytoplasm:81.3%
7 56 37 0
ΔromR
ΔromX
MglA-mVenus
mean fluorescence in cytoplasm:99.9%
9 0 0 91
mean fluorescence in cytoplasm:99.2%
36 1 2 61
MglB-mCherry
mean fluorescence in cytoplasm:96.3%
69 16 6 9
mean fluorescence in cytoplasm:89.5%
53 42 5 0
RomR-mCherry
mean fluorescence in cytoplasm:67.7%
6 75 19 0
mean fluorescence in cytoplasm:67.7%
53 42 5 0

Figure 26. RomX localizes in bipolar asymmetric pattern.
(A) Localization of RomX-YFP. Upper left panel shows snapshot, lower left panel shows time-lapse fluorescence microscopy at 30 s intervals. Cells were transferred from liquid culture to a thin agar pad on a microscope slide and imaged by fluorescence microscopy. The fluorescence signal for each pole and cytoplasm was calculated and plotted in the upper right graph. Cyan dot represents the mean. To distinguish between different localization patterns, the ω value that represents asymmetry between the polar clusters was calculated from the equation:

$$\omega = \frac{total\ fluorescence\ at\ pole\ 1 - total\ fluorescence\ at\ pole\ 2}{total\ fluorescence\ at\ pole\ 1 + total\ fluorescence\ at\ pole\ 2}$$

By definition, pole 1 is the pole with the highest fluorescence. The ω value is between 0 (bipolar symmetric localization) and 1 (unipolar localization). The localization patterns are binned from the ω values as follows: unipolar (ω > 0.9), bipolar asymmetric (0.9 > ω > 0.2) and bipolar symmetric (ω<0.2). Diffuse localization was determined when no polar signal was detected. The localization patterns observed are indicated in the schematics. n>200. Scale bar: 5 µm.
(B) Localization of RomX-YFP in indicated strains. Left panels show fluorescent microscopy image. Cells were treated as in A. Percent of fluorescence signal for each pole and cytoplasm were calculated and plotted in the left graph. Cyan dot represents the mean. The localization patterns observed are indicated in the schematics. n>200. Scale bar: 5 µm.
(C) Localization of MglA-mVenus, MglB-mCherry and RomR-mCherry in indicated strains. Cells were treated as in A. Left panel shows fluorescent microscopy image. Percent of fluorescence signal for each pole and cytoplasm were calculated and plotted on the upper graph. Cyan dot represents the mean. The localization patterns observed are indicated in the schematics. n>200. Scale bar: 5 µm.

2.2.4 RomX is polar targeting determinant of MglA

Lack of RomX or RomR causes diffuse localization of MglA. Similarly, an inactive, GDP-locked form of MglA localizes diffusely (Leonardy *et al.*, 2010). Additionally, RomX displays diffuse localization in the absence of RomR. So, RomX and RomR act together to stimulate polar localization of MglA-GTP. We thought of four models to explain how RomX and RomR could bring about polar localization of MglA-GTP: (1) RomX together with RomR or alone acts as an MglA GEF; (2) RomX together with RomR or alone inhibits MglB GAP activity; (3) RomX is an MglA-GTP polar targeting determinant and is sandwiched between RomR and MglA-GTP; (4) combinations of these activities.

To explore these possibilities, we determined localization of MglA^{Q82A}-mVenus, which is locked in the GTP-bound, in the presence and absence of RomX or RomR. First, motility assays with *mglA*^{Q82A} and *mglA*^{Q82A}*-mVenus* mutants showed no differences between the two strains (Figure 27, A). Moreover, MglA^{Q82A}-mVenus accumulated in all investigated mutants at similar level as the native fusion protein in WT (Figure 27, B).

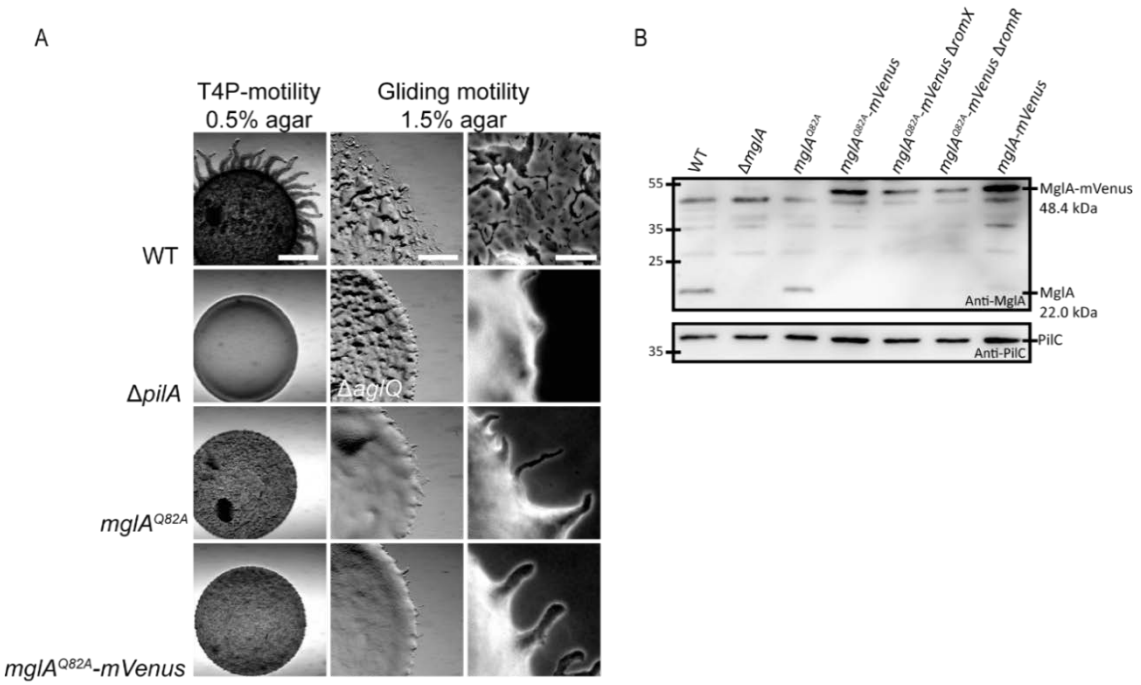

Figure 27. MglA^{Q82A}-mVenus is a functional fluorescent fusion protein.
(A) Motility assay of *mglA^{Q82A}-mVenus.* Motility assay performed as in Figure 21, A. Scale bars, 1000 μm (T4P-dependent motility), 500 μm (gliding motility – left panel) and 50 μm (gliding motility – right panel). **(B)** Immunoblot of MglA^{Q82A}-mVenus. Cells were grown in liquid culture, harvested, and total protein (1 mg per lane) was separated by SDS–PAGE and analyzed by immunoblot using α-MglA. MglA and MglA-mVenus with calculated molecular masses are indicated. Immunoblot with α-PilC serves as loading control.

As previously reported (Miertzschke *et al.*, 2011, Keilberg *et al.*, 2012, Treuner-Lange *et al.*, 2015), MglA^{Q82A} localized in a bipolar symmetric pattern with a cluster that "oscillates" between the cell poles (Figure 28, A). The "oscillating" cluster is a large complex of the Agl/Glt motility machinery. Because this machinery contains the GTP-locked MglA^{Q82A} variant and, therefore, is insensitive to MglB at the lagging cell pole, cells move one cell length before reversing leaving the impression of an oscillating cluster (Miertzschke *et al.*, 2011, Keilberg *et al.*, 2012, Treuner-Lange *et al.*, 2015). By contrast, MglA^{Q82A}-mVenus in the absence of RomR or RomX mostly localized to the "oscillating" cluster and the cytoplasm (Figure 28, A). Quantitative localization analysis revealed that difference in the cytoplasmic signal was statistically significant (t-test $p<0.001$) (Figure 28, B). These localization patterns suggest that one of the functions of RomX is to act as a polar targeting determinant for MglA-GTP, i.e. RomR recruits RomX to a pole and RomX recruits MglA-GTP.

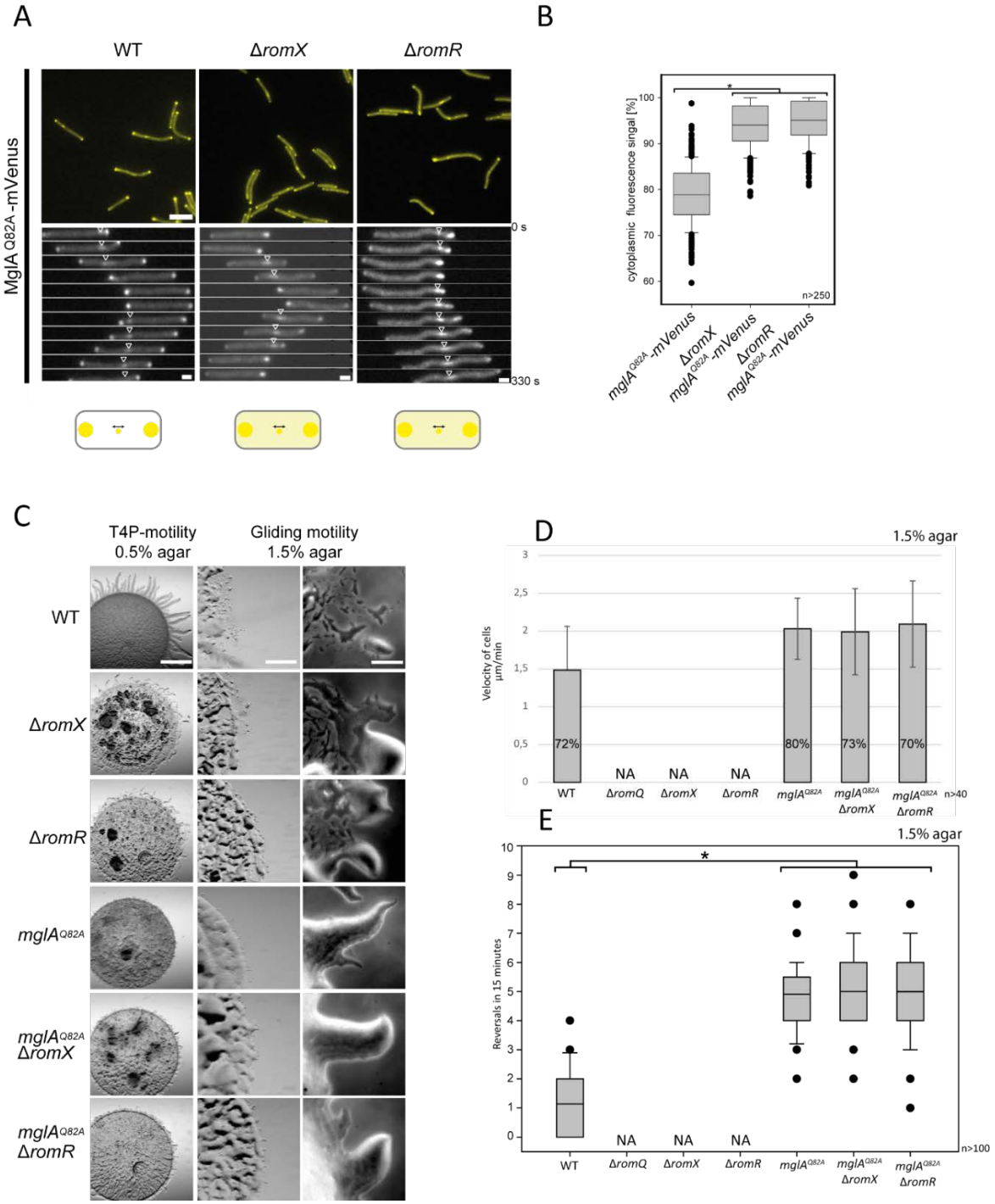

Figure 28. Polar recruitment of MglA-GTP depends on RomX and RomR.

(A) Snapshots and time-laps microscopy of MglA^{Q82A}-mVenus in indicated strains. Cells were treated as in Figure **26** and imaged by time-laps fluorescence microscopy at 30s intervals. Scale bar: 5 µm for snapshots and 1 µm for time-lapses.

(B) Analysis of the cytoplasmic fluorescence of MglA^{Q82A}-mVenus in indicated strains. Shown are boxplots of the measured integrated cytoplasmic fluorescence, boxes enclose the 25th and 75th percentile, whiskers represent the 10th and 90th percentile, and dots outliers. Student's t-test was employed for statistical analysis and * indicates p< 0.001. n>250.

(C) *mglA^{A82A}* is epistatic to *romX* and *romR*. Motility assays as described in Figure 21 comparing single mutant *mglA^{Q82A}*, Δ*romX* and Δ*romR* to double *mglA^{Q82A}*Δ*romX* and *mglA^{Q82A}*Δ*romX* mutants. Bars, 1000 µm (T4P-dependent motility), 500 µm (gliding motility – left panel) and 50 µm (gliding motility – right panel).

(D) Velocity of WT and selected mutants on 1.5% agar, 0.5% CTT. Single moving cells were tracked for 15 min. Graph presents velocity of the cells in µm/min ± standard deviation. Student's t-test was employed for statistical analysis and * indicates $p < 0.001$. $n>20$ for each of two independent experiment. Number in each column represents percent of moving single cells. $n>450$ for each of two independent experiment. NA – not applicable; Δ*aglQ*, Δ*romX*, Δ*romR* were not moving as single cells in the tested conditions.
(E) Reversal frequency of WT and selected mutants on 1.5% agar, 0.5% CTT. Shown are boxplots of the measured reversals of isolated cells for 15 min, boxes enclose the 25th and 75th percentile, whiskers represent the 10th and 90th percentile, and dots outliers. Student's t-test was employed for statistical analysis and * indicates $p < 0.001$. $n>50$. NA – not applicable; Δ*aglQ*, Δ*romX*, Δ*romR* mutants were not moving as single cells in the tested conditions.

Additionally, we tested whether MglA locked in the GTP bound form can bypass the motility defects caused by lack of RomR or RomX. In agreement with previous observations (Miertzschke *et al.*, 2011), the *mglA*^{Q82A} mutant hyper-reversed and formed short flares on 0.5% agar and displayed no single cell at the colony edge after 24 hours on 1.5% agar (Figure 28, C). As previously reported (Keilberg *et al.*, 2012), the double *mglA*^{Q82A}Δ*romR* mutant showed motility phenotype similar to *mglA*^{Q82A} mutant. Furthermore, the double *mglA*^{Q82A}Δ*romX* mutant also had the phenotype of the *mglA*^{Q82A} mutant (Figure 28, C). Next, analysis of single cells moving by gliding motility was performed. WT moved with a velocity of 1.46 µm/min and 70% of single cells were moving. As previously observed, Δ*aglQ*, Δ*romX* and Δ*romR* mutants did not move as a single cell on 1.5% agar. The *mglA*^{Q82A} mutant moved faster than WT with an average velocity of 2.09 µm/min and 84% of single cells were moving. Furthermore, the *mglA*^{Q82A}Δ*romX* and *mglA*^{Q82A}Δ*romR* mutants moved on 1.5% agar with higher velocity than WT (Figure 28, D). Moreover, the percent of moving cells in the case of *mglA*^{Q82A}Δ*romX* and *mglA*^{Q82A}Δ*romR* mutants was comparable to WT and the *mglA*^{Q82A} mutant (Figure 28, D). The *mglA*^{Q82A} mutant hyper-reversed with on average 4.8 reversals per 15 minutes (Figure 28, E). Furthermore, the *mglA*^{Q82A}Δ*romX* and *mglA*^{Q82A}Δ*romR* mutants showed a similar hyper-reversing phenotype (Figure 28, E). Thus, RomX and RomR are not required for gliding motility when MglA is locked in the GTP-bound form. Additionally, the *mglA*^{Q82A} mutation is epistatic to the Δ*romX* and Δ*romR* mutations. Altogether these observations suggest that MglA-GTP acts downstream of RomX and RomR.

2.2.5 Formation of focal adhesion depends on RomX and RomR in the presence of MglB

MglA-GTP is an integral part of the gliding motility machinery and localizes to the focal adhesion complexes (Treuner-Lange *et al.*, 2015). To further investigate hypothesis

that RomX and RomR influence nucleotide state of MglA, we focused on the localization of MglA in focal adhesion complexes. To visualize MglA in the focal adhesion complexes we used TIRF microscopy to only visualize fluorescent fusions proteins that are localize close to the cell-substratum contact surface.

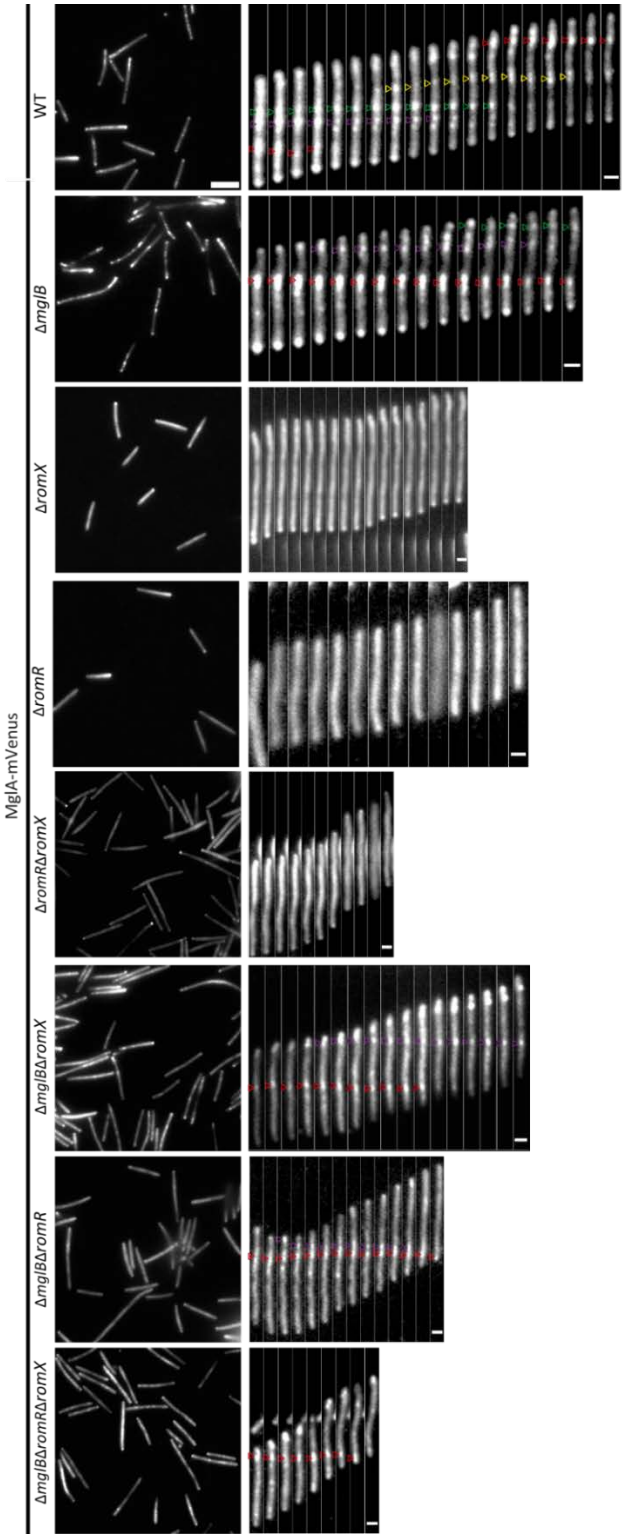

Figure 29. MglA localization to focal adhesion complexes depends on RomX and RomR.
TIRF microscopy of MglA-mVenus in indicated strains. First column presents pictures done in in TIRF microscopy, second shows TIRF time-lapse microscopy at 20 s intervals. Scale bar for snapshots: 5µm; for time lapses montages: 1 µm.

MglA-mVenus showed localization in the focal adhesion complexes. When cells were moving, these clusters stayed stationary with respect to the substratum. Additionally, MglA-mVenus clusters assembled at the leading cell pole and disassembled near the lagging cell pole (Figure 29). In the Δ*mglB* mutant, MglA-mVenus in the focal adhesion complexes was also visible. By contrast, in the Δ*romX*, Δ*romR* and double Δ*romX*Δ*romR* mutants, MglA-mVenus did not localize to the focal adhesion complexes (Figure 29). Importantly, MglA-mVenus localized to focal adhesion complexes in Δ*mglB*Δ*romX*, Δ*mglB*Δ*romX* and triple deletion Δ*mglB*Δ*romR*Δ*romX* mutants (Figure 29). Previously, we showed that MglA locked in the GTP-bound form localizes in a single focal adhesion complex independently of RomX and RomR (Figure 28, A). These observations support the idea that RomX and RomR are necessary for assembly of the focal adhesion complexes only when nucleotide state of MglA is regulated by MglB. Moreover, the data support the idea that RomX together with RomR have the opposite function on MglB, and thus, may act as an MglA GEF or inhibit MglB GAP activity.

To further analyse the formation of focal adhesion complexes in the absence of RomX and/or RomR, we localized AglZ, which is an integral part of the gliding machinery (Mignot *et al.*, 2007). First, AglZ-YFP accumulation in the investigated strains was tested. AglZ-YFP accumulated at similar levels in the absence and presence of MglB, RomX and RomR in single, double and triple deletion mutants (Figure 30).

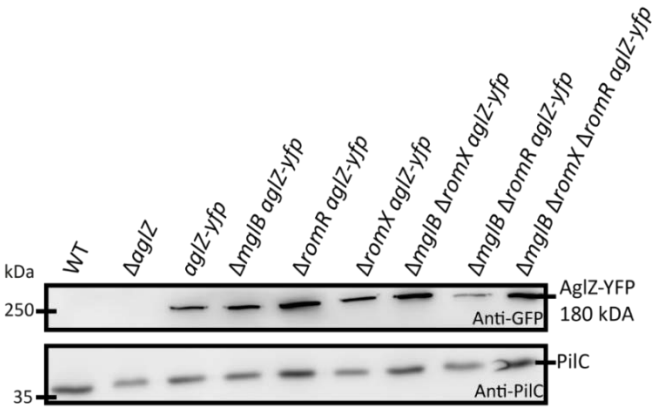

Figure 30. AglZ-YFP is stable in the absence or presence of MglB, RomX and RomR in single, double and triple deletion mutants.

Immunoblot of AglZ-YFP. Cells were grown and protein separation as in Figure 24. SDS-PAGE analyzed by immunoblot using α-GFP. AglZ-YFP with calculated molecular mass is indicated. Immunoblot with α-PilC serves as a loading control.

AglZ localized unipolarly with clusters distributed along the cell length. Additionally, when cells were moving these clusters stayed stationary with respect to the substratum. Moreover, clusters were assembled at the leading cell pole. In the absence of

MglB, we observed more AglZ-YFP clusters. Additionally, these clusters stayed stationary with respect to the substratum and were assembled at the leading cell pole. By contrast, and as observed for MglA, we did not observe AglZ-YFP clusters along the cell body in the absence of RomX or RomR. Importantly, in the Δ*mglB*Δ*romX*, Δ*mglB*Δ*romR* and Δ*romX*Δ*romR*Δ*mglB* mutants, AglZ-YFP was observed in the focal adhesion complexes when visualized by TIRF microscopy. Detailed comparisons indicated that although superficially similar, the focal adhesion complexes in these three mutants displayed three notable differences to those formed in WT. First, they "slipped" the contact to the substratum and moved within a cell, i.e. they were not stationary with respect to the substratum. Second, they moved in opposite directions within a cell. Third, they disassembled away from the lagging cell pole (Figure 31). To tally these differences, we quantified the movement of Agl/Glt complexes within cells and the lifetime of individual Agl/Glt complexes. As shown in Figure 32, in the Δ*mglB* Δ*romX*, Δ*mglB* Δ*romR* and Δ*romX*Δ*romR*Δ*mglB* mutants, the Agl/Glt complexes moved a significantly longer distance per min within cells and had significantly shorter lifetimes than in WT and Δ*mglB* cells. Altogether, these findings are consistent with the observation that the Δ*mglB* mutation only partially suppresses the gliding defects in the Δ*romX* and Δ*romR* mutants, and the Δ*mglB*Δ*romX* and Δ*mglB*Δ*romR* cells move with a significantly lower speed than WT and Δ*mglB* cells (Figure 23, B). We conclude that RomX and RomR are not only important for formation of focal adhesion complexes but also for their correct adhesion and stability. Furthermore, the data suggest that RomX and RomR also play a role in setting the directionality or polarity of the focal adhesion complexes. We speculate, that we did not observe lack of polarization and stability of the focal adhesion complexes in the Δ*mglB*Δ*romX*, Δ*mglB*Δ*romR* and Δ*mglB*Δ*romX*Δ*romR* mutants for MglA-mVenus, because this fusion protein is only partially functional.

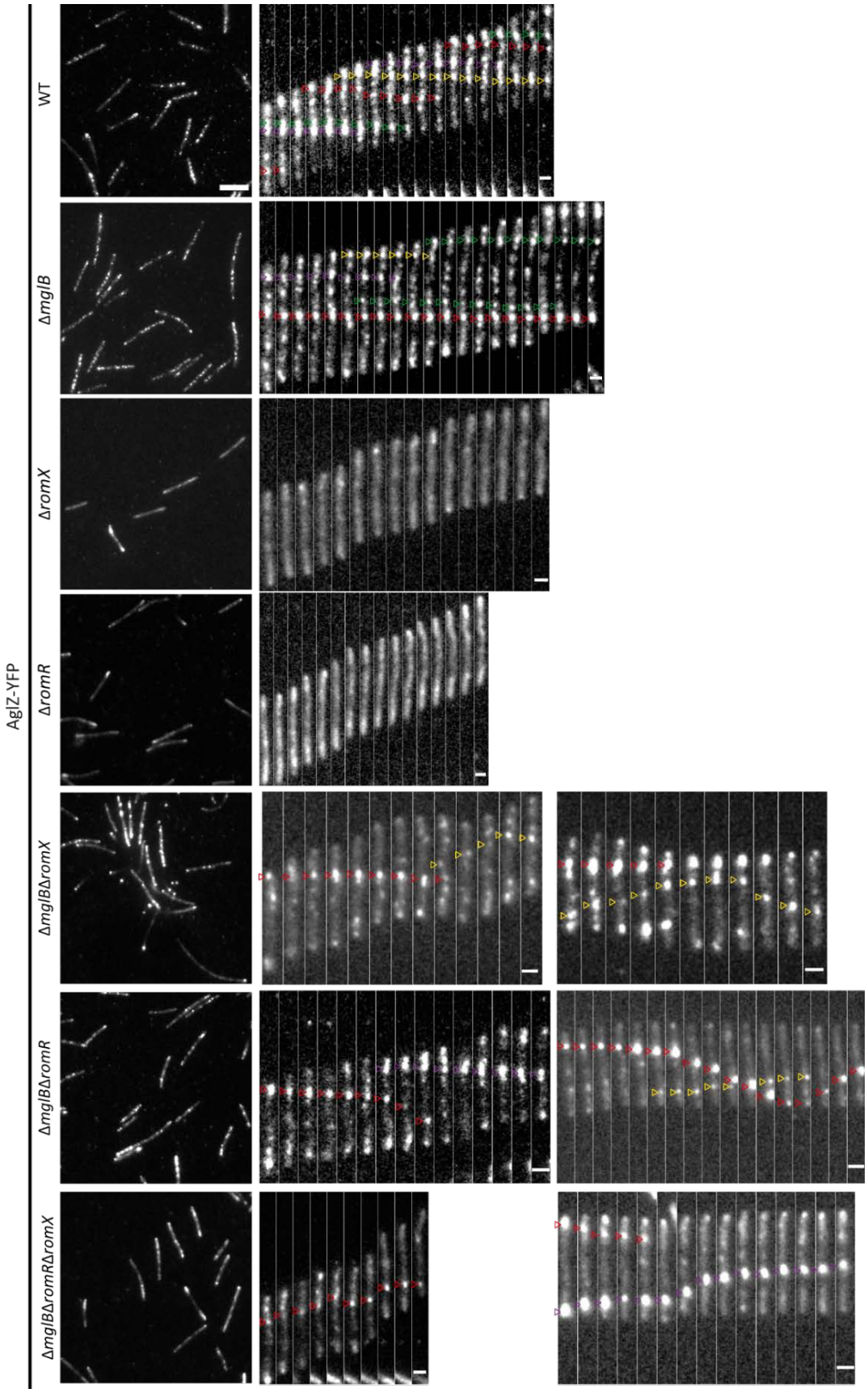

Figure 31. AglZ localization to focal adhesion complexes depends on RomX and RomR.
TIRF microscopy of AglZ-YFP in indicated strains. First column presents pictures done in in TIRF microscopy, second (and third for selected strains) shows TIRF time-lapse microscopy at 20 s intervals. Scale bar for snapshots: 5µm; for time lapses montages: 1 µm.

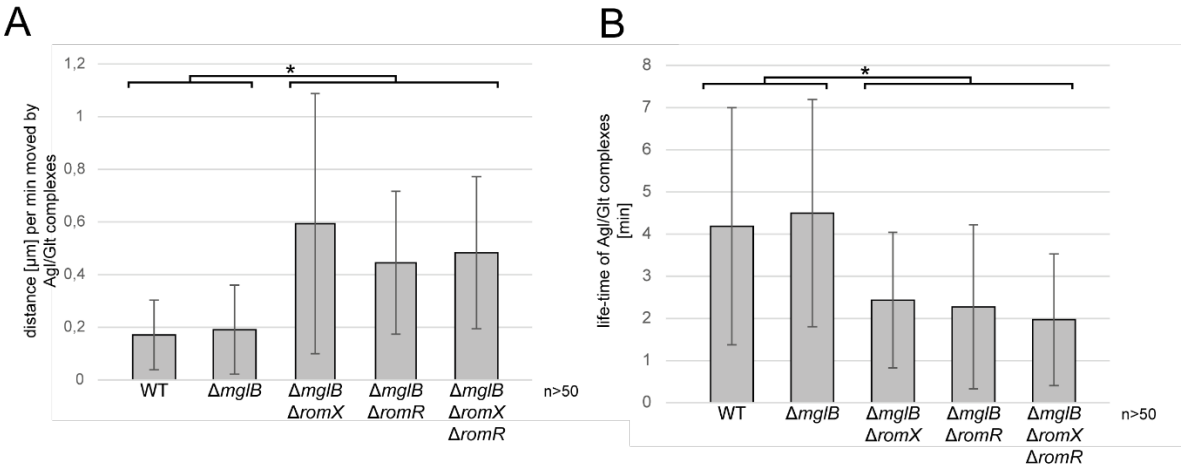

Figure 32. RomX and RomR are important for adhesion and stability of the focal adhesion complexes.

(A) Distance moved per minute by Agl/Glt complexes within cells (AglZ-YFP was used as a marker for the focal adhesion complexes) in WT and selected mutants. Graph shows distance moved by focal adhesion complexes per min within cells ± standard deviation. Student's t-test was employed for statistical analysis and * indicates $p < 0.001$. $n > 50$. In this experiment, cells were observed on chitosan coated glass by TIRF microscopy. Time-lapse recordings were done with 20s time resolution. For the analysis, kymographs of single cells were prepared. In the kymographs, high intensity tracks were semi-automatically followed.

(B) Lifetime of Agl/Glt complexes in WT and selected mutants. Graph presents lifetime of the focal adhesion complexes in min ± standard deviation. Student's t-test was employed for statistical analysis and * indicates $p < 0.001$. $n > 50$. Experiment and analysis as in A.

2.2.6 Focal adhesion immobility depends on RomX and RomR

The focal adhesion complexes formed in the absence of MglB as well as RomR and/or RomX are more mobile within cells. To further investigate this phenomenon, we localized $MglA^{Q82A}$-mVenus, which is locked in the GTP-bound form, using TIRF microscopy in the presence and absence of RomX or RomR (Figure 33). We observed multiple clusters of $MglA^{Q82A}$-mVenus along the cell body. $MglA^{Q82A}$-mVenus in the absence of RomX or RomR also localized to focal adhesion complexes along the cell body. Some of these clusters remained stationary with respect to the substratum when cells were moving, while other clusters "slipped" the contact to the substratum and moved within a cell, i.e. they were not stationary with respect to the substratum or clusters moved in opposite directions within a cell (Figure 33). We quantified these differences as described above and found that the focal adhesion complexes formed in the absence of RomX or RomR moved a significantly longer distance per min within cells (Figure 34, A) but had the same lifetime as in the presence of RomX and RomR (Figure 34, B). In addition, the focal adhesion complexes formed in the presence of $MglA^{Q82A}$ and RomR as well as RomX had the same mobility within cells as focal adhesion complexes formed in the presence of $MglA^{WT}$ protein (compare Figure 32, A and Figure 34, A). We conclude

that RomX and RomR are important for immobility of the focal adhesion complexes while MglA locked in the GTP-bound form has no effect on the mobility of the focal adhesion complexes. Moreover, RomX and RomR are not important for stability of the focal adhesion complex in strains with MglA locked in the GTP bound form. Finally, our data suggest that RomX and RomR are giving correct directionality to the focal adhesion complexes.

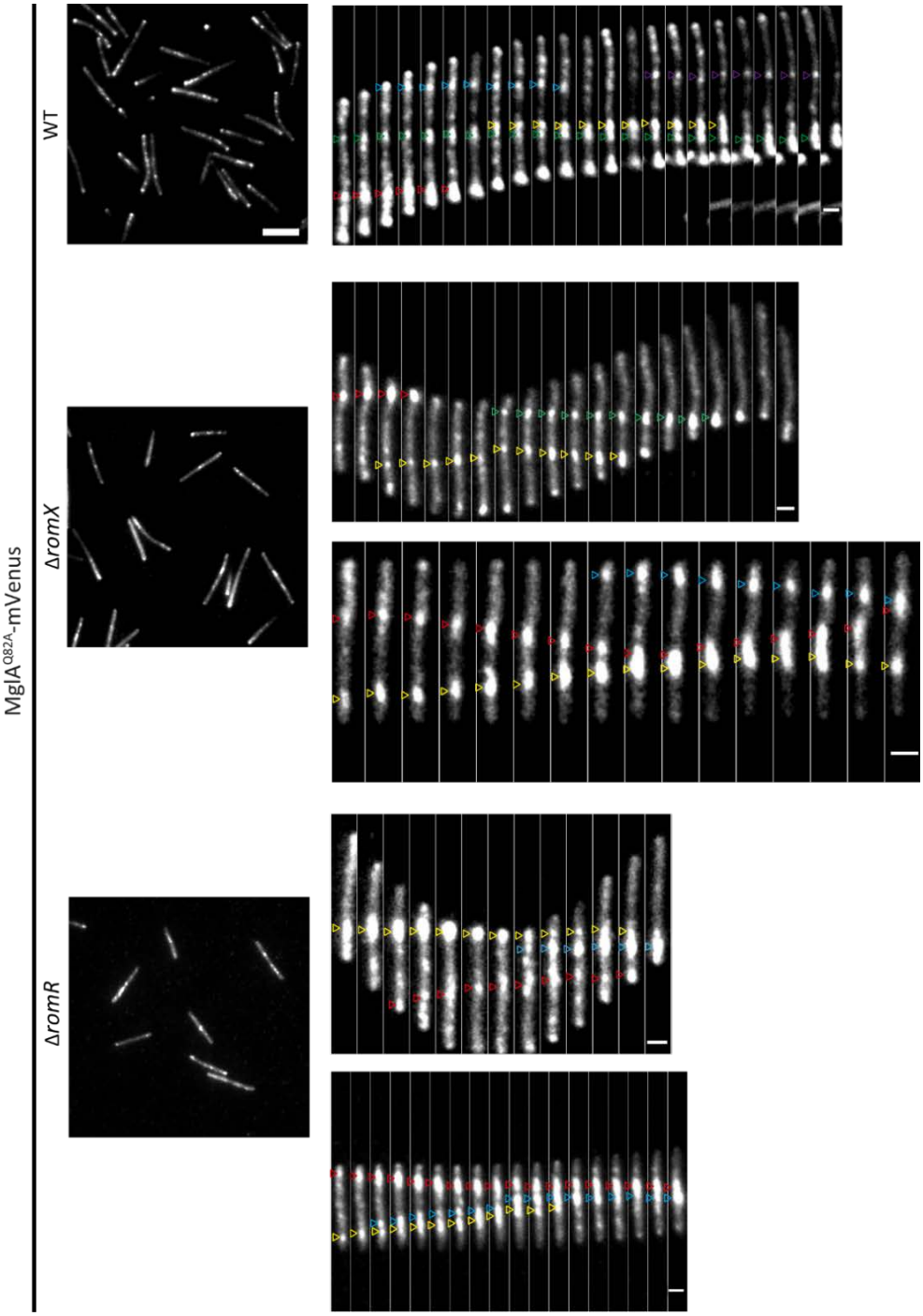

Figure 33. Polarization of the focal adhesion complexes depends on RomX and RomR.
TIRF microscopy of MglA^{Q82A}-mVenus in indicated strains. First column presents pictures done in in TIRF microscopy, second shows TIRF time-lapse microscopy at 20 s intervals. Scale bar for snapshots: 5µm; for time lapses montages: 1 µm.

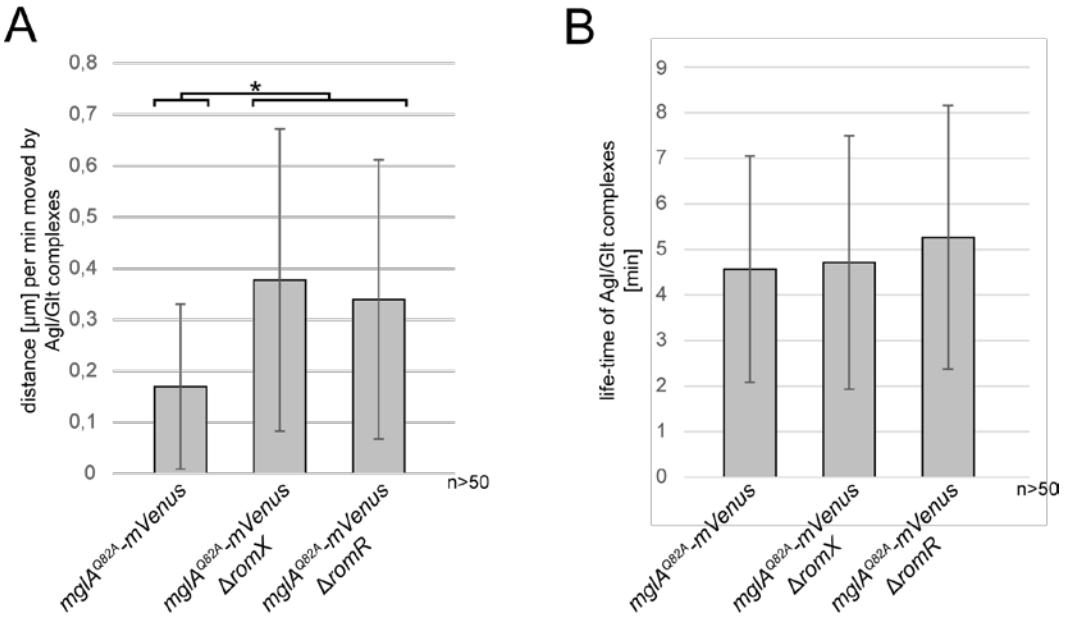

Figure 34. RomX and RomR are important for adhesion of the focal adhesion complexes in strains with MglA locked in the GTP bound form.
(A) Mobility of Agl/Glt complexes ($MglA^{Q82A}$-mVenus was used as a marker for the focal adhesion complexes) in selected strains with MglA locked in the GTP bound form. Graph shows distance moved by focal adhesion complexes per min within cells ± standard deviation. Student's t-test was used for statistical analysis and * indicates $p < 0.001$. n>50.Experiment and analysis were performed as in Figure 32, A.
(B) Lifetime of Agl/Glt complexes in selected mutants. Graph presents lifetime of the focal adhesion complexes in min ± standard deviation. n>50. Experiment and analysis as in Figure 32, A.

2.2.7 RomX and RomR localize to focal adhesion complexes

The data presented so far are consistent with the idea that RomR and RomX in addition to recruiting MglA-GTP to the leading cell pole, may also function to inhibit MglB GAP activity or function as an MglA GEF. Based on quantification of the fluorescence signal of the MglB-mCherry fusion, which is only detected as a full-length protein in immunoblots (Figure 24, C), more than 90% of MglB is localized diffusely in the cytoplasm. To further explore the idea that RomR and/or RomX could inhibit MglB GAP activity or function as an MglA GEF, we hypothesized that RomR and/or RomX would localize to the focal adhesion complexes to replenish MglA-GTP in case of MglB stimulated GTP hydrolysis by MglA. To explore this idea, we colocalized RomX with AglQ, which is a subunit of the Agl motor and localizes to the focal adhesion complexes (Sun *et al.*, 2011).

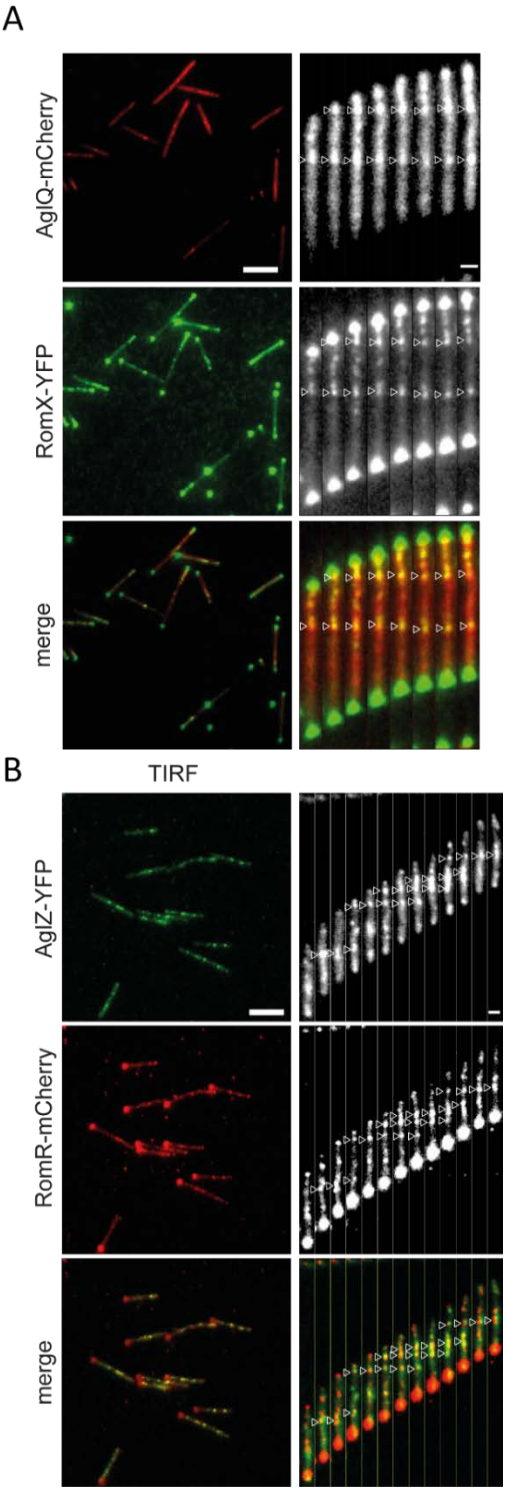

Figure 35. RomX and RomR localize to the focal adhesion complexes.
(A) AglQ colocalizes with RomX. Co-localization of AglQ and RomX observed on chitosan coated glass. First column presents pictures done TIRF microscopy, second shows TIRF time-lapse microscopy at 20 s intervals. Scale bar: 5 µm. for time lapses montages: 1 µm
(B) AglZ colocalizes with RomR. Co-localization of AglZ and RomR observed on chitosan coated glass. First column presents pictures done in TIRF microscopy, second shows TIRF time-lapse microscopy at 20 s intervals. Scale bar for snapshots: 5µm; for time lapses montages: 1 µm.

AglQ-mCherry and RomX-YFP localized to clusters along the cell body when visualized using TIRF microscopy. Moreover, AglQ-mCherry and RomX-YFP colocalized in these clusters. Furthermore, these clusters were assembled at the leading

cell pole and remained stationary with respect to the substratum when in moving cells (Figure 35, A). Similarly, RomR-mCherry colocalized with AglZ-YFP in focal adhesion complexes. We conclude that RomX as well as RomR are incorporated into the focal adhesion complexes.

2.2.8 RomX incorporation into the focal adhesion complexes depends on RomR

As previously observed, RomX-YFP localized in the bipolar asymmetric pattern and in focal adhesion complexes when visualized by TIRF microscopy. As expected, in cells of the Δ*mglA* mutant, RomX-YFP was only unipolarly localized because the focal adhesion complexes do not assemble in the absence of MglA. In the absence of MglB, RomX-YFP was incorporated into the focal adhesion complexes. Next, we asked if the incorporation of RomX into the focal adhesion complexes depends on RomR. As expected, RomX-YFP was also diffusely localized in the absence of RomR (Figure 36). Importantly, we did not observe RomX-YFP in the focal adhesion complexes in the double Δ*mglB*Δ*romR* mutant (Figure 36). The data suggests that RomX requires RomR for incorporation into the focal adhesion complexes.

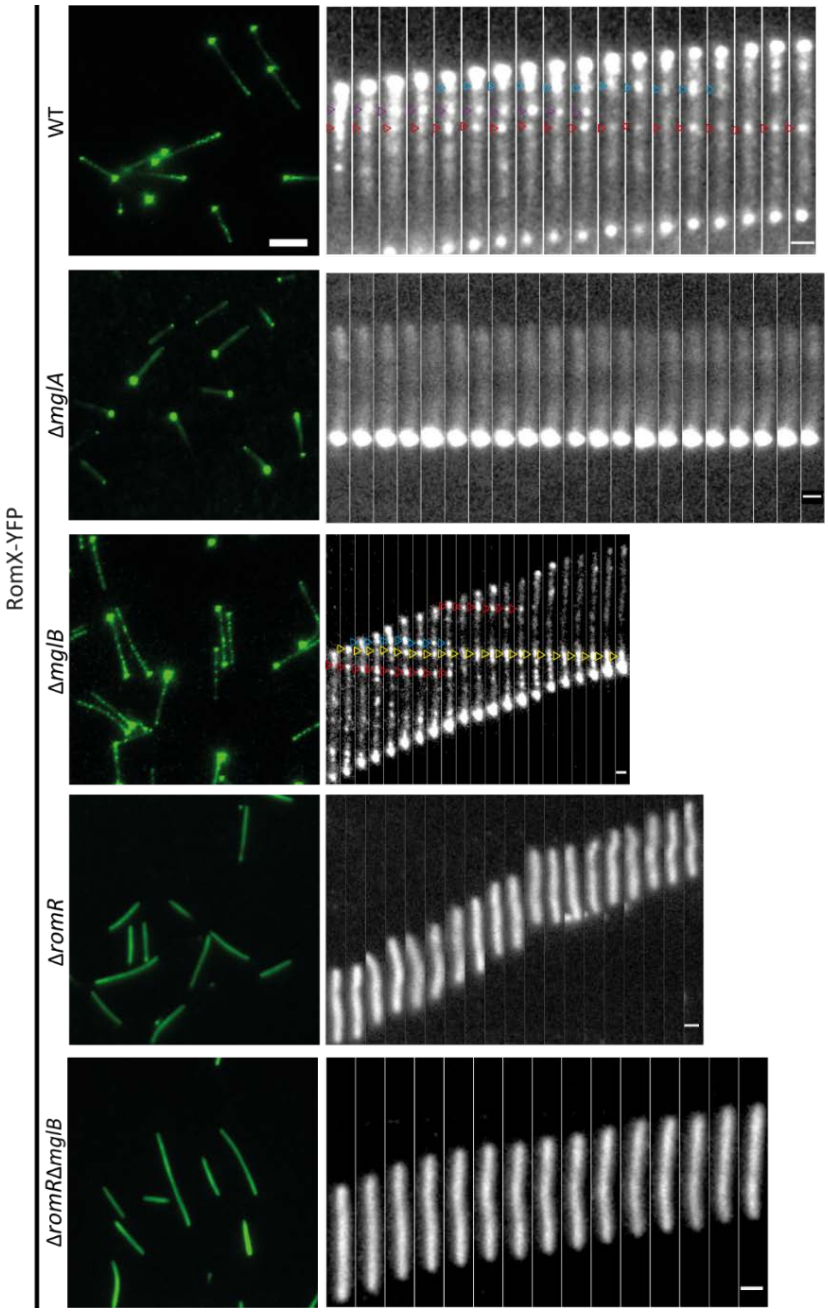

Figure 36. RomX localization to focal adhesion complexes depends on MglA and RomR.
TIRF microscopy of RomX-YFP in indicated strains. First column presents pictures done in in TIRF microscopy, second shows TIRF time-lapse microscopy at 20 s intervals. Scale bar for snapshots: 5 µm; for time lapses montages: 1 µm.

2.2.9 RomR incorporation into focal adhesion complexes is independent of RomX

Subsequently, we asked if the incorporation of RomR into the focal adhesion complexes depends on RomX. As previously observed, RomR-mCherry localized in the bipolar asymmetric pattern as well as in focal adhesion complexes when visualized by TIRF microscopy (Figure 37). As expected, in the Δ*mglA* mutant, RomR-mCherry did

not localize to the focal adhesion complexes while it still localized to focal adhesion complexes in the Δ*mglB* mutant. Moreover, and as expected, RomR was not incorporated into focal adhesion complex in the absence of RomX (Figure 37). Importantly, RomR localized to focal adhesion complexes in the double deletion Δ*mglB*Δ*romX* mutant (Figure 37). The data suggests that RomR does not depend on RomX for incorporation into the focal adhesion complexes.

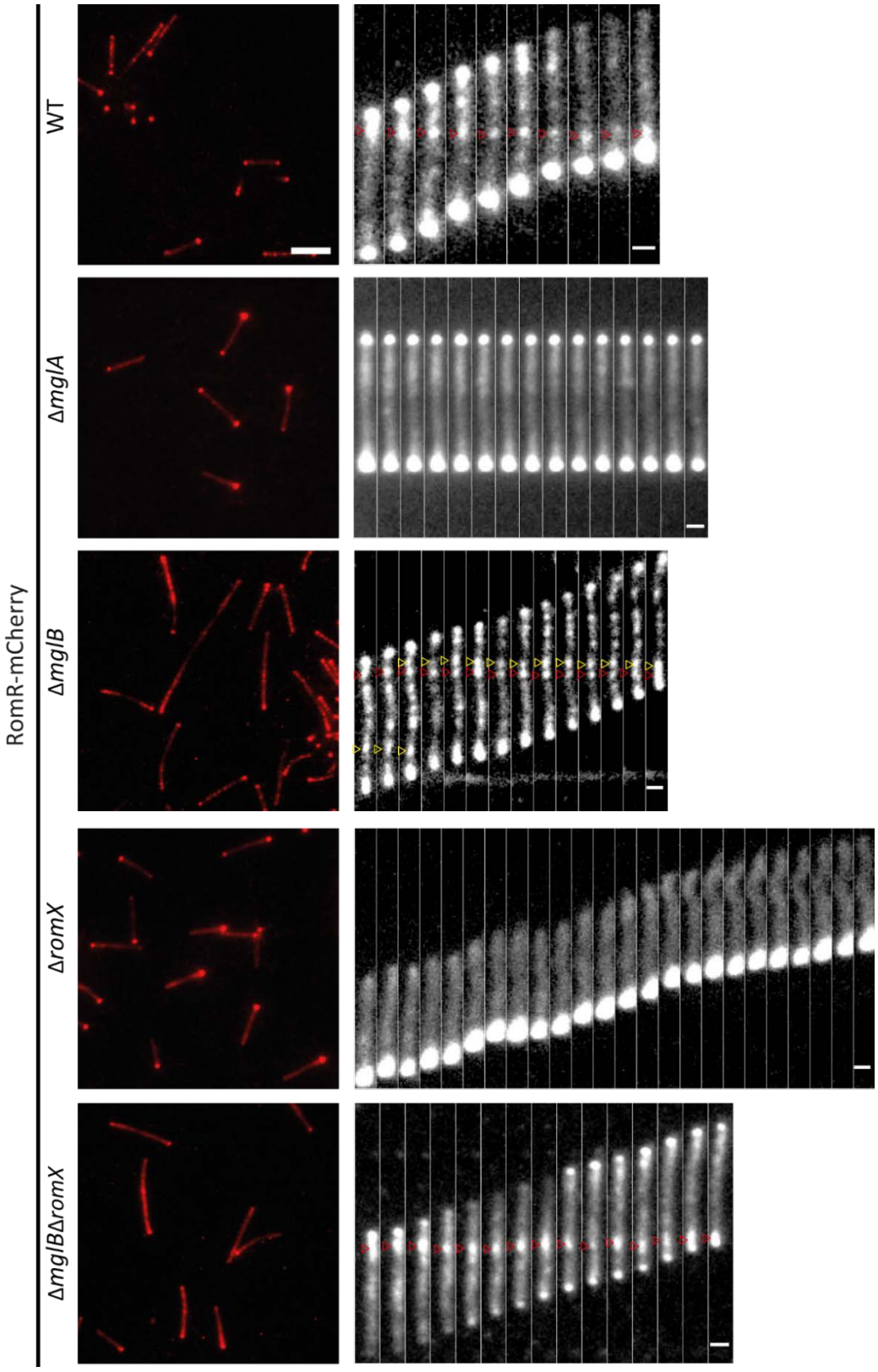

Figure 37. RomR localization to focal adhesion complexes depends on MglA and RomX.
TIRF microscopy of RomR-mCherry in indicated strains. First column presents pictures done in in TIRF microscopy, second shows TIRF time-lapse microscopy at 20 s intervals. Scale bar for snapshots: 5 µm; for time lapses montages: 1 µm.

2.2.10 RomX interacts with MglA and RomR in the bacterial two hybrid system

To finally test whether RomX interacts directly with MglA, MglB, and/or RomR, we first used the bacterial two hybrid system (Figure 38). To this end, full length MglA, MglB and RomX as well as the three domains of RomR (Receiver, linker and C-terminal part (see Figure 15) were fused to the T18 and T25 fragments of the *Bordetella pertussis* adenylate cyclase. As a positive control, we used the plasmids pUT18C-zip and pKT25-zip, which express T18 and T25 fragments fused to leucine zippers that provide strong interactions. As a negative control, we used cells co-transformed with one plasmid expressing T18-zip or T25-zip and the other plasmid expressing the bait fused to T25 or T18, respectively.

We confirmed known interactions: MglA–MglB, MglB–RomR as well as self-interaction of MglB (Miertzschke *et al.*, 2011, Keilberg *et al.*, 2012). Moreover, RomR-REC, RomR-Linker and RomR-C were observed to interact. Importantly, RomX was found to self-interact and to interact with MglA and the RomR receiver domain (Figure 38, A). These results are in agreement with the localization data and the hypothesis that RomX acts between RomR and MglA in the regulation of polarity and motility.

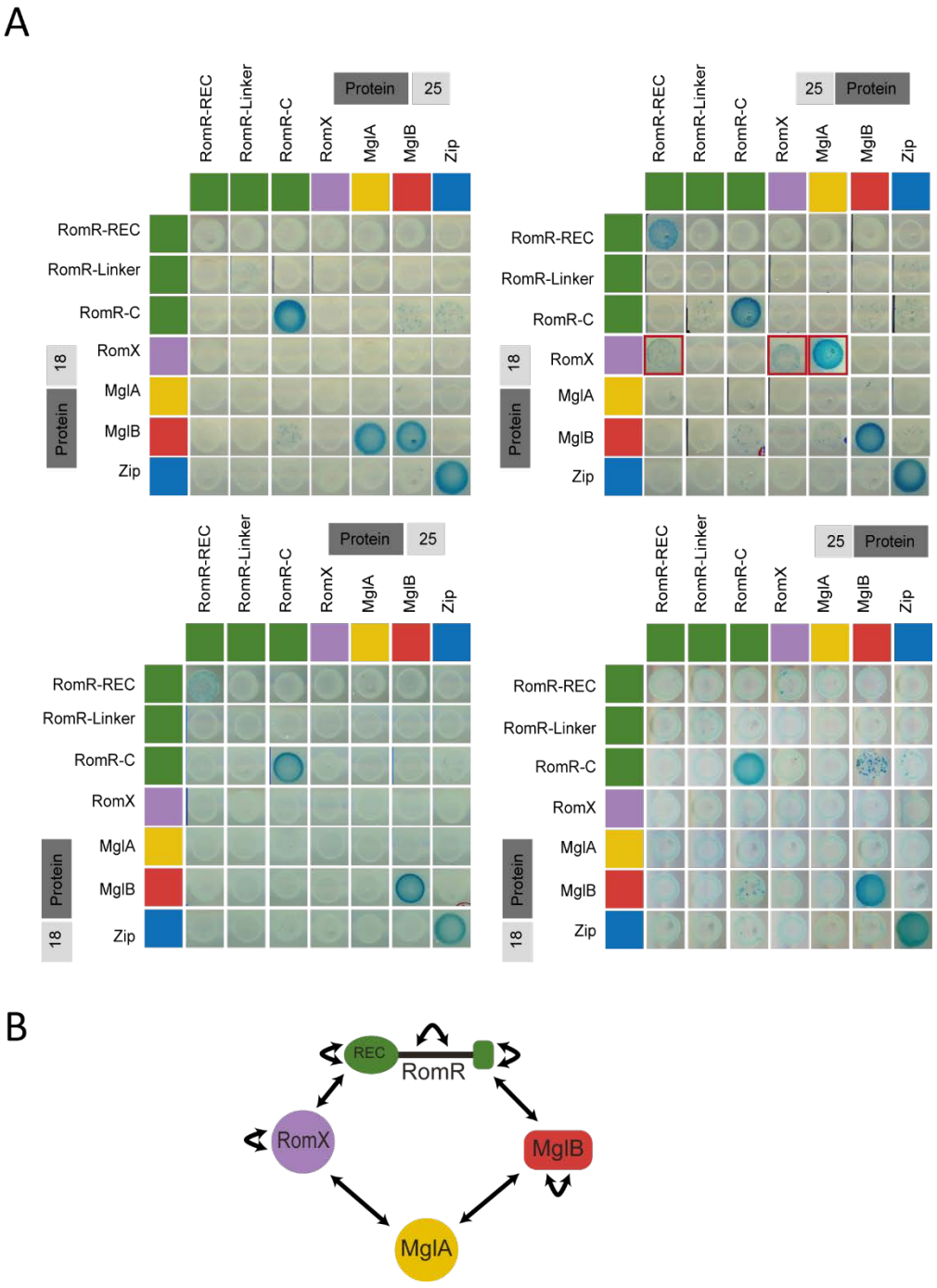

Figure 38. RomX interacts with RomR receiver domain and MglA in BACTH.
(A) Interaction between indicated proteins in fusion with T18 or T25 adenyl cyclase fragment. Novel interactions between RomX – RomR-Receiver domain (REC) and RomX – MglA and RomX self-interaction are indicated in red. Blue colonies indicate interaction, while white colonies indicate no interactions.
(B) Model for proteins interactions found in this study.

2.2.11 RomX/RomR complex interacts with MglA-GTP

To further test for direct interacts between MglA, RomR and RomX we turned to *in vitro* experiments. To this end, we purified C-terminal His6-tagged MglA (MglA-His_6),

N-terminal His6-tagged RomX (His_6-RomX), N-terminal Strep-tagged RomX (Strep-RomX), N-terminal MalE-tagged RomR (MalE-RomR) and MalE (Figure 39).

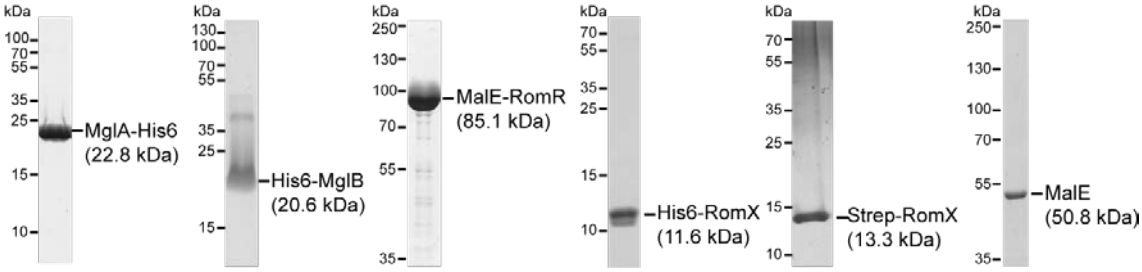

Figure 39. SDS-PAGE gels with the purified indicated proteins.
SDS-PAGE gels show selected fractions after the size exclusion chromatography. Molecular size marker and calculated molecular weights of proteins are indicated.

We first tested whether RomX interacts to form a stable complex with RomR or MglA in pull-down experiments. When MalE-RomR was bound to an amylose resin, it bound His_6-RomX whereas His_6-RomX neither bound to the resin on its own nor in the presence of MalE (Figure 40, A). We conclude that RomX and RomR interact directly. Moreover, when Strep-RomX was bound to Strep-Tactin beads, it bound MglA-GTP but MglA-GDP whereas MglA-GTP did not bind to the beads (Figure 40, B). We conclude that RomX forms a stable complex with MglA-GTP but not with MglA-GDP.

To test whether RomR, RomX and MglA can form a heteromeric complex, MalE-Rom was bound to the amylose resin with or without His_6-RomX. In the absence of His_6-RomX, binding of MglA-GTP and MglA-GDP to MalE-RomR was not observed (Figure 40, C). However, when the amylose resin contained His_6-RomX bound to MalE-RomR, MglA-GTP but not MglA-GDP was retained (Figure 40, D). Because neither MglA-GTP nor MglA-GDP bind stably to RomR in this assay, these data strongly suggest that MglA-GTP interacts with RomX in the RomX/RomR complex.

Previously, a weak interaction between RomR and MglA in pull-down experiments using a His6-RomR protein and a GST-MglA protein was reported (Keilberg *et al.*, 2012). Here, we used an MglA-His_6 protein because this protein has GTPase activity *in vitro* and this activity is stimulated by MglB (see below). We speculate that the difference between the data reported here and previously are due to the use of different purified proteins. We conclude that MglA-GTP but not MglA-GDP interacts with the RomR/RomX to form a stable complex leading to the formation of a RomR/RomX/MglA-GTP complex (Figure 40, E). These results are in agreement with the observations *in vivo* that RomR recruits RomX to a pole and RomX is a polar targeting determinant of MglA-GTP.

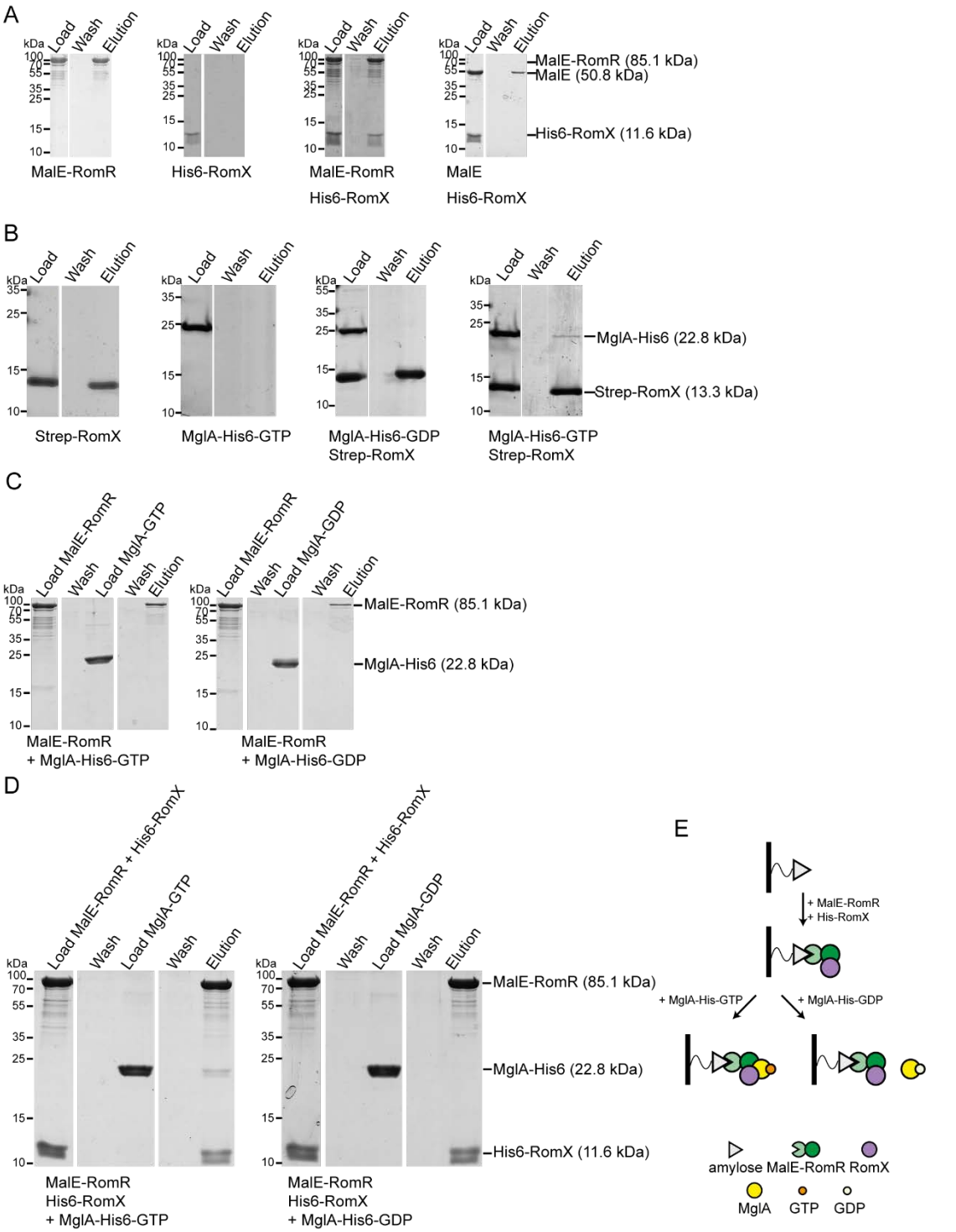

Figure 40. MglA-GTP interacts with RomR/RomX complex *in vitro*.

(A) 1st panel: MalE-RomR can be bound to amylose resin. Purified MalE-RomR was applied to an amylose column. 2nd panel: His_6-RomX does not bound to amylose resin. Purified His_6-RomX was applied to an amylose column. 3rd panel: MalE-RomR and His_6-RomX interact. Purified MalE-RomR and His_6-RomX were mixed and applied on an amylose column. 4th panel: His_5-RomX does not interact with MalE. Purified MalE and His_5-RomX were mixed and applied on an amylose column.

(B) Strep-RomX interacts with MglA-His_6-GTP but not MglA-His_6-GDP *in vitro*. Strep-RomX and MglA-His_6-GTP or MglA-His_6-GDP were mixed and immobilized on the strep-tactin magnetic beads. Proteins were eluted with buffer supplemented with biotin.

(C) MalE-RomR does not interact with MglA-His_6 *in vitro*. MalE-RomR was immobilized on the column, subsequently MglA-His_6-GTP or MglA-His_6-GDP were applied.

(D) RomR/RomX complex interacts with MglA-GTP. MalE-RomR and His_6-RomX were mixed and immobilized on the amylose column, subsequently MglA-His_6-GTP or MglA-His_6-GDP were applied. Proteins were eluted with buffer supplemented with maltose.
(E) Schematic representation of experiment from D.
For all pull-downs shown are proteins from load, last wash before elution and/or before MglA-His_6 loading, MglA-His_6 loading (if was loaded) and elution.

2.2.12 RomX and/or RomR do not inhibit MglB GAP and MglA GTPase activity

Our cell biology data suggest that one of the function of RomX and RomR is to stimulate MglA-GTP accumulation in the cell. One possibility to achieve this would be to inhibit MglB GAP or MglA GTPase activity. In order to test the hypothesis, GTPase assay was performed. A low level of intrinsic activity of MglA alone was observed. No GTPase activity for MglB, RomX and RomR were detected. MglB, as expected, stimulated MglA GTPase activity whereas RomX, RomR and RomX/RomR did not. Moreover, RomX and/or RomR pre-incubated with MglB did not interfere with MglB GAP activity (Figure 41, left part). Similarly, when RomR and/or RomX was pre-incubated with MglA-GTP before addition of MglB, we did not observe inhibition of MglB GAP activity (Figure 41, right part). We conclude that RomX and/or RomR do not inhibit MglB GAP activity.

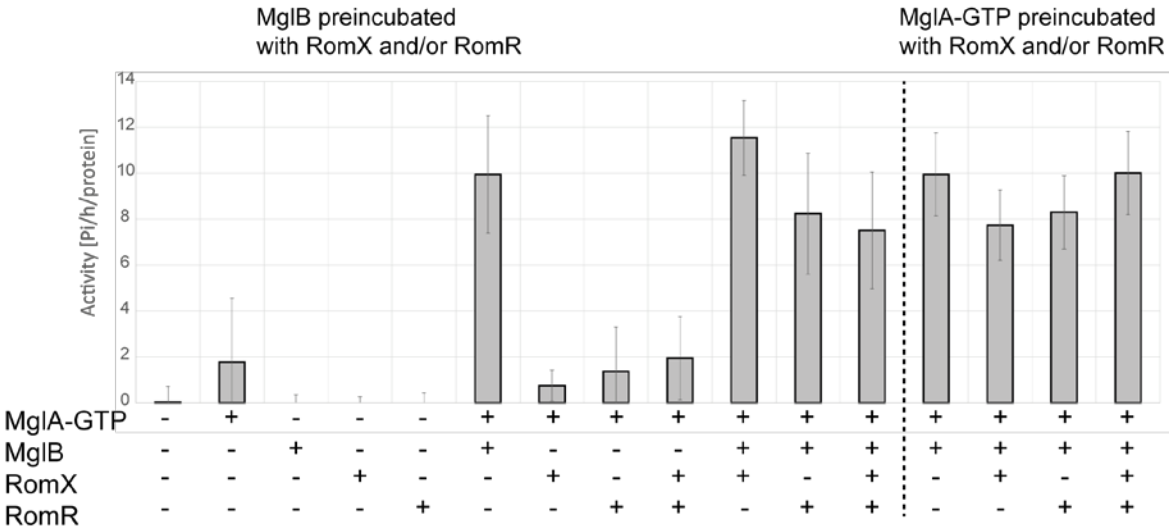

Figure 41. RomX and/or RomR do not inhibit MglA GTPase and MglB GAP activity.
Specific GTPase activity of 3 µM MglA, 6 µM MglB, 6 µM RomX, 6 µM RomR and combinations of the proteins in the presence of 1 mM GTP. Experiment was performed in triplicates and graph shows mean ± SD.

2.2.13 RomX/RomR complex stimulates MglA nucleotide exchange

To test whether RomX and/or RomR have MglA GEF activity, we monitored GDP to GTP exchange using two different experimental set-ups.

In the first set-up, MglA-His_6 was preloaded with the fluorescent GDP analog N-methylanthraniloyl (mant)-GDP before MalE-RomR and/or His_6-RomX were added. Subsequently, excess of GTP was added and the decrease in fluorescence intensity associated with release of mantGDP and binding of GTP by MglA-His_6 was monitored. MglA spontaneously exchanged mantGDP for GTP slowly and the exchange rate was not affected by BSA, which served as a negative control (Figure 42, A). RomX and RomR independently did not stimulate the nucleotide exchange rate. Importantly, in the presence of both, RomX and RomR, the two proteins synergistically stimulated the nucleotide exchange rate supporting that the RomX/RomR complex has MglA GEF activity (Figure 42, A).

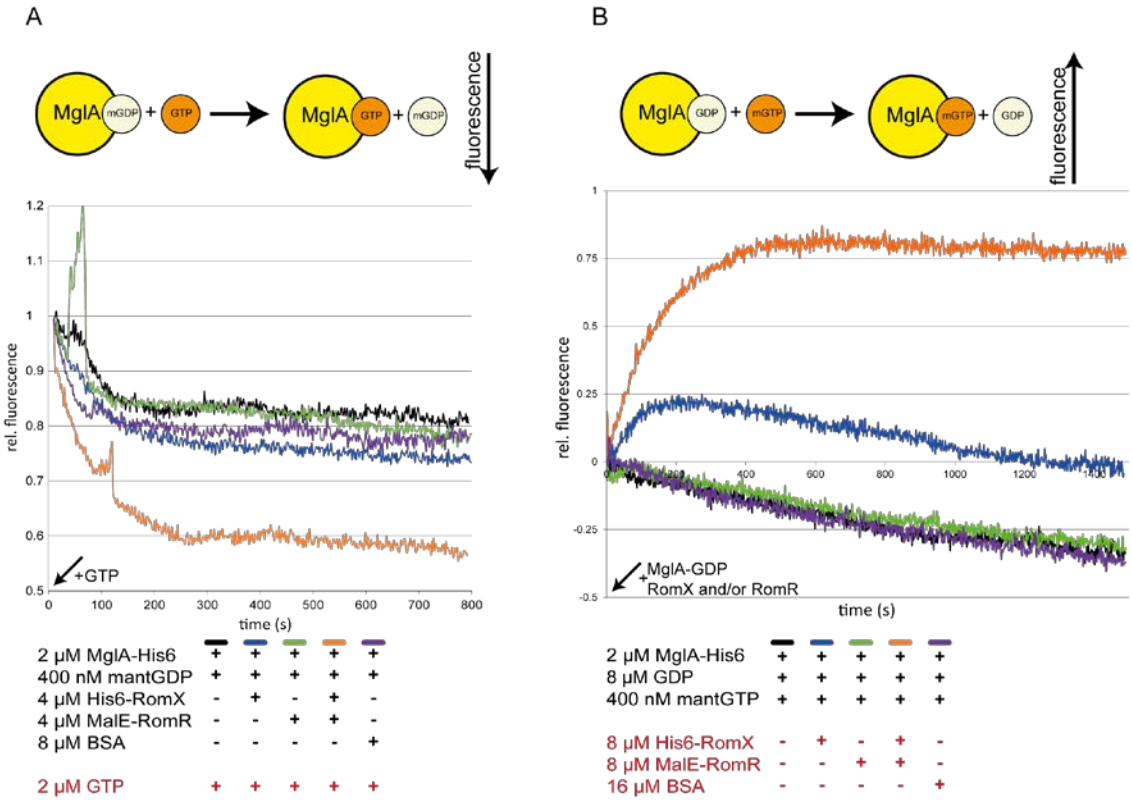

Figure 42. RomX/RomR complex stimulates MglA nucleotide exchange.
(A) MglA was loaded with mGDP and mGDP release was measured in real time (as shown in the scheme above) in the absence and in the presence of RomX, RomR, RomX/RomR or BSA. Arrow indicates a start of the reaction by adding GTP. Fluorescence was measured every second.
(B) MglA was loaded with GDP and mGTP binding was measured in real time (as shown in the scheme above) in the absence and in the presence of RomX, RomR, RomX/RomR or BSA. Arrow indicates start of the reaction by adding MglA-GDP or MglA-GDP and RomX, RomR, RomX/RomR or BSA.

In the reciprocal experiment, MglA-His_6 was preloaded with GDP, then mantGTP was added followed by addition of His_6-RomX and/or MalE-RomR or BSA, and the increase in fluorescence intensity associated with release of GDP and binding of mantGTP by MglA-His_6 was followed. In the presence of MglA alone or together with RomR or BSA no increase in fluorescence intensity was observed indicating that GDP was not being exchanged for mantGTP (Figure 42, B). After addition of only RomX, a transient increase in fluorescence intensity was observed. However, in the presence of RomX together with RomR a significant increase in fluorescence intensity was observed indicating GDP for mantGTP exchange by MglA (Figure 42, B). We speculate that the reason why no spontaneous exchange of GDP for mantGTP by MglA was observed in this experiment is due to the 20-fold higher concentration of GDP compared to mantGTP. Note than in the experiment in Figure 42, A in which spontaneous exchange of mantGDP for GTP by MglA was observed, GTP was added in 5-fold excess of mantGDP. Based on the *in vitro* experiments, we conclude that the RomR/RomX complex has MglA GEF activity and also interacts directly with MglA-GTP. *In vivo* these two activities would bring about polar localization of MglA-GTP by increasing the concentration of MglA-GTP via the GEF activity and by RomX/RomR binding and recruiting MglA-GTP directly to a pole.

Binding of effectors or a GAP to a small GTPase containing a bound mant-nucleotide can cause a change in mant fluorescence (Kuhlmann *et al.*, 1997, Leonard *et al.*, 1998, Hemsath *et al.*, 2005). To exclude the possibility that the increase in fluorescence intensity observed in the experiment in Figure 42, B in the presence of the RomR/RomX complex was caused by simple binding of RomR/RomX to the MglA/mantGTP complex a control experiment was performed. In this experiment, we tested the change in fluorescence of mantGTP bound to MglA following addition of RomX and/or RomR. As a positive control, we used MglA preloaded with GDP and then added mantGTP with RomX and RomR as described in the previous experiment. We did not observe an increase in fluorescence for MglA/mantGTP alone or with RomX, RomR or BSA. After addition of the RomX/RomR complex to MglA/mantGTP, we detected an increase in fluorescence. However, the increase was lower than in the mantGTP exchange experiment with RomX and RomR (Figure 43). Thus, the data support that the increase in mant fluorescence for the previous experiment is mainly due to the binding of mantGTP by MglA and not the RomR/RomX complex interacting with MglA/mantGTP. Furthermore, because we are so far not able to purify nucleotide free MglA (data not

shown) we cannot exclude that the increase in fluorescence observed upon addition of the RomR/RomX complex to MglA/mantGTP is a consequence of increased binding of mantGTP to MglA. Regardless, the data is consistent and support the conclusion that RomX/RomR complex is a GEF and stimulates MglA nucleotide exchange.

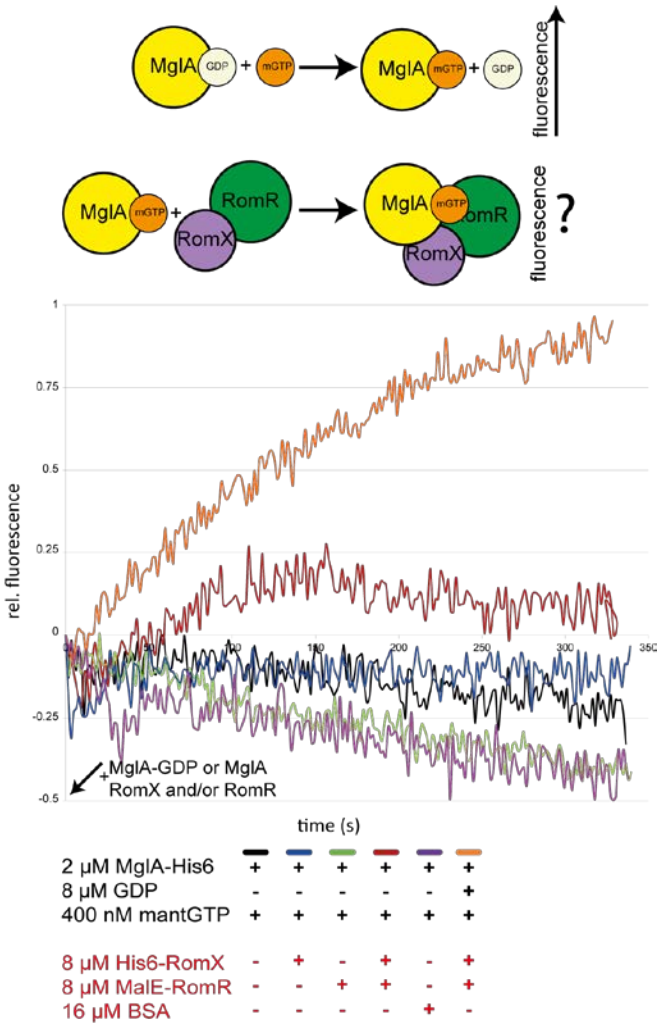

Figure 43. RomX/RomR complex binds to MglA-GTP.
MglA was loaded with GDP and mGTP binding was measured in real time in the presence of RomX/RomR complex (as shown in the scheme above; orange line on the graph) or MglA was loaded with mGDP and change of the fluorescence intensity due to possible interaction with MglA was measured in real time (as shown in the scheme above) in the absence and in the presence of RomX, RomR, RomX/RomR or BSA. Arrow indicates start of the reaction by adding MglA-GDP and RomX/RomR or MglA with or without RomX, RomR, RomX/RomR or BSA.

2.3. Characterization of RomY in *Myxococcus xanthus*

Alignment of all 28 identified RomY homologs revealed a conserved N-terminal region, a proline rich low complexity region of variable length, and a conserved C-terminal motif (Figure 44, A). None of these domains matches any currently characterized domain models.

The genetic neighborhood of *romY* is conserved in closely related species; however, the flanking genes did not suggest any function in regulation of motility. In *M. xanthus*, the ABC transporter FtsEX involved in cell division is encoded downstream of *romY* and immediately upstream of *romY* is the gene encoding the carotenoid synthesis regulator, *carF* (Figure 44, B).

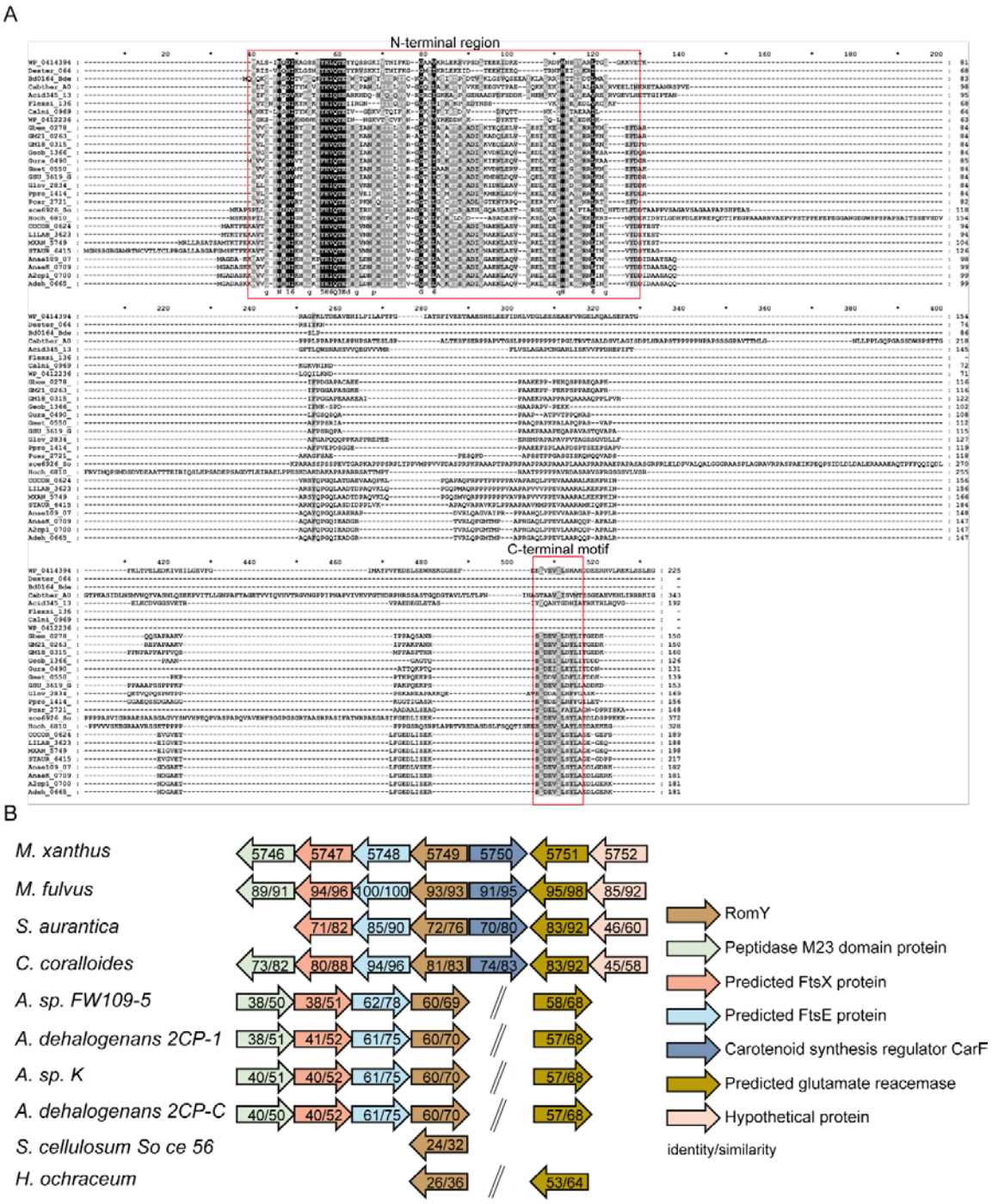

Figure 44. Bioinformatics analysis of RomY

(A) Alignment of identified RomY homologs. N-terminal conserved region and C-terminal conserved motif are indicated.

(B) Conservation of *romY* neighbourhood in selected myxobacteria. Genes are depicted as arrows. Arrow orientation indicates coding direction. Homologous proteins are indicated in same colours. Numbers in arrows in *M. xanthus* display gene number. Numbers in arrows (outside of *M. xanthus*) indicate identity and similarity of their encoded protein to their *M. xanthus* homolog. Numbers were obtained from Pairwise Sequence Alignement of protein using EMBOSS Needle. Right part shows predicted proteins functions based on the NCBI BLAST and conserved domain analysis (Marchler-Bauer *et al.*, 2017)

2.3.1 RomY is important for both motility systems

In order to test whether RomY is involved in motility and/or its regulation we generated an in-frame *romY* deletion. The Δ*romY* mutant showed very short flares on

0.5% agar in comparison to the WT strain. In the case of gliding motility, we observed fewer single cells for the Δ*romY* mutant in comparison to WT on 1.5% agar (Figure 45). To confirm that the motility defects in the Δ*romY* mutant was caused by lack of RomY, we generated a complementation strain in which a RomY-YFP fusion protein was expressed ectopically under the control of the native promoter. This strain did not show motility defects (Figure 45). Based on these experiments we conclude that RomY is important for both T4P-dependent and gliding motility.

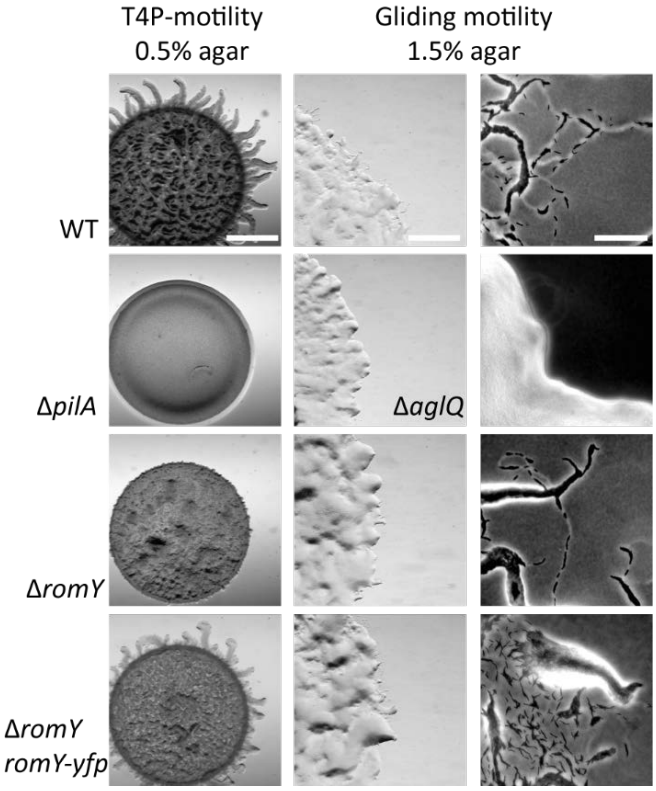

Figure 45. *romY* mutant shows defect in T4P-dependent and gliding motility.
Motility assay as described in Figure 21 compares WT to the Δ*romY* mutant. Scale bars, 500 µm (T4P-dependent motility), 500 µm (gliding motility – left panel) and 50 µm (gliding motility – right panel).

2.3.2 RomY acts in the same pathway as MglA, MglB, RomR and RomX

Next, we tested whether RomY acts in the same pathway as MglA, MglB, RomR and RomX. To this end, genetic epistasis experiments were performed (Figure 46). Both Δ*mglA* and Δ*mglA*Δ*romY* mutants had a flat colony edge on 0.5% as well as on 1.5% agar. This suggests that MglA acts downstream of RomY. The Δ*mglB* mutant was indistinguishable from the Δ*romY* mutant under both conditions. Both strains showed very short flares on 0.5% agar and only few single cells at the colony edges on 1.5% agar. Furthermore, the same phenotype was observed for the double deletion Δ*mglB*Δ*romY*

mutant under both conditions. Moreover, measured expansions of the colonies after 24 hours of the Δ*mglB*, Δ*romY* and Δ*mglB*Δ*romY* mutants were very similar and the differences in colony expansion were not statistically significant (t-test $p>0.01$). Based on this observation we conclude that lack of the RomY caused the same defect as Δ*mglB* and the double deletion caused no additive effect. The Δ*romR* mutant showed misformed flares on 0.5% agar and the Δ*romR*Δ*romY* mutant had a similar phenotype. On 1.5% agar, the double Δ*romR*Δ*romY* mutant showed more single cells at the colony edge than the Δ*romR* mutant and a colony expansion after 24 hours that was comparable to that of the Δ*romY* mutant. Both Δ*romX* and Δ*romX*Δ*romY* mutants had short misformed flares in contrast to the very short flares of the Δ*romY* mutant. On 1.5% agar, the double Δ*romX*Δ*romY* mutant showed a larger colony expansion after 24 hours in comparison to the single Δ*romX* mutant and somewhat similarly to the Δ*romY* mutant. Furthermore, the differences in colony expansion after 24 hours were statistically significant (t-test $p<0.01$) (Figure 46, A).

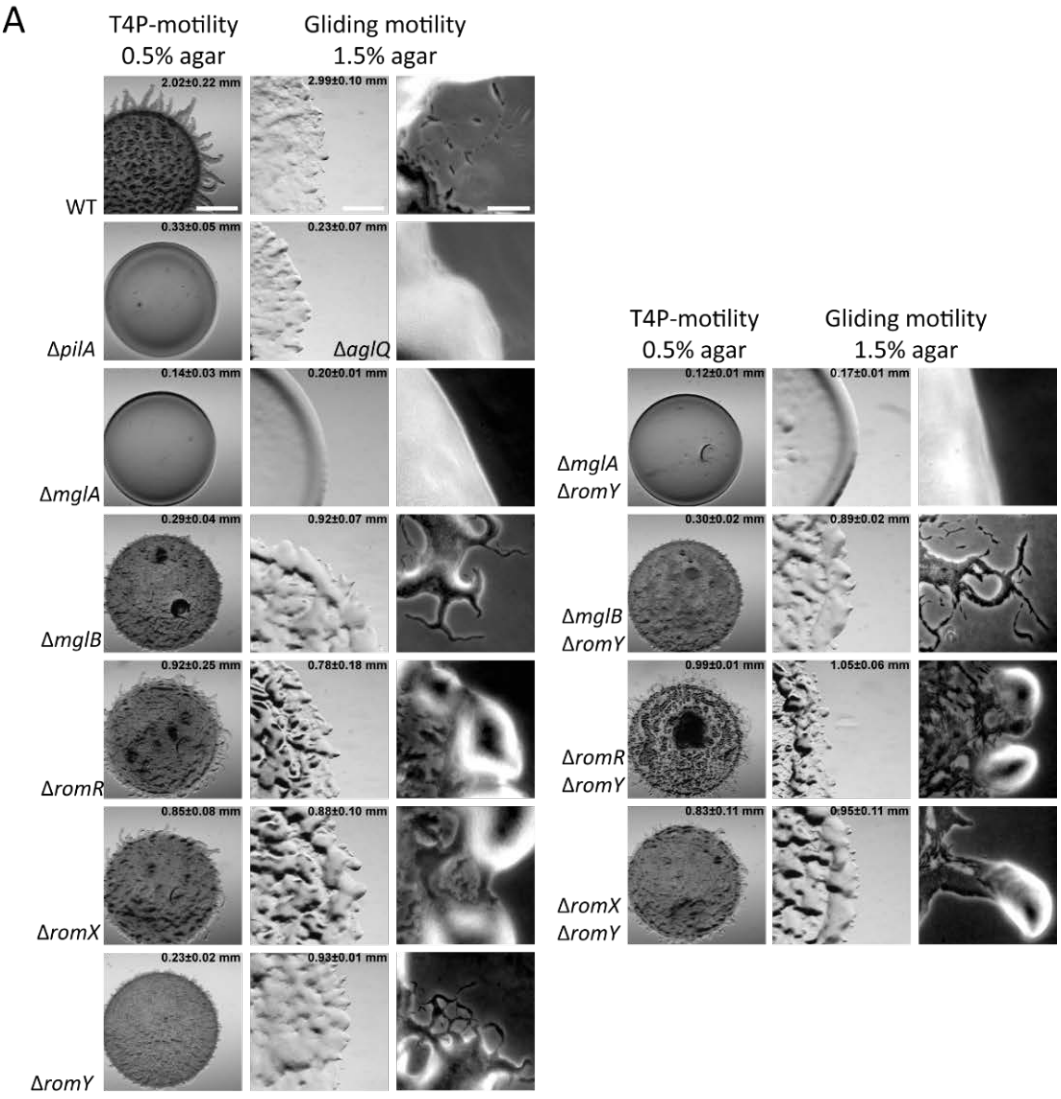

Figure 46. RomY acts in the same pathway as MglA, MglB, RomR and RomX.

(A) Motility assay as described in Figure 21 compares single and double mutants of *romY*, *mglA*, *mglB*, *romX* and *romR*. The numbers indicate the increase in colony diameter in mm ± standard deviation from three technical replicates after 24h. Scale bars, 1000 µm (T4P-dependent motility), 500µm (gliding motility – left panel) and 50 µm (gliding motility – right panel).

(B) Reversal frequency of WT and selected mutants on 1.5% TPM agar. Shown are boxplots of the measured reversals of isolated cells for 15 min, boxes enclose the 25th and 75th percentile, whiskers represent the 10th and 90th percentile, and dots outliers. Student's t-test was employed for statistical analysis and * indicates $p < 0.001$. $n > 50$.

The epistasis experiment suggested that RomY acts in the same pathway as MglA, MglB, RomR and RomX. Moreover, comparison of the Δ*mglB* and Δ*romY* mutants suggested that lack of MglB and RomY cause the same motility defects. Because lack of MglB causes cells to hyper-reverse, we quantified the reversal frequency on 1.5% agar of the Δ*romY* mutant. Under the tested conditions, WT reversed on average 1.40 times in 15 min while the Δ*mglB* mutant reversed on average 3.41 times in 15 min. Importantly, the Δ*romY* mutant also hyper-reversed and with an average of 3.5 reversals in 15 min. In the double Δ*mglB*Δ*romY* mutant, we did not observe additive effects of the single deletions. (Figure 46, B). Thus, the Δ*romY* mutant is hyper-reversing and RomY acts in the same pathway as MglA, MglB. RomR and RomX.

2.3.3 RomY localization studies

MglA, MglB, RomR and RomX are polarly localized and mutually depend on each other for polar asymmetry and localization (chapter 2.2.4). We decided to test whether RomY is polarly localized and whether localization of RomY depends on MglA, MglB, RomR and RomX.

First, we tested accumulation and stability of RomY-YFP fusion protein in the Δ*romY* mutant, as well as in absence of MglA, MglB, RomR and RomX. The RomY protein in WT was detected by α-RomY antibodies. Moreover, RomY-YFP accumulated in the complementation strain at a slightly higher level than the native protein in the WT. RomY-YFP accumulated at similar level as in the complementation strain in the absence of MglA, MglB, RomR and RomX (Figure 47).

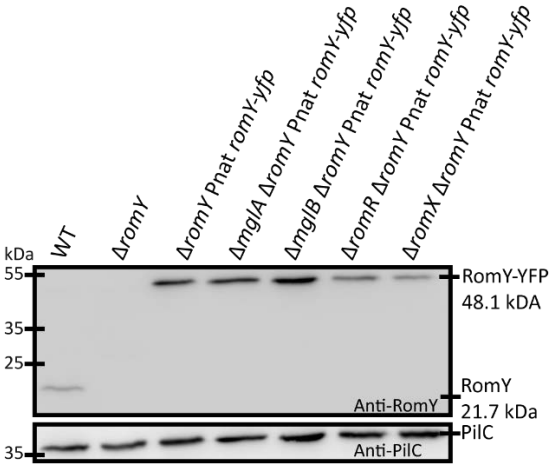

Figure 47. RomY-YFP is stable in investigated mutants.
Immunoblot of RomY-YFP. Cells were grown in liquid culture, harvested, and total protein (1 mg per lane) was separated by SDS–PAGE and analyzed by immunoblot using α-RomY. RomY and RomY-YFP with calculated molecular masses are indicated. Immunoblot with α-PilC serves as loading control.

RomY-YFP localized predominantly unipolarly with the cluster at the lagging cell pole. Moreover, when cells reversed, RomY-YFP changed localization to the new lagging cell pole (Figure 48, A). RomY-YFP localized predominantly in a unipolar pattern in the absence of MglA. RomY-YFP localized mostly diffusely throughout the cytoplasm in the absence of MglB. In the absence of RomR, RomY-YFP localization shifted towards more diffuse throughout the cytoplasm. However, more than 50% of cells still showed a polar RomY-YFP cluster. In the absence of RomX, RomY-YFP localized predominantly diffusely throughout the cytoplasm (Figure 48, B). Nevertheless, the effect of the Δ*romX* mutation on RomY localization was not as strong as in the case of the Δ*mglB* mutation. Therefore, polar localization of RomY depends strongly on MglB and less on RomR and RomX.

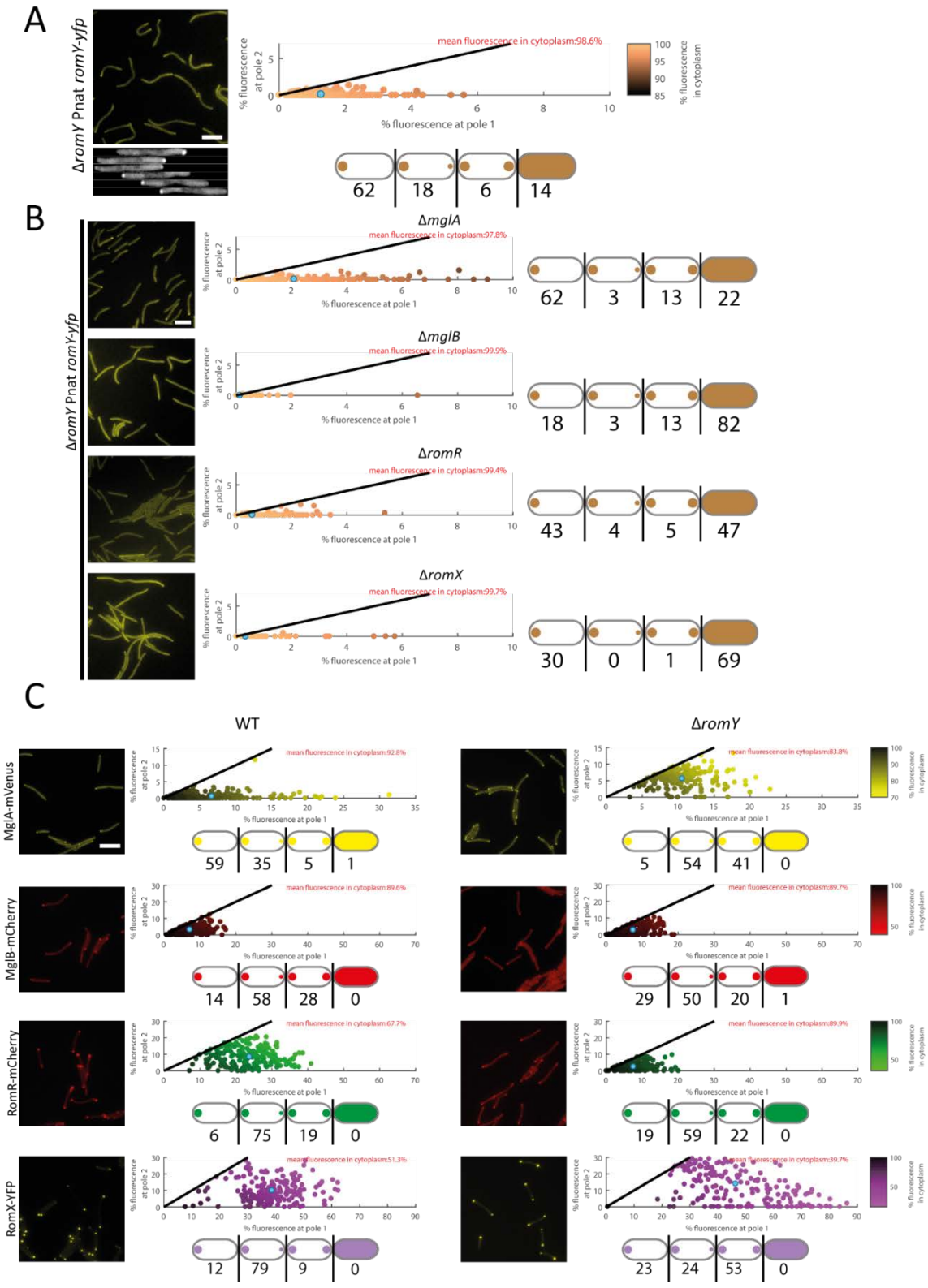

Figure 48. RomY localizes predominantly at the lagging pole.

(A) Localization of RomY-YFP. Upper left panel shows snapshot, lower left panel shows time-lapse fluorescence microscopy at 30 s intervals. Cells were treated as in Figure 26. Percent of fluorescence signal for each pole and cytoplasm were calculated and plotted on the upper right graph. Cyan dot represents the mean. The localization patterns observed are indicated in the schematics. The ratios between polar signals were calculated to distinguish between unipolar, asymmetric bipolar and symmetric bipolar localization as in figure 26. Scale bar: 5 µm. n>200.

(B) Localization of RomY-YFP in indicated strains. Left panels show fluorescent microscopy pictures. Cells were treated as in Figure 26. Percent of fluorescence signal for each pole and cytoplasm were calculated and plotted on the left graph. Cyan dot represents the mean. The localization patterns observed are indicated in the schematics. The ratios between polar signals were calculated to distinguish between unipolar, asymmetric bipolar and symmetric bipolar localization as in figure 26. n>200. Scale bar: 5 µm.
(C) Localization of MglA-mVenus, MglB-mCherry and RomR-mCherry in indicated strains. Cells were treated as in Figure 26. Left panel shows fluorescent microscopy picture. Percent of fluorescence signal for each pole and cytoplasm were calculated and plotted on the upper graph. Cyan dot represents the mean. The localization patterns observed are indicated in the schematics. The ratios between polar signals were calculated to distinguish between unipolar, asymmetric bipolar and symmetric bipolar localization as in figure 26. n>200. Scale bar: 5 µm.

In the reciprocal experiments, we observed that MglA predominantly localized in a unipolar pattern in WT and changed localization towards bipolar asymmetric and symmetric in the absence of RomY. Thus, polar asymmetry of MglA depends on the RomY. MglB, in the absence of RomY, localized in a bipolar asymmetric pattern as in WT. RomR, in the absence of RomY, localized predominantly in the bipolar asymmetric pattern as in WT. However, in the absence of RomY less RomR was polarly bound. Thus, RomY helps RomR to bind to the poles. RomX localized mostly in the bipolar asymmetric pattern in WT and in the absence of RomY, we observed a shift towards a more bipolar symmetric pattern. Also, more RomX was polarly bound in the absence of RomY in comparison to WT. Thus, polar asymmetry of RomX depends on RomY (Figure 48, C).

2.3.4 RomY interacts with RomX and MglA in bacterial two hybrid system

To test whether RomY interacts directly with MglA, MglB, RomR or RomX, we performed bacterial two hybrid experiments. In these experiments, we found that RomY self-interacts and also interacts with RomX and MglA (Figure 49, A).

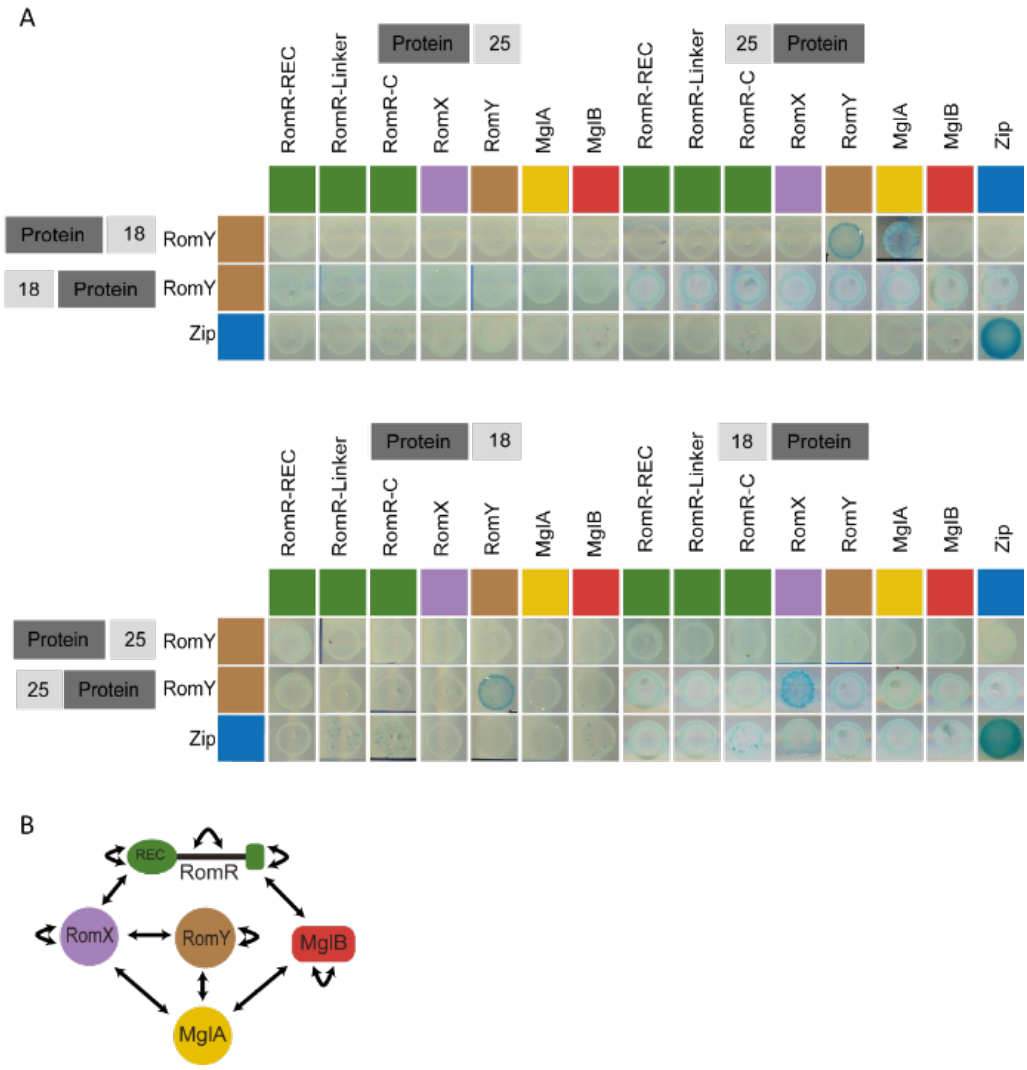

Figure 49. RomY interacts with RomX, MglA and itself in BACTH.
(A) Interaction between indicated proteins in fusion with T18 or T25 adenyl cyclase fragment. Blue colonies indicate interaction, while white colonies indicate no interactions.
(B) Model for proteins interactions found in all performed BACTH studies.

2.4 Characterization of the importance of RomR for reversals

2.4.1 Δ*romR* and Δ*romX* mutants respond to IAA

The RomR response regulator was suggested to be the central output of the Frz system because its substitution of the phosphorylatable Asp residue in the receiver domain to Glu, which has been reported to mimic the phosphorylated state in many response regulators (Domian *et al.*, 1997), and Gln, which cannot be phosphorylated and mimics the non-phosphorylated form, caused a hyper-reversal and hypo-reversal phenotype, respectively (Keilberg *et al.*, 2012, Leonardy *et al.*, 2007). Thus, phosphorylation of RomR could link signaling by the Frz system to the polarity switch (Leonardy *et al.*, 2007). Additionally, it has been shown that a Δ*romR* mutant does not

reverse while cells are moving by T4P-dependent motility (Guzzo *et al.*, 2015). As reported here, cells that lack RomX also do not reverse while moving by T4P-dependent motility. To test whether RomX and/or RomR are essential to generate an output of the Frz system, we artificially increased Frz signaling in Δ*romX* and Δ*romR* mutants by adding isoamyl alcohol (IAA) to cells. The exact target of IAA is not known; however, its action strictly depends on the Frz system and IAA activates the Frz system (McBride *et al.*, 1992, Bustamante *et al.*, 2004).

We tested T4P-dependent motility on 0.5% agar in the presence of gradually increasing IAA concentrations (Figure 50). In the absence of IAA, WT formed flares, the Δ*pilA* mutant that served as a negative control did not, and the Δ*frzE* mutant showed misformed flares. The Δ*romX* and Δ*romR* mutants formed short misformed flares. Importantly, increasing concentrations of IAA caused the formation of shorter flares in all strains except the Δ*frzE* mutant that was not affected by IAA (Figure 50). We conclude that IAA in the absence of RomX or RomR still induces reversals.

We also tested the effect of IAA on glding motility on 1.5% agar (Figure 50). Without IAA, WT showed single cells at the colony edge while the Δ*aglQ* mutant did not. Δ*frzE* mutant showed single cells at the colony edge comparable to WT. For the Δ*romX* and Δ*romR* mutants, only movement of groups of cells was observed. Also, for gliding motility increasing concentrations of IAA caused fewer visible single cells at the colony edges in all strains except the Δ*frzE* mutant that was not affected by IAA (Figure 50). We conclude that IAA in the absence of RomX or RomR still induces reversals. In total, these data suggests that neither RomX nor RomR are essential for the output of the Frz system.

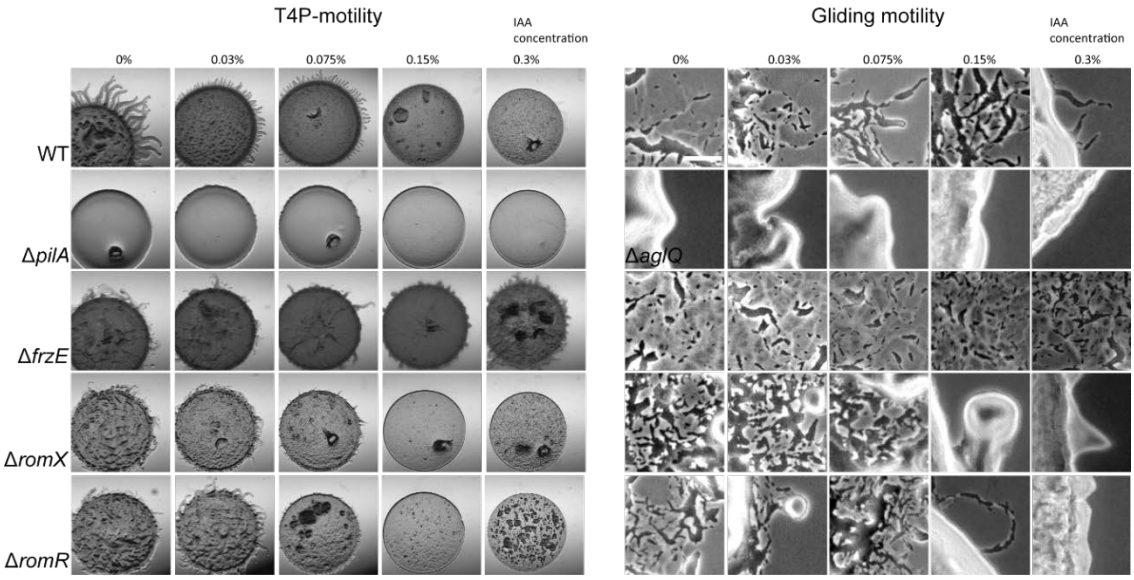

Figure 50. **The Δ*romX* and Δ*romR* strains are sensitive to IAA.**
Motility assays as in Figure 21; right part show colony after 24h on the 0.5% CTT, 0.5% agar plates without and with indicated IAA concentrations. Light part show colony after 24h on the 0.5% CTT, 1.5% agar plates without and with indicated IAA concentrations. Bars, 1000 μm (T4P-dependent motility – left part), 50 μm (gliding motility – right part).

To confirm the effect of IAA on motility observed in the population-based assay, we analysed single cells moving by T4P-dependent motility in the absence and presence of IAA. As shown in Figure 51, the Δ*aglQ* mutant reversed on average 0.62 times in 10 minutes while the Δ*aglQ*Δ*romR* and Δ*aglQ*Δ*romX* mutants did not reverse. As reported previously (Blackhart & Zusman, 1985), the Δ*aglQ*Δ*frzE* mutant did not reverse. However, in the presence of 0.3% IAA, the reversal frequency of the Δ*aglQ*, Δ*aglQ*Δ*romX* and Δ*aglQ*Δ*romR* mutants increased while the Δ*aglQ*Δ*frzE* mutant was not affected by IAA (Figure 51). Therefore, artificial activation of Frz signaling increases the reversal frequency of the normally non-reversing Δ*romX* and Δ*romR* mutants, supporting that RomR and RomX are not essential to generate the output of the Frz system.

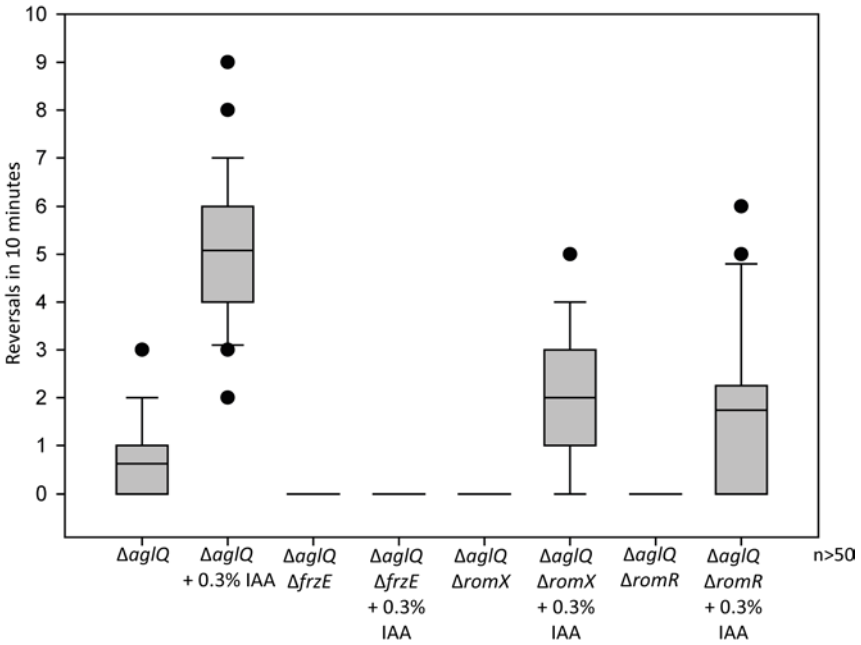

Figure 51. The Δ*romX* and Δ*romR* mutants are IAA sensitive.
Reversal frequency of WT and selected mutants on 1% methylcellulose with or without 0.3% IAA. Shown are boxplots of the measured reversals of isolated cells for 10 min, boxes enclose the 25th and 75th percentile, whiskers represent the 10th and 90th percentile, and dots outliers. n>50.

2.4.2 Mimicking and blocking of possible RomR phosphorylation site has no effect on the motility

To further investigate how RomR is important for reversals induced by the Frz system, we ectopically expressed RomR^{D53E}, which has been suggested to mimic the phosphorylated state of RomR (Leonardy *et al.*, 2007, Keilberg *et al.*, 2012), and RomR^{D53N}, which cannot be phosphorylated and mimics the non-phosphorylated form (Leonardy *et al.*, 2007, Keilberg *et al.*, 2012), under the control of the strong, constitutively active *pilA* promoter. Unfortunately, both variants of RomR did not accumulate (data not shown). Next, *romR*, *romR^{D53E}* and *romR^{D53N}* were expressed ectopically under control of a vanillate inducible promotor.

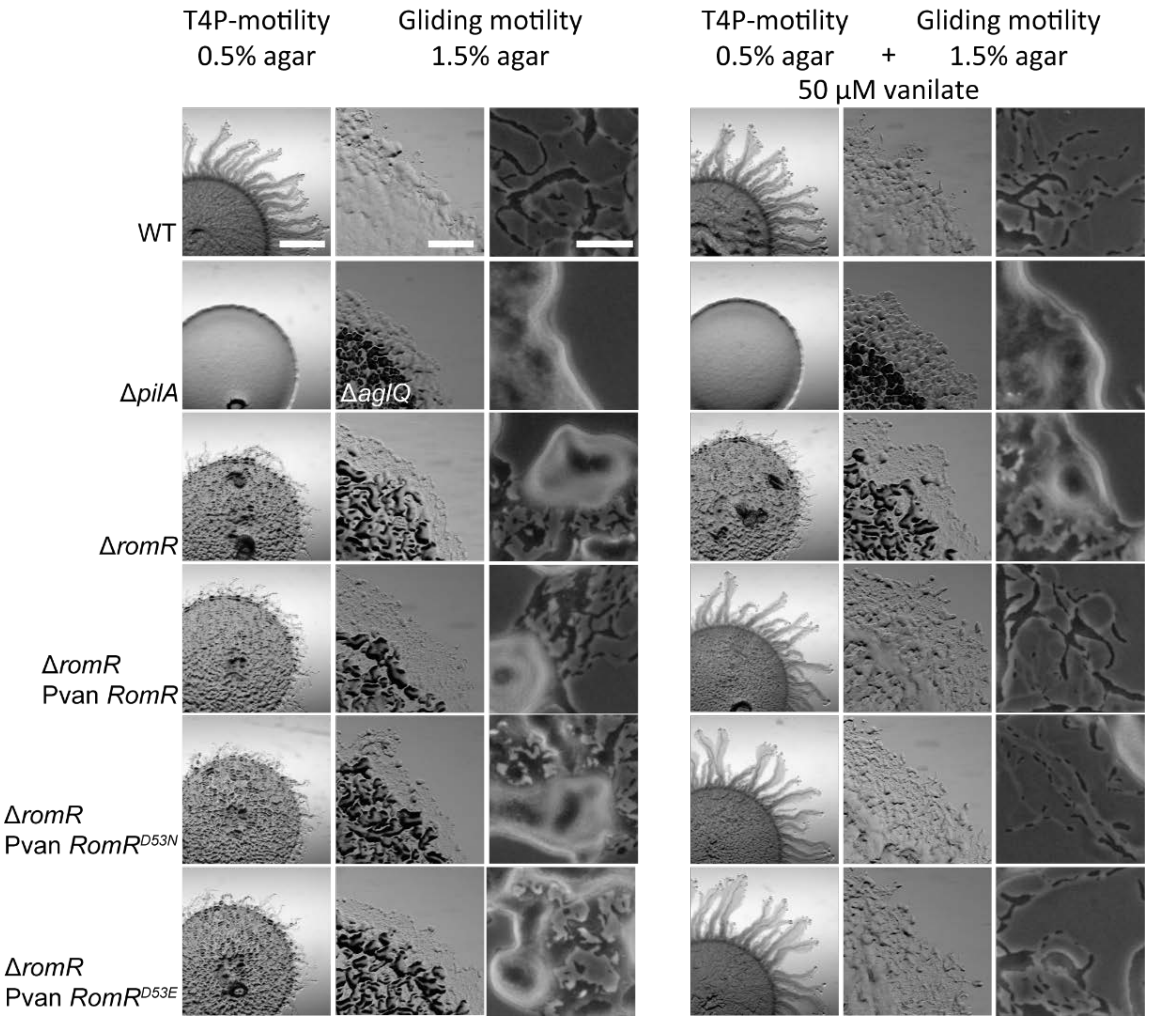

Figure 52. Mimicking or blocking phosphorylation site of RomR has no effect on the motility.
Motility assay as described in Figure 21; right columns show colony after 24h of growth on the plates with 50 µM vanillate used as an inducer. Bars, 1000 µm (T4P-dependent motility), 500µm (gliding motility – left panel) and 50 µm (gliding motility – right panel).

In the absence of inducer, the strains expressing *romR*, *romR*^{D53N} or *romR*^{D53E} showed the Δ*romR* phenotype. On plates with and without 50 µM vanillate, WT showed flares on 0.5% agar and single cells at the colony edge on 1.5% agar (Figure 52). Therefore, vanillate has no effect on motility. Furthermore, strains that expressed *romR*, *romR*^{D53N} or *romR*^{D53E} under the control of the inducible promotor were indistinguishable from WT in the presence of 50 µM vanillate (Figure 52). Thus, blocking and mimicking of possible phosphorylation site of RomR has no effect on the motility.

To further investigate the effect of possible RomR phosphorylation on reversals, we examined single cells expressing *romR*, *romR*^{D53N} or *romR*^{D53E}. Synthesis of the RomR variants was induced in suspension with 50 µM vanillate and samples were withdrawn at different time points to determine the accumulation level of RomR variants. In the absence of vanillate, none of the RomR variants accumulated (Figure 53, A). After

2 hours, the accumulation level of the RomR variants had reached the WT level. After 3 hours, the level of the RomR variants were higher than in WT (Figure 53, A). At all time points, the strains expressing *romR*, *romR*^{D53N} and *romR*^{D53E} behaved similarly with respect to reversals (Figure 53, B).

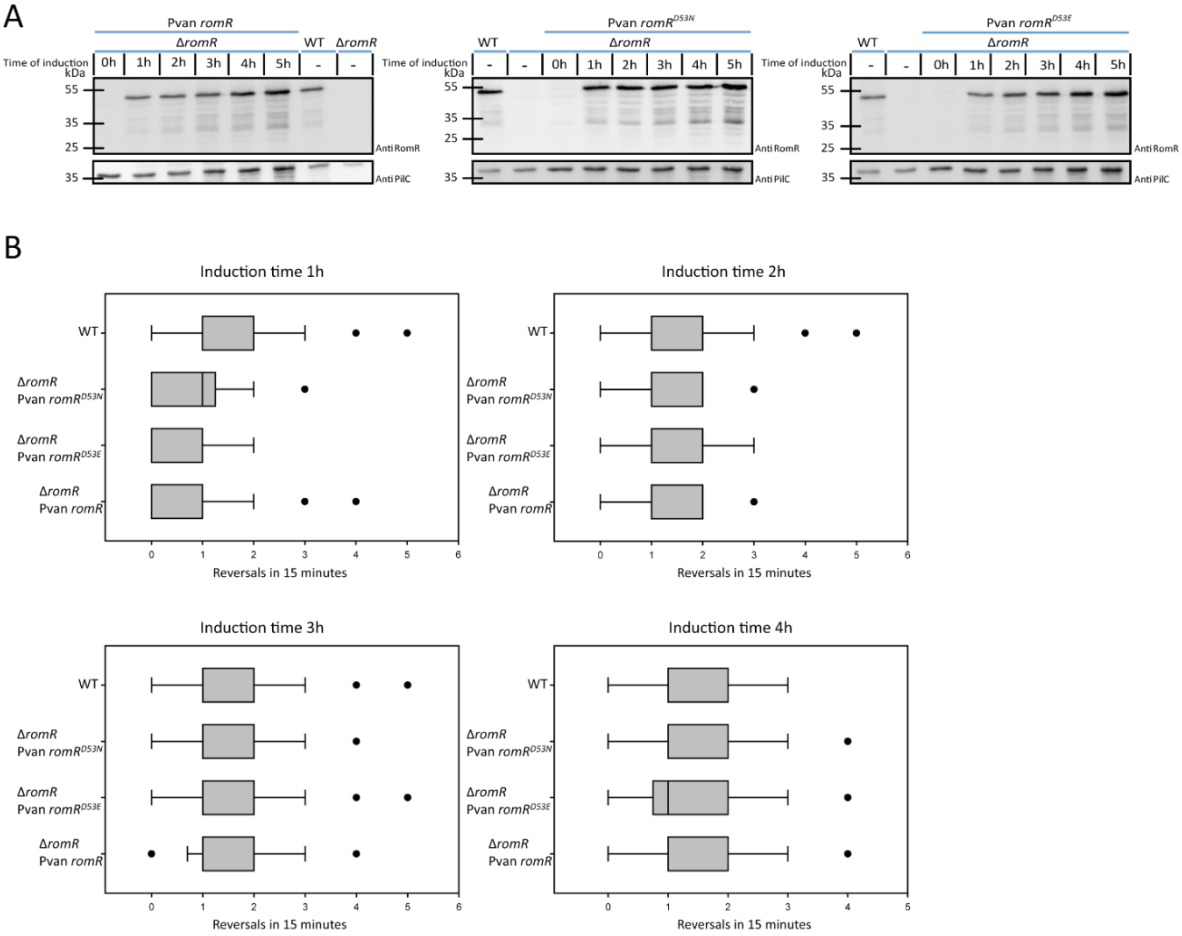

Figure 53. Mimicking or blocking phosphorylation site of RomR has no effect on the reversal frequency when cell are moving by gliding motility.

(A) Immunoblots of RomR. Details of experiment are explained in text. Total protein (1 mg per lane) was separated by SDS–PAGE and analyzed by immunoblot using α-RomR. Immunoblot with α-PilC serves as a loading control.

(B) Reversal frequency of WT and selected mutants on 1.5% TPM agar. Shown are boxplots of the measured reversals of isolated cells for 15 min, boxes enclose the 25th and 75th percentile, whiskers represent the 10th and 90th percentile, and dots outliers. Δ*romR* was not moving as single cells in the tested conditions.

In previous experiment, we induced synthesis of the RomR variants over time. Next, we analysed the effect of the RomR variants on the reversal frequency in steady state after 8 generation of induction in the presence of 15 µM vanillate (Figure 54, A). As expected, *romR*, *romR*^{D53N} and *romR*^{D53E} mutants that were growing for 8 generations without inducer showed no RomR accumulation (Figure 54, A) and no sufficient movement to calculate reversals. In the presence of 15 µM vanillate, RomR, RomR^{D53N}

and RomR^{D53E} accumulated to WT level (Figure 54, A) and *romR*, *romR*^{D53N} and *romR*^{D53E} mutants had the same reversal frequency as WT (Figure 54, B). Therefore, blocking and mimicking of possible RomR phosphorylation have no effect on the reversal frequency.

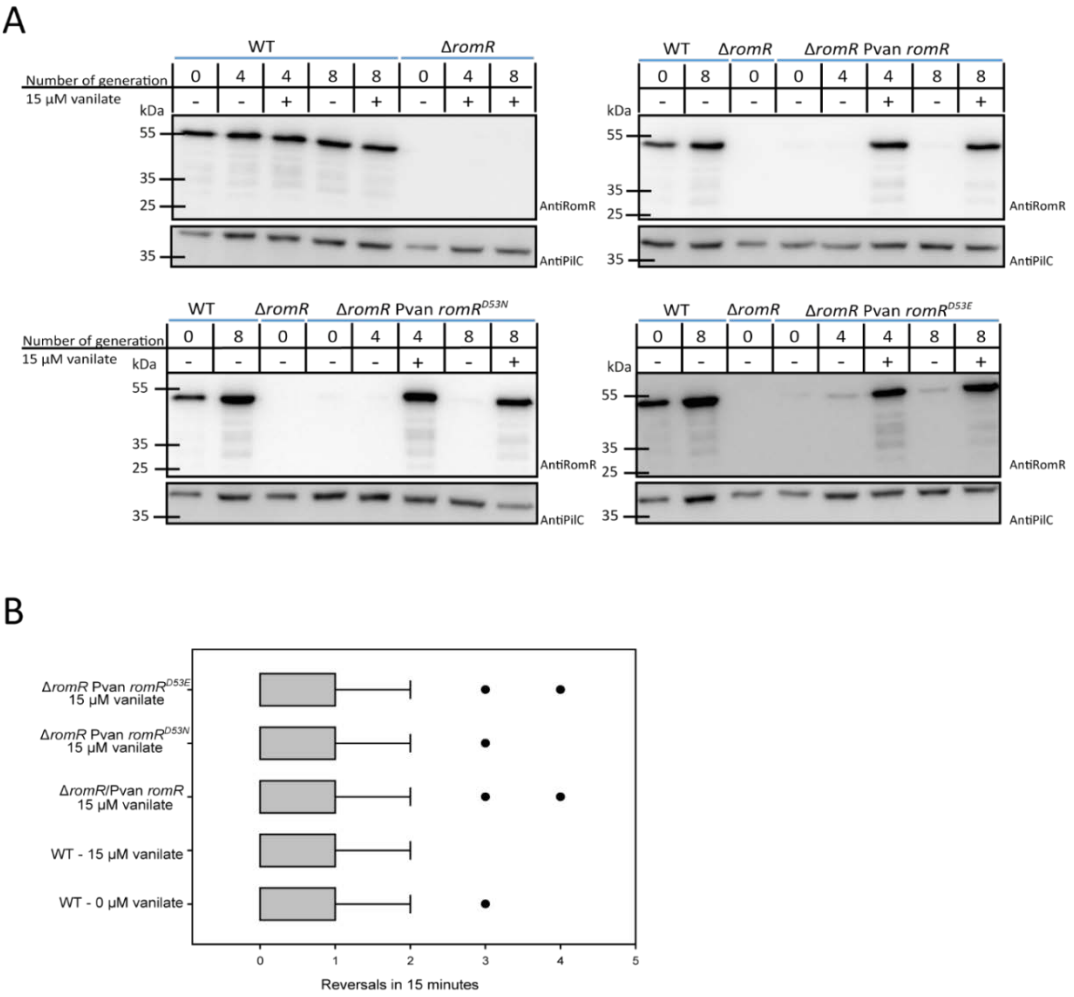

Figure 54. Mimicking or blocking phosphorylation site of RomR has no effect on the reversal frequency.

(A) Immunoblots of RomR. Details of experiment explained in text. Total protein (1 mg per lane) was separated by SDS–PAGE and analyzed by immunoblot using α-RomR. Immunoblot with α-PilC serves as a loading control.

(B) Reversal frequency of WT and selected mutants on 1.5% TPM agar. Shown are boxplots of the measured reversals of isolated cells for 15 min, boxes enclose the 25th and 75th percentile, whiskers represent the 10th and 90th percentile, and dots outliers. Δ*romR* was not moving as single cells in the tested conditions.

3. Discussion

To identify additional proteins that may regulate motility in *M. xanthus* we sought in 1611 prokaryotic genomes for genes with the same genomic distribution as *romR*. We identified two genes that encode uncharacterized proteins without any conserved domains that could indicate their function. These two proteins, named RomX and RomY, have not been identified before in screens for genes involved in gliding, T4P-dependent motility or regulation of reversals. We speculate that the small size of *romX* (264 bp) and *romY* (651 bp) decreases the possibility of random insertion during transposon mutagenesis. Therefore, bioinformatics analysis serves as a powerful tool to find new proteins potentially involved in different cellular processes.

3.1 RomX regulates cell polarity together with MglA, MglB and RomR

The small GTPase MglA regulates cell motility and polarity in a nucleotide-dependent manner. Active MglA-GTP localizes at the leading pole and stimulates motility while MglA-GDP is the inactive form and localizes diffusely throughout the cytoplasm. Moreover, MglA-GTP localizes to the focal adhesion complexes as an integral part of the gliding machinery. The nucleotide-bound state of MglA is regulated by the cognate GAP protein MglB that stimulates GTPase activity of MglA and mainly localizes to the lagging cell pole. Both proteins depend for their localization on the response regulator RomR (Leonardy *et al.*, 2010, Zhang *et al.*, 2010, Miertzschke *et al.*, 2011, Keilberg *et al.*, 2012, Patryn *et al.*, 2010, Treuner-Lange *et al.*, 2015, Zhang *et al.*, 2012).

Generally, *romX* is found in genomes that contain *mglA, mglB* and *romR* suggesting that RomX is functionally connected to MglA, MglB and RomR. In this study, we have shown that RomX is important for both motility systems. Furthermore, more detailed studies show that RomX is necessary for gliding motility and regulates reversals in the T4P-dependent motility system. Furthermore, epistasis experiments showed that RomX acts in the same pathway as MglA, MglB and RomR. Δ*romX* and Δ*romR* mutants share the same motility phenotype and the double deletion Δ*romR*Δ*romX* mutant did not show an additive phenotype. Strikingly, deletion of *mglB* partially restored gliding motility in the Δ*romX* and Δ*romR* mutants, suggesting that MglB acts downstream of RomX and RomR. Furthermore, epistasis experiments suggest that RomX and RomR have opposite function to MglB. Finally, strains that lack RomX or RomR and have MglA locked in the

GTP bound form show completely restored gliding motility and reversals. In conclusion, we suggest that RomX and RomR act upstream of MglB and MglA-GTP (Figure 55).

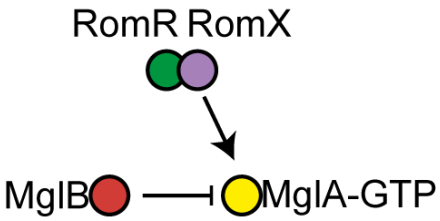

Figure 55. RomX together with RomR act upstream of MglB and MglA-GTP in the regulation of polarity in motility of *M. xanthus*.
Arrow shows stimulation while T-bar shows inhibition.

RomX localizes in a bipolar asymmetric pattern similarly to RomR. RomX polar localization depends on RomR, and MglA polar localization depends on RomX and RomR. However, RomR polar localization is RomX independent. MglA only binds to the cell pole in its active GTP bound form (Leonardy *et al.*, 2010, Zhang *et al.*, 2010, Keilberg *et al.*, 2012, Zhang *et al.*, 2012). MglA locked in the GTP-bound form ($MglA^{Q82A}$) localizes in a bipolar pattern; however, polar localization is strongly impaired in the absence of RomX and RomR. These data suggest that at the leading cell pole RomR binds RomX that, in turn, recruits MglA-GTP. To further investigate the possibility that RomX and RomR form a functional protein complex at the cell pole, we compared localization of RomR and RomX in the absence of MglA and MglB. Both, RomR and RomX localize mainly unipolar in the absence of MglA. This is a common pattern of localization of the motility regulatory proteins in the absence of MglA and was previously described for FrzS, MglB, RomR and MglC (Zhang *et al.*, 2012, Keilberg *et al.*, 2012, McLoon *et al.*, 2015). By contrast, in the absence of MglB, MglA, RomR and RomX change localization toward bipolar symmetric. These localization patterns support the idea that RomR and RomX form a complex at the cell pole. Furthermore, in pull-down experiments with purified proteins, RomR interacts with RomX and RomX interacts with MglA-GTP. Furthermore, the RomR/RomX complex interacts with MglA-GTP. Moreover, RomR does not interact with MglA-GTP and MglA-GDP. Together with the observations from bacterial two hybrid system, where direct interactions RomX-RomR and RomX-MglA were observed, we propose a model in which RomR binds to the leading pole and, in turn, recruits RomX. Next, the RomR/RomX complex binds MglA-GTP to form a RomR/RomX/MglA-GTP complex.

3.2 RomR/RomX complex acts as an MglA GEF

Epistasis analysis has shown that MglA-GTP acts downstream of RomX and RomR. Moreover, quantitative analysis of motility parameters (velocity and reversal frequency) of gliding cells showed no differences between *mglA*^{Q82A}, *mglA*^{Q82A}Δ*romX* and *mglA*^{Q82A}Δ*romR* mutants. Thus, the gliding motility defects caused by Δ*romX* and Δ*romR* mutations can be bypassed by high MglA-GTP concentration. Similarly, the defects in gliding motility in the absence of RomR or RomX are corrected in the absence of MglB. Based on these observations we hypothesized, that the RomR/RomX complex not only functions as a polar binding determinant of MglA-GTP but also plays a role in the regulation of the nucleotide-bound state of MglA. *In vitro* analyses with purified porteins demonstrated that neither RomR alone, RomX alone nor the RomR/RomX complex inhibit MglA GTP hydrolysis. Similarly, RomR and/or RomX do not inhibit MglB GAP activity. However, the RomR/RomX complex stimulates MglA nucleotide exchange. Thus, we conclude that the RomR/RomX complex is an MglA GEF. In total, the RomR/RomX complex has two functions. First, it has MglA GEF activity. Second, it binds MglA-GTP. *In vivo* both activities contribute to a high local concentration of MglA-GTP at the leading pole.

The interaction between GTPases and their cognate GEFs have been extensively studied in eukaryotes. In the current model, a GEF associates with the GDP-bound GTPase forming a low affinity complex. Upon nucleotide release, the GEF forms a high affinity complex with nucleotide free GTPase. Upon binding of GTP, a low affinity complex is formed again and, finally, the GEF is released (Bos *et al.*, 2007). The mechanism of the RomR/RomX GEF activity remains to be investigated. In particular, it will be interesting to investigate whether the catalytic part of the complex is formed by both proteins or whether one of the two proteins undergoes structural changes in the RomR/RomX complex in that way allowing it to function as a GEF. Of note, the active site of the TRAPP complex, which has Rab1 GEF activity, is assembled from several subunits (Cai *et al.*, 2008). Activation of a GEF by an interaction partner was described for the Ras GEF Sos that is activated by the interaction with the adaptor Grb2 (Aronheim *et al.*, 1994) and p115RhoGEF in which GEF activity is activated by interaction with subunits of heterotrimeric G proteins (Fukuhara *et al.*, 2001).

We have shown that RomR/RomX complex has two distinct activities with respect to MglA: GEF and binding of MglA-GTP at the leading cell pole. GEF proteins that also bind to their cognate small Ras GTPase in their GTP-bound form were described for some

eukaryotic GEFs. Detailed biochemical studies revealed that the interaction is part of a positive feedback loop and activates the GEF, in turn, leading to accumulation of GTPase-GTP (Margarit *et al.*, 2003, Menetrey *et al.*, 2007, Richardson *et al.*, 2012, Cohen *et al.*, 2007, Chen *et al.*, 2010, Lin *et al.*, 2006). So far, we do not have any evidence that RomR/RomX and MglA localization involves a similar positive feedback loop.

In eukaryotes, the GEFs of the five subfamilies of small GTPases are structurally unrelated. Interestingly, neither RomX nor RomR show sequence similarity to known GEF proteins. Therefore, the RomR/RomX complex may represent a new family of GEFs. Previously, it has been shown that the GAP of MglA, MglB, belongs to new group of GAPs proteins with a unique mechanism of stimulating GTP hydrolysis (Miertzschke *et al.*, 2011). Interestingly, MglA and MglB are widespread in prokaryotes (Keilberg *et al.*, 2012, Wuichet &Søgaard-Andersen, 2014) whereas RomR and RomX have a more narrow distribution, suggesting the existence of other GEFs for MglA-like proteins.

3.3 Formation of focal adhesion complexes depends on RomX and RomR

MglA-GTP is an integral part of focal adhesion complexes. MglA-GTP is incorporated into the focal adhesion complexes at the leading cell pole and focal adhesion complexes are disassembled at the lagging cell pole due to MglB GAP activity there (Zhang *et al.*, 2010, Patryn *et al.*, 2010, Keilberg *et al.*, 2012, Treuner-Lange *et al.*, 2015). Moreover, experiments with inactive MglA-GDP provided evidence that only active, MglA-GTP stimulates gliding motility (Leonardy *et al.*, 2010). In the non-gliding Δ*romX* and Δ*romR* mutants, MglA does not localize to focal adhesion complexes. Moreover, when we used AglZ-YFP as a readout for formation of the focal adhesion complexes, we confirmed lack of focal adhesion complex formation in the absence of RomX and RomR. We speculate that lack of gliding motility and focal adhesion complexes could be a result of non-sufficient MglA-GTP concentration. To test this hypothesis, we generated an in frame deletion of *mglB* in the backgrounds of *mglA-mVenus*Δ*romX*, *mglA-mVenus*Δ*romR* and *mglA-mVenus*Δ*romX*Δ*romR*. In the absence of MglB and RomX and/or RomR, we observed MglA-mVenus in the focal adhesion complexes. Moreover, we confirmed these observations by detecting AglZ-YFP in the focal adhesion complexes. Thus, RomX and RomR are necessary for focal adhesion complex formation only when the MglA nucleotide-bound state is tightly regulated by its cognate GAP MglB. Moreover, these data are in agreement with the analysis of gliding motility in single cells in which we observed partial recovery of the gliding motility in the double Δ*mglB*Δ*romX* and

Δ*mglB*Δ*romR* mutants. Also, these observations are consistent with our model in which RomR/RomX comples acts as an MglA GEF and stimulates MglA-GTP concentration at the leading cell pole and in focal adhesion complexes. These observations also suggest that a sufficient level of MglA-GTP accumulates in the absence of MglB, RomR and RomX to stimulate assembly of the gliding motility complexes. Along the same lines, even in the presence of MglB, a sufficiently high level of MglA-GTP accumulates to stimulate T4P-dependent motility.

3.4 RomX and RomR localize to the focal adhesion complexes

Quantification of the fluorescence signal of the MglB-mCherry fusion, which is only detected as a full-length protein in immunoblots, showed that more than 90% of MglB is localized diffusely in the cytoplasm. Based on this observation, we hypothesized that RomR/RomX complex may localize to the focal adhesion complexes to replenish MglA-GTP in case of MglB stimulated GTP hydrolysis by MglA. To this end, we observed that the motor protein AglQ colocalizes with RomX and AglZ colocalizes with RomR. All proteins are incorporated into the focal adhesion complexes at the leading cell pole and disassemble near lagging cell pole. Interestingly, in the double Δ*mglB*Δ*romR* mutant we did not observe RomX in the focal adhesion complexes. By contrast, RomR localizes to focal adhesion complexes in the Δ*mglB*Δ*romX* mutant. Furthermore, RomR localizes to focal adhesion complexes in the absence of RomX in the strain with MglA locked in the GTP bound form. Therefore, we speculate that RomR interacts directly with one or more of the cytoplasmic components of the gliding machinery. Additionally this data strongly suggest that RomR is a binding scaffold for RomX in the focal adhesion complexes. We conclude that RomX and RomR are new cytoplasmic components of the focal adhesion complexes; however, as opposed to all other proteins in these complexes, RomR and RomX are only essential for formation of these complexes in the presence of MglB.

3.5 RomX and RomR are important for attachment, stability and directionality of the focal adhesion complexes

Previously, the focal adhesion complexes were described to be assembled at the leading cell pole, stay stationary in the respect to the substratum in moving cell and disassemble near the lagging cell pole (Mignot *et al.*, 2007, Jakobczak *et al.*, 2015).

Recent studies also revealed clusters moving along the cell body. In moving cells, these clusters are assembled at the leading cell pole and move towards the lagging cell pole. In non-moving cells multiple dynamic focal adhesion complexes assemble at one cell pole and move to the opposite cell pole. Dynamic focal adhesion complexes are thought to be unattached motility complexes (Faure *et al.*, 2016).

Quantitative analysis of the movement of focal adhesion complexes within cells showed that in the absence of RomX and RomR in strains with high MglA-GTP concentration (Δ*mglB* mutants or with MglA locked in the GTP-bound form) these complexes are assembled and more motile than in WT. We would like to propose that these motile focal adhesion complexes do not produce or produce less force to propel a cell. Therefore, we speculate that RomX and RomR are important for the correct assembly of functional focal adhesion complexes. Moreover, in Δ*mglB*Δ*romX*, Δ*mglB*Δ*romR* and Δ*mglB*Δ*romX*Δ*romR* mutants we observe a shorter lifetime of the focal adhesion complexes. Therefore, RomX and RomR are also important for their stability. However, shorter lifetime can be explained by lower MglA-GTP concentration than in WT, as there is no effect on the stability of focal adhesion complexes in *mglA*^{Q82A}-*mVenus*Δ*romX* and *mglA*^{Q82A}-*mVenus*Δ*romR* mutants. We observe only partially restored gliding motility in the Δ*mglB*Δ*romX* and Δ*mglB*Δ*romR* mutants and fully restored gliding in *mglA*^{Q82A}Δ*romX* and *mglA*^{Q82A}Δ*romR* mutants, thus, we speculate that the main motility defect is coming from instability of the focal adhesion complexes. However, we cannot exclude the additive effect of the instability and intracellular mobility of the focal adhesion complexes.

Qualitative analysis of the focal adhesion complexes in the absence of *romX* and *romR* in the strains with elevated MglA-GTP concentration shows loss of the directionality. For some cells, we observe focal adhesion complexes that are assembled at the opposite cell poles and are moving in opposite directions. Loss of the directionality is observed in the strains with increased mobility of the focal adhesion complexes. However, it remains unclear, if increase of mobility leads to loss of directionality.

Taken together, we conclude that RomX and RomR by localizing to the focal adhesion complexes help to maintain their attachment, stability and directionality. It remains unclear whether the only role of RomR is to bring RomX to the focal adhesion complexes. Lack of attachment and loss of directionality of focal adhesion complexes are observed when RomX is absent and RomR is present in the focal adhesion complexes. It remains unknown how RomR/RomX complex binds to the focal adhesion complexes and

what the mechanism of action is to stimulate focal adhesion complexes attachment and directionality.

3.5 RomX/RomR establishes front-rear polarity, cell asymmetry and gliding motility by its triple function

We propose the following three functions of RomR and RomX: First, RomR binds RomX at the leading cell pole. Second, the RomR/RomX complex by its GEF activity stimulates the formation of a local pool MglA-GTP at this pole. RomR/RomX binds MglA-GTP forming a RomR/RomX/MglA-GTP complex at the leading cell pole. Third, the RomR/RomX/MglA-GTP complex is loaded onto the focal adhesion complexes. The RomR/RomX complex stimulates the stability of focal adhesion complexes by replenishing MglA-GTP in these complexes in case of MglB stimulated MglA GTPase activity. RomX or the RomX/RomR complex by a so far unknown mechanism is giving directionality and increases adhesion of the focal adhesion complexes. At the lagging cell pole, GTPase activity of MglA-GTP is stimulated by MglB, GTP is hydrolysed to GDP and focal adhesion complex is disassembled (Figure 56, A and B).

A

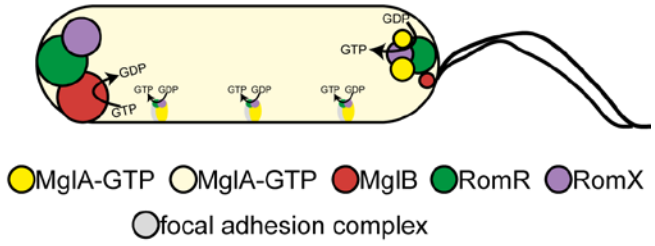

B

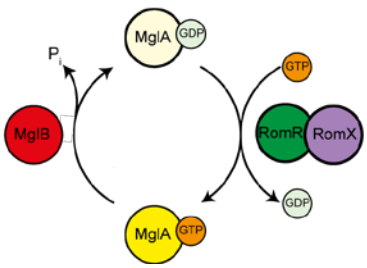

Figure 56. Model for RomX/RomR complex actions in the cell.
(A) Spatial organization of the motility regulatory proteins. Description in text. Arrow from GDP to GTP indicates RomR/RomX GEF activity on MglA. Arrow from GTP to GDP indicates hydrolysis of GTP by MglA stimulated by MglB.
(B) Model for MglA GTP/GDP cycle.

In eukaryotes, small Ras-like GTPases play an important role in regulation of cell polarity and motility and function in spatially organized manners (Jaffe & Hall, 2005, Charest & Firtel, 2007, Kortholt & van Haastert, 2008, Chiou *et al.*, 2017). Small GTPases may be spatially regulated by the colocalization with their cognate GEF. This has been described for Cdc42 and Cdc24 from *Saccharomyces cerevisiae* at the bud site (Chiou et al 2017) and for Rab5 and its cognate GEF Rabex-5 in the early endosomes (Blumer *et al.*, 2013). Alternatively, the activated GTPase colocalizes with its GEF(s) and is spatially separated from its cognate GAP, as is the case during invagination of epithelial cells during embryogenesis in *Drosophila* where the two Rho1 GEFs colocalize with Rho1 at the apical membrane while the single Rho1 GAP localizes to the basolateral membrane (Simões *et al.*, 2006). Thus, colocalization of MglA with the RomR/RomX complex, separation from MglB and spatial control of MglA activation are similar to mechanisms observed in eukaryotes. Particularly challenging question is how MglA, MglB, RomR and RomX become asymmetrically localized. For some of above described eukaryotic systems, positive feedback plays a crucial role in acquiring asymmetry. However, as mentioned before, there is no evidences for such a positive feedback loop for RomR/RomX and MglA. More detailed biochemical studies are required to get better insight into how asymmetry is established.

3.6 RomY regulates cell polarity together with MglA, MglB, RomR and RomX

Generally, *romY* occurs in genomes together with *mglA*, *mglB* and *romR* suggesting a functional connection to regulation of the cell motility. We confirmed our predictions by analyzing motility of an in-frame *romY* deletion strain. Lack of RomY causes formation of shorter flares on 0.5% agar and less single cells movement on 1.5% agar in comparison to WT. Thus, RomY seems to be important for regulation of motility rather than movement *per se*. Moreover, the finding that the Δ*romY* mutant hyper-reverses supports the hypothesis that RomY plays a role in regulation of the reversal frequency in both motility system. Epistasis experiment shows that RomY acts in the same pathways as MglA, MglB, RomR and RomX. Moreover, Δ*mglB* and Δ*romY* mutants share the same motility phenotype and the double Δ*mglB*Δ*romY* mutant does not show additive phenotype. Furthermore, quantitative reversal frequency analysis shows no statistically relevant difference between Δ*mglB*, Δ*romY* and Δ*mglB*Δ*romY* mutants. For Δ*romR*Δ*romY* and Δ*romX*Δ*romY* mutants, we observe partially restored gliding motility. Based on our previous studies on Δ*romX*Δ*mglB* and Δ*romR*Δ*mglB* mutants and

observations of the partial complementation of the gliding motility, we speculate that lack of RomY, similarly to lack of MglB, increases MglA-GTP concentration.

To further understand RomY function in the regulation of polarity we determined RomY localization dependencies. RomY localizes mainly at the lagging cell pole. Surprisingly, in the absence of RomY, MglA localizes mainly in the bipolar pattern. Furthermore, RomX shows strong shift towards bipolar symmetric localization in the absence of RomY. RomR, in the absence of RomY, does not show shift towards more symmetric localization, however we observe strongly increased signal from the cell body. Interestingly, similar localization changes for MglA, RomX and RomR we observe in the absence of MglB. Based on the data we thought of two possible mechanisms of RomY action: RomY stimulates MglB GAP activity or RomY has GAP activity on its own. However, we did not observe direct interaction between RomY and MglB. Of note, we are unable to exclude direct interactions between MglB and RomY based on the negative results from the bacterial two hybrid system. Nevertheless, we observe that polar localization of RomY strongly dependents on MglB suggesting a functional connection between these two proteins. Interestingly, we have found that RomY directly interacts with MglA and RomX. The function of the MglA-RomY interaction is unknown. RomY may stimulate GTPase activity directly or by interacting with MglA may stimulate MglB GAP activity. Further studies are necessary to identify the function of RomY in regulation of polarity. GTPase assay could also directly answer whether RomY is a GAP, directly stimulates MglA GTPase activity or stimulates MglB GAP activity.

In two (out of 28 species that *romY* was originally found) species *romY* is present without *mglB* arguing against the idea that RomY stimulates MglB GAP activity. Well described example of organism with *mglA*, *romR* and *romY* but without *mglB* is *Bdellovibrio bacteriovorus*. *B. bacteriovorus* is small predatory deltaproteobacterium, which invades other Gram-negative bacteria wherein it replicates. *Bdellovibrio* can encounter their prey by fast motility, driven by flagellum in liquid environment (Iida *et al.*, 2009), or by twitching motility driven by T4P on a solid surface. *B. bacteriovorus* does not show social T4P-dependent motility as in *M. xanthus*. *B. bacteriovorus* requires T4P for invasion into the prey cell periplasm. The Δ*mglA B. bacteriovorus* strain is hypo-piliated and unable to invade prey (Lambert *et al.*, 2011). *B. bacteriovorus* MglA ($MglA_{Bb}$) shares significant sequence similarity to MglA from *M. xanthus* ($MglA_{Mx}$) with 64% protein identity and 82% similarity (Milner *et al.*, 2014). Major difference is in a P-loop region that is important for GTP hydrolysis (Miertzschke *et al.*, 2011). The P-loop

region of $MglA_{Bb}$ contains a serine at residue 21; the corresponding G21S substitution in eukaryotic RAS proteins locks them in the GTP-bound form (Sei *et al.*, 2009). Moreover, $MglA_{Mx}^{G21V}$ is insensitive to MglB and thus locked in the GTP bound form (Miertzschke *et al.*, 2011). Taken all together, $MglA_{Bb}$ is most probably locked in the GTP bound state. Of course, we are not able to exclude that $RomY_{Bb}$ has GAP activity and by a mechanism that is different from that of MglB, stimulates $MglA_{BB}$ GTPase activity and thus $MglA_{Bb}$ cycles between GTP and GDP bound state. However, up to date the function of RomY in *B. bacteriovorus* is unknown.

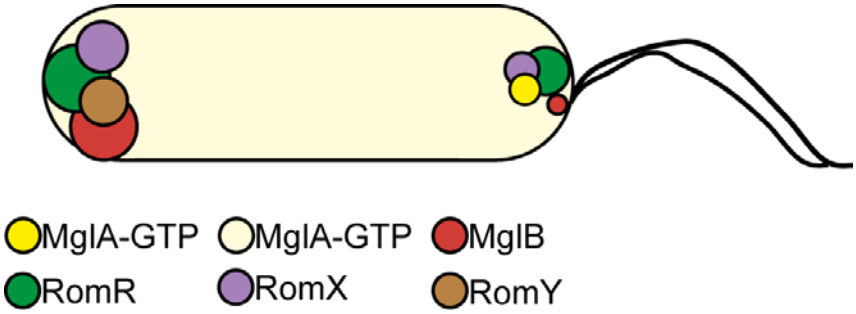

Figure 57. Model of polar localization of proteins involved in the regulation of motility in *M. xanthus*. Proteins colour on the model correspond to the colours in the legend.

In this study, we identified two new proteins that are important for the polarity of motility in *M. xanthus*, RomX and RomY. Furthermore, we have found that RomX and RomY show dynamic polar localization similarly to other proteins that are involved in the regulation of motility – RomR, MglA and MglB (Figure 57). All these proteins mutually depend on each other for the correct localization. We have shown that, two proteins localize to the cell pole independently – RomR and MglB. We hypothesize that MglB form directly or indirectly a localization landmark for RomY. We have shown that RomR recruits RomX, which, in turn, recruits MglA-GTP. So far, the exact mechanism how *M. xanthus* cells establish correct polarity and protein asymmetry remains unclear. Further protein interaction analysis together with extensive localization studies could be helpful in gaining detailed insight into regulation of polarity.

3.7 RomX and RomR are not essential for generating an output from the Frz system

RomR was previously thought to be the central output of the Frz system. However, direct connection between RomR and the Frz system is not known up to date (Leonardy *et al.*, 2007, Keilberg *et al.*, 2012, Guzzo *et al.*, 2015). Our detailed studies show that

Δ*romX* and Δ*romR* mutants do not glide but still show T4P-dependent movement on WT level, however they do not reverse. To test whether RomX or/and RomR may be essential for generating an output from the Frz system we took advantage of IAA that simulates Frz dependent reversals. On the population level, using motility assay as a read out, we have found that both Δ*romX* and Δ*romR* mutants respond to the IAA in the same way as WT. Moreover, analysis of single cells shows that reversals of the Δ*romX* and Δ*romR* mutants can be artificially increased by the addition of IAA. However, stimulation of reversals does not reach the WT level. Previously, it has been shown that Δ*romR* mutant is insensitive to the IAA. This observation was done by tracking oscillations of FrzS-YFP, protein important for T4P-dependent motility that localize mainly at the leading cell pole (Guzzo *et al.*, 2015). We suggest that lack of RomR decreases dynamic oscillations of FrzS and it cannot be correlated with cellular reversal. Moreover, our studies in which cells were growing for 24 hours on medium with the IAA clearly show that Δ*romR* and Δ*romX* mutants are IAA sensitive. The data does not definitively rule out that RomX and RomR are not a part of signal transduction from the Frz system. It has been shown that reversals of the Δ*frzZ* mutant, that lacks the output protein of the Frz system, could be induced by the IAA and this stimulation is at a lower level than for WT (Guzzo *et al.*, 2015). MglA-GTP at the leading cell pole is thought to play a regulatory role for Frz dependent reversals. In the current model of the Frz system dependent reversals, phosphorylated output of the Frz system (FrzZ) interacts at the leading pole with MglA-GTP and releases it from this cell pole (Kaimer & Zusman, 2013). We hypothesize that artificially increased activity of the Frz system and thus, high level of phosphorylated output(s) of this system, can bypass the absence of MglA-GTP at the leading cell pole in the Δ*romR* and Δ*romX* mutants.

RomR contains response regulator domain with putatively phosphorylable conserved aspartic acid residue (Leonardy *et al.*, 2007, Keilberg *et al.*, 2012). However, phosphorylation of RomR has not been shown and a kinase that could phosphorylate RomR is not known. Previously, it was hypothesized that the Frz system could phosphorylate RomR by an unknown mechanism. For many response regulators it was shown that phosphorylation of a conserved aspartic acid residue is required for activity (Stock *et al.*, 2000). Blocking phosphorylable residue by a mutation of aspartic acid (D) to the asparagine (N) results in loss of the ability of phosphorylation and thus, loss of activity. Mutation of aspartic acid (D) to glutamic acid (E) was shown to partially mimic phosphorylation state for some response regulators (Domian *et al.*, 1997). For *romR*

insertional mutant expressing *romR*^{D53N}*-gfp* under the control of the strong, constitutively active *pilA* promoter, no reversals were observed for 50 cells for 10 minutes. Phosphorylation mimicking mutant (*romR*::nptII P$_{pilA}$*romR*^{D53E}*-gfp)* has shown 1.5 fold more reversals than strain expressing *romR-gfp* (Leonardy *et al.*, 2007). Moreover, later studies with RomR-GFP variants expressed under the *pilA* promoter in the in frame *romR* deletion mutant have shown similar patterns. Blocking RomR phosphorylation resulted in hypo-reversing strain, however, some reversals were still observed. Mimicking of the RomR phosphorylation generated hyper-reversing strain but this effect was less prominent than in the previous studies (Keilberg *et al.*, 2012). We revisited function of potential RomR phosphorylation by testing motility phenotypes of mutants that express RomR variant that mimics phosphorylation or is blocked in the phosphorylation site.

Our population-based experiments show no differences between wild type version of RomR, RomR with blocked phosphorylation and mimicking phosphorylation for the T4P-dependent and gliding motility. In our experimental conditions, all three tested variants of RomR behave like WT. We confirmed our observations in two independent experiments in which we analyzed reversals of single gliding cells. We do not observe statistically significant differences in reversal frequency between WT and strains that express RomR, RomR^{D53N} and RomR^{D53E} as an only copy of RomR. Thus, RomR phosphorylation is not regulating reversal frequency under the conditions tested. Based on the data, we concluded that RomR is not essential for generating an output from the Frz system. In the experiment in which we induced *romR*, *romR*^{D53N} and *romR*^{D53E} over the time, we found that a low level of RomR causes cells to hypo-reverse. We hypothesize that strong overexpression of RomR may lead to the hyper-reversing cells. However, so far we do not have any experimental evidence to confirm this hypothesis, future studies with RomR overexpression could be performed to give directly answer whether RomR overexpression will lead to hyper-reversing cells. Nevertheless, we would like to propose that RomR concentration effect on the reversal frequency could explain previously published observations (Leonardy *et al.*, 2007, Keilberg *et al.*, 2012).

4. Materials and Methods

4.1 Chemicals, equipment and software

All chemicals, enzymes and kits are listed together with their suppliers in the Table 1. All devices together with their manufacturers and applications are listed in the Table 2. Specific softwares together with their manufacturers are listed in the Table 3.

Table 1. Reagents, enzymes, antibiotics and kits

Reagents	**Supplier**
Chemicals	Roth (Karlsruhe), Merck (Darmstadt), Sigma-Aldrich (Taufkirchen
Media components, agar	Roth (Karlsruhe), Merck (Darmstadt), Difco (Heidelberg), Invitrogen (Darmstadt)
Rabbit antisera	Eurogentec (Seraing, Belgium)
Goat anti-rabbit IgG, goat anti-rabbit IgG DyLight 549	Pierce/Thermo Scientific (Dreieich)
Anti-GFP monoclonal antibody Anti-mCherry	Roche Diagnostics GmbH (Mannheim) BioVision
Anti-mouse sheep IgG antibody, horseradish peroxidase linked	GE Healthcare Europe GmbH (Freiburg)
Nitrocellulose membrane	GE Healthcare Europe GmbH (Freiburg)
SDS gel electrophoresis size standards Pageruler™ Plus Prestained Protein Ladder	Pierce™ Thermo Scientific™ (Darmstadt)
Luminata Western HRP Substrate	Millipore Merck Chemicals GmbH (Schwalbach)
Oligonucleotides	Eurofins MWG Operon (Ebersberg) Invitrogen™ life technologies (Karlsruhe)
2-log DNA Ladder	New England Biolabs (NEB) (Frankfurt a. M.)
Enzymes	
Antarctic Phosphatase	New England Biolabs (Frankfurt a. M.)
T4 DNA Ligase	Fermentas (St. Leon-Rot)
restriction enzymes	Fermentas (St. Leon-Rot), New England Biolabs (Frankfurt a. M.)
5 PRIME MasterMix	5 PRIME GmbH (Hamburg)
Phusion High-Fidelity DNA Polymerase	Thermo Scientific (Dreieich)
Q5 High-Fidelity DNA Polymerase	New England Biolabs (Frankfurt a. M.)
Antibiotics	
kanamycin sulfate,	Roth (Karlsruhe)

ampicillin sodiumsulfate,	
gentamycin sulfate,	
oxytetracycline dehydrate,	
tetracycline hydrochloride	
Streptomycin sulfat	
Kits	
DNA purification (plasmid DNA), PCR purification, Gel purification	Zymo Research (Freiburg), Qiagen (Hilden), Macherey-Nagel (Düren)
DNA purification (chromosomal DNA)	Epicentre Biotechnologies (Wisconsin,USA)

Table 2. Equipment

Application	**Device**	**Manufacturer**
Cell disruption	Branson Sonifier 250, French pressure cell press	G. Heinemann (Schwäbisch Gmünd) SLM instruments (Urbana, IL)
Centrifugation	Centrifuge 5424, Centrifuge 5424 R, Multifuge X1R., Mega Star 1,6R	Eppendorf (Hamburg), Thermo Scientific (Dreieich), VWR International GmbH (Darmstadt)
PCR	Mastercycler personal, Mastercycler epgradient	Eppendorf (Hamburg)
Thermomixer	Thermomixer compact	Eppendorf (Hamburg)
DNA illumination	UVT_20 LE	Herolab (Wiesloch)
DNA illumination and documentation	E-BOX VX2 imaging system	Bio-Rad (München)
Protein electrophoresis	Mini-PROTEAN® 3 cell	Bio-Rad (München)
Western blotting	TransBlot®Turbo™ Transfer System, Hoefer™ TE77	Bio-Rad (München), Amersham (Freiburg)
Chemiluminescence detection	Luminescent image analyzer LAS-4000	Fujifilm (Düsseldorf)
Microscopes	MZ75 Stereomicroscope, M205FA Stereomicroscope, DM IRE2 Inverted microscope, DMi8 Inverted microscope, DMi6000B inverted microscope, DM6000B	Leica (Wetzlar)
Determination of optical densities,	Ultrospec 2100 pro Sprectrophotometer,	GE Healthcare Europe GmbH (Freiburg),

nucleic acids absorption	Nanodrop ND-1000 UV-Vis spectrophotometer, DS11+	Nanodrop (Wilmington), DeNovix Inc. (Wilmington)
Multifunktionsreared Infinite M200 pro with Monochromatoroptics	Detection of absorption changes during enzymatic assay	Tecan Deautschland GmbH (Crailsheim)
ÄKTA pure with Fraction collector F9-C -5 ml Strep Traap HP -5 ml HiTrap Q HP -5 ml MBPTrapHP -5 ml HITrap Chelating HP -HiLoad 16/600 Superdex 200 pg -HiLoad 16/600 Superdex 75 pg	Size, affinity purification of recombinant proteins, anion exchange chromatography, exclusion chromatography	GE Healthcare Europe GmbH (Freiburg)
Measuring of mant fluorescence	ISS PC1 spectrofluorometer with a cooled photomultiplier	ISS (USA)

Table 3. Software

Application	**Software**	Supplier
Data analysis of microscopy pictures	Metamorph® v 7.7.5.0, ImageJ 1.51s	Molecular Devices (Union City, CA), Wayne Rasband (National Institutes of Health, USA)
Automatic detection of cells on the microscopy pictures	Oufti	Jacobs-Wagner Lab (Paintdakhi *et al.*, 2016)
Automatic analysis of fluorescence signals	MATLAB R2016b	The MathWorks, Inc (Natcik, USA)
Checking of DNA and proteins sequences, in silico cloning of plasmids and data management of DNA, protein and plasmid sequences.	Vector NTI advance software, suite 11, DNASTAR	Invitrogen™ life technologies (Karlsruhe), DNASTAR, Inc (Madison, USA)
Preparation of kymograph and its analysis	Icy	Icy - copyright 2017 - Institut Pasteur (de Chaumont *et al.*, 2012)

4.2 Media

E. coli cells were cultivated in Luria-Bertani (LB) liquid media or on LB agar plates with 1.5% agar concentration. *M. xanthus* cells were cultivated in CTT media or on CTT

agar plates with 1.5% agar concentration. Motility assays of *M. xanthus* were performed on A- or S-motility plates. Media composition is described in Table 4.

Table 4. Growth media for *E. coli* and *M. xanthus*

Media	**Composition**
E. coli	
LB medium	1% (w/v) tryptone, 0.5% (w/v) yeast extract, 1% (w/v) NaCl
2 x YT	16 g Bacto tryptone, 5 g yeast extract, 5 g NaCl, pH 7.2
LB agar plates	LB medium, 1.5% (w/v) agar
M. xanthus	
CTT	1% (w/v) Bacto casitone, 10 mM Tris-HCl pH 8.0, 1 mM potassium phosphate buffer pH 7.6, 8 mM MgSO4
CTT agar plates	CTT medium, 1.5% agar
CTT soft agar	CTT medium, 0.5% agar
Motility assays	
A-motility plates (Hodgkin & Kaiser, 1977)	0.5% CTT, 1.5% agar
S-motility plates (Hodgkin & Kaiser, 1977)	0.5% CTT, 0.5% agar
Microscopy media	
TPM agar	10 mM Tris-HCl pH 7.6 1 mM KH2PO4 pH 7.6 8 mM MgSO4 1.5% agar
MC7	10 mM MOPS, pH 7.0, 1 mM CaCl2
Methylcellulose solution	MMC 1% methylcellulose
Chitosan 100x solution	2M acetic acid 15mg/ml chitosan

The adequate antibiotics were added to cultures when needed. For the protein induction in *E. coli* IPTG was added, for *M. xanthus* vanilate and for selection X-GAL or galactose were added (Table 5)

Table 5. Additives used for *E. coli* and *M. xanthus*

Additive	Final concentration	Dissolved in
E. coli		
Ampicillin sodium sulfate	100 µg/ml	H_2O
Tetracyclin	15 µg/ml	99.99% ethanol
Kanamycin sulfate	50 µg/ml	H_2O
5-Brom-4-chlor-3-indoxyl-β-D-galactopyranosid (X-gal)	40 µg/ml	Dimethylformamide
IPTG	1mM	H_2O
M. xanthus		
Kanamycin sulfate	50 µg/ml	H_2O
Oxytetracycline	10 µg/ml	0.1M HCl
Galactose	2.5%	H_2O
Isoamyl alcohol	0.03%-0.3%	
Vanilate	15µM-150µM	H_2O (adjusted to pH 7.6 with KOH)

4.3 Microbial methods

4.3.1 *E. coli* strains used in this study

Table 6. *E. coli* strains used in this study

Strain	Relevant characteristics	Source or reference
Mach1	ΔrecA1398 endA1 tonA Φ80ΔlacM15 ΔlacX74 hsdR(rK-mK+)	Invitrogen (Darmstadt)
TOP10	F- mcrA Δ(mrr-hsdRMS-mcrBC) Φ80lacZΔM15 ΔlacX74 recA1 araD139 Δ(ara leu) 7697 galU galK rpsL (StrR) endA1 nupG	Invitrogen™ life technologies (Karlsruhe)
BTH101	F- cya-99 araD139 galE15 galK16 rpsL1 (StrR) hsdR2 mcrA1 mcrB1	Euromedex, (Souffelweyersheim, France)
Rosetta 2 (DE3)	F-ompT hsdSB(rB-mB-) gal dcm(DE3) pRARE2(CmR)	Novagen/Merck (Darmstadt)

4.3.2 *M. xanthus* strains used in this study

For strains containing plasmid integrated at the Mx8 *attB* site, the gene expressed including promoter driving the expression is indicated in brackets.

Table 7. *M. xanthus* strains used in this study

Strain	Genotype	Source or reference
DK1622	Wild type	(Kaiser, 1979)
DK10410	Δ*pilA*	(Wu & Kaiser, 1996)
SA5293	Δ*algQ*	(Jakobczak *et al.*, 2015)
SA3683	Δ*romX*	Daniela Keilberg
SA6974	Δ*romX*, Δ*pilA*	This work
SA7123	Δ*romX*, Δ*aglQ*	Anna Potapova
SA5990	Δ*romX*; *attB::*pDK131 (P_{nat}*romX-yfp*)	Daniela Keilberg
SA6997	Δ*romX*; *attB::*pDK157 (P_{nat} *romX*)	Daniela Keilberg
SA3300	Δ*romR*	(Keilberg *et al.*, 2012)
SA9676	Δ*romR*, Δ*pilA*	This work
SA7110	Δ*romR*, Δ*algQ*	Anna Potapova
SA8802	Δ*frzE*	Dorota Skotnicka
SA7135	Δ*frzE*, Δ*algQ*	Anna Potapova
SA4420	Δ*mglA*	(Miertzschke *et al.*, 2011)
SA3387	Δ*mglB*	(Leonardy *et al.*, 2010)
SA6300	Δ*mglA*, Δ*romX*	Daniela Keilberg
SA3615	Δ*mglB*, Δ*romX*	Daniela Keilberg
SA3619	Δ*romR*, Δ*romX*	Daniela Keilberg
SA3936	Δ*mglB*, Δ*romR*	(Keilberg *et al.*, 2012)
SA3631	Δ*mglA*, Δ*romX*; *attB::*pDK131 (P_{nat}*romX-yfp*)	Daniela Keilberg
SA3635	Δ*mglB*, Δ*romX*; *attB::*pDK131 (P_{nat}*romX-yfp*)	Daniela Keilberg
SA3633	Δ*romR*, Δ*romX*; *attB::*pDK131 (P_{nat}*romX-yfp*)	Daniela Keilberg
SA3636	Δ*romY*, Δ*romX*; *attB::*pDK131 (P_{nat}*romX-yfp*)	Daniela Keilberg
SA8185	*mglA-mVenus*	Luis Carreira
SA7593	Δ*mglB*, *mglA-mVenus*	Luis Carreira
SA8369	Δ*romR*, *mglA-mVenus*	Luis Carreira
SA7580	Δ*romX*, *mglA-mVenus*	Luis Carreira
SA7577	Δ*romY*, *mglA-mVenus*	Luis Carreira

SA6963	*mglB-mCherry*	(Keilberg *et al.*, 2012)
SA3971	Δ*mglA*, *mglB-mCherry*	(Keilberg *et al.*, 2012)
SA3966	Δ*romR*, *mglB-mCherry*	(Keilberg *et al.*, 2012)
SA6935	Δ*romX*, *mglB-mCherry*	This work
SA6911	Δ*romY*, *mglB-mCherry*	This work
SA7507	*romR-mCherry*	Luis Carreira
SA7579	Δ*mglA*, *romR-mCherry*	Luis Carreira
SA8308	Δ*mglB*, *romR-mCherry*	Luis Carreira
SA8172	Δ*romX*, *romR-mCherry*	Luis Carreira
SA8306	Δ*romY*, *romR-mCherry*	Luis Carreira
SA3833	$mglA^{Q82A}$	(Keilberg *et al.*, 2012)
SA8183	$mglA^{Q82A}$*-mVenus*	Luis Carreira
SA8191	Δ*romR*, $mglA^{Q82A}$*-mVenus*	Luis Carreira
SA8190	Δ*romX*, $mglA^{Q82A}$*-mVenus*	Luis Carreira
SA7108	$mglA^{Q82A}$, Δ*romR*	Anna Potapova
SA6962	$mglA^{Q82A}$, Δ*romX*	This work
SA6960	$mglA^{Q82A}$, Δ*romX; attB::*pDK131 (P_{nat}*romX-yfp*)	This work
SA6957	$mglA^{Q82A}$, Δ*romR*, Δ*romX; attB::*pDK131 (P_{nat}*romX-yfp*)	This work
SA7113	$mglA^{Q82A}$, Δ*romR*; *attB::* pSH700 (P_{pilA}*romR-gfp*)	Anna Potapova
SA6958	$mglA^{Q82A}$, Δ*romX*, Δ*romR*; *attB::* pSH700 (P_{pilA}*romR-gfp*)	This work
SA6932	Δ*romR*; *attB::* pSH700 (P_{pilA}*romR-gfp*)	This work
SA6984	Δ*romX*, Δ*romR*, *mglA-mVenus*	This work
SA6985	Δ*mglB*, Δ*romX*, *mglA-mVenus*	This work
SA6996	Δ*mglB*, Δ*romR*, *mglA-mVenus*	This work
SA6986	Δ*mglB*, Δ*romX*, Δ*romR*, *mglA-mVenus*	This work
MxH2262	Δ*aglZ*	(Zhang *et al.*, 2010)
SA6987	*aglZ::aglZ-yfp* (pSL65)	This work
SA9100	Δ*mglB*, *aglZ::aglZ-yfp* (pSL65)	This work
SA6990	Δ*romR*, *aglZ::aglZ-yfp* (pSL65)	This work
SA6988	Δ*romX*, *aglZ::aglZ-yfp* (pSL65)	This work
SA6994	Δ*mglB*, Δ*romR*, *aglZ::aglZ-yfp* (pSL65)	This work
SA6993	Δ*mglB*, Δ*romX*, *aglZ::aglZ-yfp* (pSL65)	This work

SA6995	Δ*mglB*, Δ*romR*, Δ*romX*, *aglZ::aglZ-yfp* (pSL65)	This work
SA6948	*AglQ-mCherry*, Δ*romX; attB::*pDK131 (P_{nat}*romX-yfp*)	This work
SA6980	*romR-mCherry*, *algZ::algZ-yfp* (pSL65)	This work
SA6989	Δ*romR*, Δ*mglB*, Δ*romX; attB::*pDK131 (P_{nat}*romX-yfp*)	This work
SA6983	Δ*mglB*, Δ*romX*, *romR-mCherry*	This work
SA6931	Δ*romR*; *attB::*pDSZ10 (P_{pilA}*RomR*^{D53N}*-gfp*)	This work
SA6934	Δ*romR*; *attB::*pDSZ11(P_{pilA}*RomR*^{D53E}*-gfp*)	This work
SA6944	Δ*romR*; *mxan18-19::*pDSZ16 (P_{van}*romR*)	This work
SA6945	Δ*romR*; *mxan18-19::*pDSZ17(P_{van}*romR*^{D53N})	This work
SA6946	Δ*romR*; *mxan18-19::*pDSZ18 (P_{van}*romR*^{D53E})	This work
SA5958	Δ*romY*	Daniela Keilberg
SA6901	Δ*romY; attB::*pDK132 (P_{nat}*romY-yfp*)	This work
SA3626	Δ*mglA*, Δ*romY*	Daniela Keilberg
SA3630	Δ*mglB*, Δ*romY*	Daniela Keilberg
SA3621	Δ*romR*, Δ*romY*	Daniela Keilberg
SA5792	Δ*romX*, Δ*romY*	Daniela Keilberg
SA6913	Δ*mglA*, Δ*romY; attB::*pDK132 (P_{nat}*romY-yfp*)	This work
SA6903	Δ*mglB*, Δ*romY; attB::*pDK132 (P_{nat}*romY-yfp*)	This work
SA6908	Δ*romR*, Δ*romY; attB::*pDK132 (P_{nat}*romY-yfp*)	This work
SA6912	Δ*romX*, Δ*romY; attB::*pDK132 (P_{nat}*romY-yfp*)	This work

4.3.3 Cultivation and storage of *E. coli* and *M. xanthus*

E. coli strains were grown in LB liquid media with 230 rpm horizontaly shaking at 37 °C or on LB agar plates at 37 °C, strain BTH 101 was grown on LB agar plates at 30 °C. The optical densities of cultures were determined photometrically at 600 nm. Glycerol

stocks for long storage were made with overnight culture by adding glycerol to the final concentration of 10%, freezing in liquid nitrogen and stored at -80 °C.

M. xanthus cells were grown on CTT agar plates at 32 °C in dark with appropriate antibiotics when necessary. For the liquid cultures, cells were harvested from the plate, resuspended in 1 ml of CTT and then transferred to the bigger volume of media. Liquid cultures were incubated with horizontal shaking 220 rpm at 32 °C. The optical density of *M. xanthus* cultures were determined photometrically at 550 nm. Glycerol stocks for long storage were made with exponentially growing culture of *M. xanthus* by adding the glycerol to final concentration 4%, freezing in liquid nitrogen and stored at -80 °C.

4.3.4 Bacterial Two Hybrid Assay (BACTH)

The Bacterial Two Hybrid system (Karimova *et al.*, 2005) was used in this studies to detect direct interactions between two proteins of interest in heterologous system in *E. coli*. Plasmids containing the T18 (pUT18 and pUT18C) and the T25 (pKT25 and pKNT25) fragment of the *Bordetella pertussis* adenylate cyclase gene were provided by the manufacturer (Euromedex, Souffelweyersheim, France). Prepared plasmids contain N-terminal or C-terminal fusions of genes of interest to T18 or T25 fragment of the adenylate cyclase. For the assay chemi-competent cell of BTH101 strain, lacking the *cyaA* gene, encoding the catalytic domain of the adenylate cyclase, were transformed with two plasmids as described by the manufacturer. Cells of reporter strain BTH101 do not produce cyclic adenosine monophosphate (cAMP). *In vivo* protein-protein interaction expressed from transformed plasmids can restore the activity of adenylate cyclase from Bordetella pertussis in E. coli BTH 101 reporter strain and produces cAMP. cAMP production leads to activity of the *lac*-operon and production of β-galactosidase. The enzyme cleaves present in growth medium X-gal, which allows for blue-white screening of colonies. To test for interactions, plasmids containing gene of interest fused with T18 fragment were used as a bait and co-transformed with a plasmid containing the second gene of interest fused to the T25 fragment. For transformation 10 ng to 25 ng of plasmid DNA were used. Co-transformed cells were plated on LB agar plates containing 100 μg/ml ampicillin, 50 μm/ml kanamycin and 1 mM IPTG. For comparison, for each screen the plasmids pUT18C-Zip and pKNT25-Zip were co-transformed as a positive control. Additionally each plasmid used used in the screen was co-transformed with pUTC-Zip or pKNT25-Zip as a negative control. Plates were incubated on 30 °C for 48 h. For direct comparison 3 corresponding colonies of each co-transformationplate were inoculated in 0.5 ml LB medium containing 100 μg/ml ampicillin, 50 μm/ml kanamycin and 1 mM

IPTG and incubated for 3 h shaking at 37 °C. After incubation 5 µl of each culture were spot with all the controls on the same LB agar plate containing 100 µg/ml ampicillin, 50 µm/ml kanamycin, 1 mM IPTG and 40 µg/ml X-gal. Plate were incubated on 30 °C for 48 h. Pictures were acquired before and after additional incubation of plates at 4 °C for 24 h and 48 h to enhance the blue color of positive colonies.

4.3.5 Motility assays for *M. xanthus*

For motility assay, *M. xanthus* cells from exponentially growing cultures were harvested at 4700 rpm for 10 min and resuspended in 1% CTT to density of 7×10^9 cells/ml. 5 µl aliquots of the resuspension were spotted on 0.5% CTT supplemented with 0.5% for T4P-dependent motility (S-motility) and 1.5% agar for gliding motility (A-motility) and incubated in dark at 32 °C. After 24h, colony morphology and colony edges were observed using a Leica MZ75 Stereomicroscope or Leica M205FA Stereomicroscope and visualized using Leica DFC280 and Hamamatsu ORCA-flash V2 Digital CMOS cameras, respectively. Additionally, on 1.5% agar colonies edges were observed using Leica DM IRE2 Inverted microscope or Leica DM6000B microscope and visualized by Leica DFC280 and Photometrics Cascade II 1024 EMCCD cameras, respectively.

4.3.6 Reversal frequency assay for *M. xanthus* on 1.5% agar, 0.5% CTT

For reversal frequency assay, 5 µl of the exponentially growing overnight culture was spotted on 0.5% CTT supplemented with 1.5% agar, covered by cover slide and incubated in dark at 32 °C. After 4 to 6h, cells were observed using Leica DMi 6000B inverted microscope or Leica DM 6000B or Leica DMi8 microscope microscope and visualized using Hamamatsu Flash 4.0 sCMOS, Photometrics Cascade II 1024 EMCCD and Leica DFC9000 GT cameras, respectively. Cells were recorded for 15 min at 30 s intervals. Analysis was done in Metamorph (Molecular Devices) and ImageJ (Wayne Rasband).

4.3.7 Reversal frequency assay for *M. xanthus* moving by the T4P-dependent motility

For T4P-dependent reversal frequency assay, 5 µl of the exponentially growing overnight culture was spotted into the 24 polystyrene well-plate (Falcon; Sarsted). After 10 minutes incubation in the dark at room temperature cells were covered with 500 µl of 1% methylcellulose in the MMC buffer (10 mM MOPS pH 7.6, 4 mM $MgSO_4$, 2 mM $CaCl_2$). Next, plates were incubated in the dark at room temperature for 30 min. Cells

were observed using Leica DM IRE2 Inverted microscope or Leica DMi8 microscope and visualized by Leica DFC280 and Leica DFC9000 GT. Cells were recorded for 10 min at 20 s intervals. Analysis was done in Metamorph (Molecular Devices) and ImageJ (Wayne Rasband).

4.3.8 Trypan blue and congo red dyes binding assay

To determine ability of *M. xanthus* to bind tryphan blue and congo red dyes plate assay was carried out. Cells from exponentially growing culters were harvested at 4700 rpm for 10 min and resuspended in 1% CTT to density of 7×10^9 cells/ml. 10 µl aliquots of resuspension were spotted on 0.5% CTT supplemented with 0.5% agar and 20 µg/ml trypan blue or 40 µg/ml congo red. Plates were incubated at 32 °C for 24h.

4.3.9 Epifluorescence microscopy

For epifluorescence microscopy, *M. xanthus* cells were placed on a thin 1.5 % agar pad buffered with TPM buffer (10 mM Tris-HCl pH 8.0, 1 mM potassium phosphate buffer pH 7.6, 8 mM MgSO4) on a glass slide and immediately covered with a coverslip. After 30 min incubation in the dart at 32 °C cells were observed using temperature controlled (32 °C) Leica DMi8 and visualized with Hamamatsu ORCA-flash V2 Digital CMOS camera. Cells on the phase contrast images were automatically detected in Oufti (Jacobs-Wagner Lab). Next, fluorescence signal for segmented cells were analyzed by custom Matlab (The MathWorks) script. Script detects polar clusters only if they have average fluorescence higher than mean of the cytoplasmic fluorescence plus two standard deviations of the cytoplasmic fluorescence and it is bigger than three pixels. Total fluorescence of the polar clusters and cytoplasm was recalculated as a percent of the total cell fluorescence. The data was plotted as a fluorescence at the pole 1 in the function of fluorescence at the pole 2 while pole 1 was always the polar cluster with higher fluorescence. Additionally, omega value that represents asymmetry between the polar clusters was calculated from the equation:

$$\omega = \frac{total\ fluorescence\ at\ pole\ 1 - total\ fluorescence\ at\ pole\ 2}{total\ fluorescence\ at\ pole\ 1 + total\ fluorescence\ at\ pole\ 2}$$

Omega value is between 0 (bipolar symmetric) and 1 (unipolar localization). The localization patterns were determined from omega value: unipolar ($\omega > 0.9$), bipolar asymmetric ($0.9 > \omega > 0.2$) and bipolar symmetric ($\omega < 0.2$). Diffuse localization was determined when script was not able to detect any polar cluster that fulfilled mentioned before criteria.

For the time-laps epifluorescence microscopy, cells were prepared as for snap shots analysis. Time-lapses were taken for 15 min with time resolution 30 s. Data was processed with Metamorph (Molecular Devices) and ImageJ (Wayne Rasband).

4.3.10 Tirf microscopy

For tirf microscopy, 50 – 150 µl of *M. xanthus* overnight, exponentially growing culture was diluted in 1 ml of the MC7 buffer (10 mM MOPS pH 7.0, 1 mM $CaCl_2$) and spotted on the chitosan coated glass and visualized after 10 min of incubation at room temperature in the dark. Chitosan coated glass was prepared as described in (Ducret *et al.*, 2013) with further modifications. Freshly prepared chitosan 100x counting solution (15 mg/ml chitosan in 2 M acetic acid) diluted 100 fold with deionized water was used for coating the µDish (IBIDI GMBH, Martinsried). 1 ml solution was incubated in the µDish for 30 min. Then, chitosan solution was removed, µDish washed with 1 ml of deionized water and 1 ml of the MC7 buffer. Cells were observed with Leica DMi8 inverted microscope with a 100x flat field apochromatic oil-immersion objective (NA=1.47) and dual color laser Leica AM TIRF MC (488 nm solid state laser used for YFP and mVenus and 561 diode laser used for mCherry imagining) and visualized with Hamamatsu ORCA-flash V2 Digital CMOS camera. TIRF images and time-lapses were taken with penetration depth of 110 nm. For the time lapses, cells were observed for 10 min with the time resolution of 20 s. Active autofocus was used to correct any changes in the objective – sample distance. Obtained data was further processed with Metamorph (Molecular Devices) and ImageJ (Wayne Rasband) and analyzed in ICE (Institut Pasteur). ICE was used to create and analyze kymographs.

4.4 Molecular biology methods

4.4.1 Plasmids and oligonucleotides

All oligonucleotides that were used in this study are listed in Table 8. Underlined sequences display restriction sites used for cloning. All plasmids used in this study are listed in Table 9.

Table 8. Oligonucleotides used in this study

Name	Sequencce (5'-3')	Purpose
RomR fw pSW105	ATCGAAGCTTATGCCCAAGAATCTGCTGG	Amplification of *romr-gfp* to clone to pSW105
GFP rv	ATCGGAATTCTTACTTGTACAGCTCGTCCAT	

RomR fw pMR	ATCGCATATGCCCAAGAATCTGCTGGTCGC	Amplification of the full length *romR*
RomR rv stop	ATCGGGAATTCGATCAGTGCTGGGTCTCTCGGTCCTTGA	
BTHRomRfw	TCGGTCTAGAGATGCCCAAGAATCTGCTGGTCGC	Amplification of the receiver domain of *romR*
BTHRecrv	ATCGGGAATTCGACACCTTGTCGAGCAGCACCTGG	
BTHGlufw	ATCGGTCTAGAGATGGCCGCGGATGGGGGC	Amplification of the C-terminal domain of *romR*
BTHRomR rv stop	ATCGGGAATTCGATCAGTGCTGGGTCTCTCGGTCCTTGA	
romX E	GAGGCTCCGTCCGAGCCGGG	Primers used for verification of *romX* deletion
romX F	CTTCTGGAGCGCCACCAGCGC	
RomY E	GGGCGGATGAGCGCCTTGCCCAGC	Primers used for verification of *romY* deletion
RomY F	TCTCGCGCGCCTCCGCGCGG	
romR E	GGAGGCGCTGCCGCACC	Primers used for verification of *romR* deletion
RomR F	GGCCCGGTACATCAGGCC	
pilaF2	CAGCAGTCCGTAGACCTGGC	Primers used for verification of *pilA* deletion
PilaE	CGCTTCCGGCCGCAGCACGG	
pilaH	CGATCACCCAGTCATCGAAG	
pilaG	CCTGGCCGCCATCGCCATCC	
MglBfwsur	ATCGGAAGCTTGCGTGAAGCCCTCATAGGTGAGC	Primers used for verification of *mglb* deletion or integration of *mglB-mcherry*
MglB sur rv	ATCGGGAATTCTCGCGCTTGTTGTACTGGA	
int18-19C forw	CCCACGGAGAGCTGCGTGAC	Primers used to verify integration at 18-19 site
int18-19C rev	GAGAAGGGTGCCGTCACGTC	
int18-19P forw	CGCAAGGCGACAAGGTGCTG	
int18-19P rev	CCCTGGCCGCCATTCGTAAC	
attB right	GGAATGATCGGACCAGCTGAA	Primers user to verify integration at Mx8 phage attachment site
attB left	CGGCACACTGAGGCCACATA	
attP right	GCTTTCGCGACATGGAGGA	
attP left	GGGAAGCTCTGGGTACGAA	
M13 uni (-43)	AGGGTTTTCCCAGTCACGACGTT	Sequencing primers
M13 rev (-49)	GAGCGGATAACAATTTCACACAGG	
KA254	GTGCGCACCTGGGTTGGCATGCG	
pKT25fw	GGCGATTCGGTGACCGATTA	
pUT18frow	TCCGGCTCGTATGTTGTGTG	
pUT18V-fw	CTGGAAACGGTGCCGGCGTC	

Table 9. Plasmids used in this study

Plasmid	Description	Reference
pSW105	P_{pilA}, kan^R	S. Weiss (MPI Marburg)
pSWU30	tet^R	(Wu *et al.*, 1997)
pMR3691	P_{van}, tet^R	(Iniesta *et al.*, 2012)
pBJ114	Kan^R, galK	(Julien *et al.*, 2000)
pDK94	pBJ114; in frame deletion of *romX*, kan^R	Daniela Keilberg, PhD thesis, 2013
pDK95	pBJ114; in frame deletion of *romY*, kan^R	Daniela Keilberg, PhD thesis, 2013
pSL37	pBJ114; in frame deletion of *romR*, kan^R	(Keilberg *et al.*, 2012)
pES2	pBJ114; in frame deletion of *mglB*, kan^R	(Leonardy *et al.*, 2010)
pDK145	pBJ114; in frame integration of *mglB-mCherry*, kan^R	(Keilberg *et al.*, 2012)
pSL65	pBJ114; in frame integration of *aglZ-yfp*, kan^R	(Leonardy *et al.*, 2010)
pLC32	pBJ114; in frame integration of *romR-mCherry*, kan^R	Luis Carreira
pMAT162	pBJ114; in frame deletion of *pilA*, kan^R	Anke Treuner-Lange
pDK131	pSW105; P_{nat}*romX-yfp*	Daniela Keilberg
pDK132	pSW105; P_{nat}*romY-yfp*	Daniela Keilberg
pDK157	pSWU30; P_{nat}*romX*	Daniela Keilberg
pSH700	pSW105; P_{pilA}*romR-gfp*	(Keilberg *et al.*, 2012)
pDSZ10	pSW105; $P_{pilA}RomR^{D53N}$-GFP	This work
pDSZ11	pSW105; $P_{pilA}RomR^{D53E}$-GFP	This work
pDSZ16	pMR3691; P_{van}*romR*	This work
pDSZ17	pMR3691; $P_{van}romR^{D53N}$	This work
pDSZ18	pMR3691; $P_{van}romR^{D53E}$	This work
pTM1	Overexpression MglA-His_6	(Zhang *et al.*, 2010)
pTM2	Overexpression His_6-MglB	(Zhang *et al.*, 2010)
pTB005	Overexpression His_6-RomX	Tobias Bender
pDK28	Overexpression MalE-RomR	(Keilberg *et al.*, 2012)
pAH159	Overexpression of Strep-RomX	Andrea Harms
pUT18	amp^R	Euromedex (France)
pUT18C	amp^R	Euromedex (France)
pKT25	kan^R	Euromedex (France)
pKNt25	kan^R	Euromedex (France)
pDK70	MglA (pKNT25)	(McLoon *et al.*, 2015)
pDK143	MglA (pKT25)	Daniela Keilberg
pDK76	MglA (pUT18)	Daniela Keilberg
pDK75	MglA (pUT18C)	(McLoon *et al.*, 2015)
pDK71	MglB (pKNT25)	(McLoon *et al.*, 2015)
pDK142	MglB (pKT25)	Daniela Keilberg
pDK77	MglB (pUT18)	Daniela Keilberg

pDK74	MglB (pUT18C)	(McLoon *et al.*, 2015)
pDK119	RomR N-terminal receiver (pKNT25)	(McLoon *et al.*, 2015)
pDK138	RomR N-terminal receiver (pKT25)	Daniela Keilberg
pDSZ13	RomR N-terminal receiver (pUT18)	This work
pDK114	RomR N-terminal receiver (pUT18C)	(McLoon *et al.*, 2015)
pDK110	RomR C-terminal (pKNT25)	(McLoon *et al.*, 2015)
pDSZ12	RomR C-terminal (pKT25)	This work
pDK117	RomR C-terminal (pUT18)	Daniela Keilberg
pDK111	RomR C-terminal (pUT18C)	(McLoon *et al.*, 2015)
pDK126	RomR Pro-rich linker (pKNT25)	(McLoon *et al.*, 2015)
pDK139	RomR Pro-rich linker (pKT25)	Daniela Keilberg
pDK126	RomR Pro-rich linker (pUT18)	Daniela Keilberg
pDK127	RomR Pro-rich linker (pUT18C)	(McLoon *et al.*, 2015)
pDK118	RomX (pKNT25)	Daniela Keilberg
pDK140	RomX (pKT25)	Daniela Keilberg
pDK113	RomX (pUT18)	Daniela Keilberg
pDK107	RomX (pUT18C)	Daniela Keilberg
pDK112	RomY (pKNT25)	Daniela Keilberg
pDK141	RomY (pKT25)	Daniela Keilberg
pAP7	RomY (pUT18)	Anna Potapova
pDK115	RomY (pUT18C)	Daniela Keilberg

4.4.2 Plasmids construction

Genomic DNA of *M. xanthus* DK1622, SA3980 or SA3981 was used to amplify DNA fragments. Plasmid construct were transformed to *E. coli* Mach1 or TOP10 cells. Purified plasmids were sequenced by the Eurofins MWG Operon (Eldersber) company to verify the correct sequences. Sequencing results were analyzed using ContigExpress from the VectorNTI advance suite 11 software (Invitrogen) or with SeqMan Pro from DNASTAR (DNASTAR) software package.

The plasmids pDSZ10 and pDSZ11 are derivatives of pSW105 and were generated for the expression of *romR*^{D53N}*-gfp* and *romR*^{D53E}*-gfp* under the control of the strong, constitutively active promotor. To amplify *romR*^{D53N}*-gfp* genomic DNA of SA3980 and primers “RomR fw pSW105” and “GFP rv” were used. To amplify *romR*^{D53E}*-gfp* genomic DNA of SA3981 and primers “RomR fw pSW105” and “GFP rv” were used. The products were cloned with *HindIII*/*EcoRI* sites to pSW105.

The plasmids pDSZ16, pDSZ17 and pDSZ18 are derivatives pf pMR3691 and were generated for the expression of *romR*, *romR*^{D53N} and *romR*^{D53E} under control of the inducible promotor. Genomic DNA of DK1622, SA3980 and SA3981 were used

respectively. To amplify *romR*, *romR*^{D53N} and *romR*^{D53E} "RomR fw pMR" and "RomR rv stop" primers were used. The products were cloned at the *NdeI*/*EcoRI* sites to pMR3691.

The plasmid pDSZ12 and pDSZ13 are derivatices of pUT18 and pKT25 respectively and were generated for testing protein-protein interaction in the Bacterial two hybrid system. pDSZ12 contains C-terminal RomR domain, DNA fragment was amplified with primers "BTHGlufw" and "BTHRomRrv stop". The product was cloned with *XbaI*/*EcoRI* sites to pKT25. pDSZ13 contains RomR N-terminal receiver domain, DNA fragment was amplified with primers "BTHRomRfw" and "BTHrecrv". Product was cloned with *XhoI*/*EcoRI* sites to pUT18.

4.4.3 Generation of in-frame deletion mutants

In-frame deletion mutants were generated by two-step homologous recombination as described (Shi *et al.*, 2008). Briefly, the upstream and downstream flanking reagion of approximately 500bp were amplified using AB and CD primer pairs. B and C primers contain overlapping compatibilie ends essential for the fusion of AB and CD fragments in a PCR reaction using A and D primers. AB and CD fragments serve as a template to generate the in-frame deletion fragment AD. Next, AD fragment was cloned into pBJ114 vector. The correct pBJ114AD plasmid was transformed into *M. xanthus* DK1622. The plasmid integration was checked by PCR reaction with E (binds upstream of A primers) and F (binds downstream to D primer), E and M13forward (binds to pBJ114), F and M13reverse (binds to pBJ144) primer pairs. One clone from up- and downstream plasmid integration was used for the second step of homologous recombination. Plasmid pBJ114 contains the selection marker *galK* (galaktokinase) gene. The gene product GalK converts galactose into galactose-1-phosphate which cannot be metabolize by *M. xanthus* and accumulates up to toxic levels when cells are grown on media supplemented with galactose. Thus, only clones that undergo second homologous recombination lost plasmid are able to grown on media with galactose. For the second homologous recombination event cells were grown in CTT liquid shaking culture to exponential growth phase. Series of dilutions were plated on CTT agar plates supplemented with 10 μg/ml gentamycin and 2.5% galactose. Galactose resistant and kanamycin sensitive clones were checked with PCR reaction using E and F, G(binds downstream of B primer) and H (binds upstream of C primer) primer pairs. The EF prime pair PCR reaction product was longer for the WT then for the deletion mutant, while GH fragment was amplified only in the WT.

4.4.4 DNA isolation from *E. coli* and *M. xanthus*

Plasmid DNA from *E. coli* was isolated using the QIAprep Spin Miniprep Kit (Qiagen) or the NuceoSpin Plasmid QuickPure kit (Macherey-Nagel) in accordance to the instructions provided by the manufacturer. Genomic DNA of *M. xanthus* was isolated using MasterPure DNA preparation Kit (Epicentre) according to the instructions provided by the manufacturer. Concentration and purity of DNA was determined with the Nanodrop ND-1000 spectrophotometer (Nanodrop, Wilmington) or with DS11+ spectrophotometer (DeNovix Inc., Wilmington). Crude genomic DNA of *M. xanthus* for colony PCR was prepared by resuspending in 50 µl H_2O cells grown on CTT agar plates and boiling for 5 min at 96°C and centrifuging the sample for one minute at 13 000 rpm. 3 µl of resulting supernatant was used for the PCR reaction.

4.4.5 Polymerase Chain Reaction (PCR)

For the amplification of specific DNA fragments, the Phusion High-Fidelity DNA Polymerase (Thermo Scientific™, Darmstadt) or Q5® Hot Start High-Fidelity DNA Polymerase (New England Biolabs, Frankfurt a. M.) was used in a total reaction volume of 50 µl. The colony PCR was performed used 5 PRIME MasterMix in total volume of 20 µl. The composition of the PCR reaction mix is described in Table 10.

Table 10. PCR reaction mix

Component	**Volume**	**Final concentration**
PCR with Phusion High-Fidelity DNA Polymerase		
Template DNA	1 µl	~50 ng
10 µM primer (each)	2.5 µl	1.25 µM
10 mM dNTPs	1 µl	0.2 mM
5 x Phusion GC buffer	10 µl	1x
5 x enhancer	10 µl	1x
DMSO	2.5 µl	5% (v/v)
Phusion DNA polymerase	0.5 µl	0.02 unit/µl
ddH_2O	To 50 µl	
PCR with Q5® Hot Start High-Fidelity DNA Polymerase		
Template DNA	1 µl	~50 ng
10 µM primer (each)	2.5 µl	1.25 µM
10 mM dNTPs	1 µl	0.2 mM
5 x Q5 Reaction Buffer	10 µl	1x
5 x Q5 High GC Enhancer	10 µl	1x
DMSO	2.5 µl	5% (v/v)
Q5 Hot Start High-Fidelity DNA	0.5 µl	0.02 unit/µl
ddH_2O	To 50 µl	

Colony PCR

Crude genomic DNA	3 µl	~ 200 ng
10 µM primer (each)	1 µl	0.5 µM
5 PRIME MasterMix	10 µl	
DMSO	2 µl	10% (v/v)
ddH_2O	To 20 µl	

The PCR programs used in this study are represented in Table 11. PCR conditions were modified depending on the primer annealing temperature and expected product size.

Table 11. PCR programs

Step	**Temperature**	**Time**	
Standard/check PCR			
Initial denaturation	98 °C	30 min	
denaturation	98 °C	30 sec	35 x
Primer annealing	5 °C below predicted melting temperature	30 sec	
elongation	72 °C	1 min/kb	
final elongation	72 °C	3 min	
hold	4 °C	∞	
Touch down PCR			
Initial denaturation	98 °C	30 min	
denaturation	98 °C	30 sec	10 x
Primer annealing	65 °C	30 sec	
elongation	72 °C	1 min/kb	
denaturation	98 °C	30 sec	10 x
Primer annealing	62 °C	30 sec	
elongation	72 °C	1 min/kb	
denaturation	98 °C	30 sec	10 x
Primer annealing	58 °C	30 sec	
elongation	72 °C	1 min/kb	
final elongation	72 °C	3 min	
hold	4 °C	∞	

4.4.6 Agarose gel electrophoresis

Nucleic acid fragments were separated by size on 1% agarose gels within 0.01% (v/v) ethidium bromide in TBE buffer (Invitrogen) at 120 V. DNA samples were mixed with 5 x DNA loading buffer (32.5 % sacharose, 5 mM EDTA, 5 mM Tris-HCl pH 7.5, 0.15% bromophenol blue). As a DNA marker the 2-log DNA ladder (NEB) was used. Agarose gels were imaged using E-BOX VX2 imaging system (PeqLab).

4.4.7 DNA restriction and ligation

Restriction of DNA fragment (0.5-2 µg) was performed with restriction endonucleases at 37 °C for 2 h. Restricted DNA was puriefied using the DNA Clean & Concentration kit (Zymo Research) according to manufacturer protocol.

Ligation reactions were performed with T4 DNA ligase (NEB). DNA fragments were ligated into vector with 3- to 5-fold molar excess of insert DNA. After 1 h at room temperature ligation mixtures were used for transformation into *E. coli* Mach1 or TOP10.

4.4.8 Preparation and transformation of chemically competent *E. coli* cells

To prepare chemical competent *E. coli* cells, the overnight culture was used to inoculate 200 ml of LB media. Cultures were grown with shaking at 230 rpm at 37 °C to an OD_{600} of 0.5 – 0.7. The cells were harvested by centrifugation at 4700 rpm for 20 min 4 °C and resuspended in 50 ml ice-cold sterile 50 mM $CaCl_2$ solution. The cells were pelleted again at the same conditions and washed again. The cells were centrifuged again in the same conditions and resuspended in 2 ml ice-cold sterile 50 mM $CaCl_2$ with 10% (v/v) glycerol solution. 50 µl aliquots of cells were frozen in liquid nitrogen and kept at -80 °C until used.

For transformation one 50 µl aliquote was thawed on ice and 10 µl of ligation mixture was added to cells and mixed carefully. After 30 min incubation on ice to perform heat shock cells were transferred to 42 °C for 1 min 30 sec. After 5 min incubation on ice, 1 ml LB-medium was added and cells were incubated for 60 min shaking at 37 °C. After harvesting, cells pellet were resuspended in 50 µl LB medium and plated on LB agar plates supplemented with appropriate antibiotics. Plates were incubated at 37 °C overnight. Grown colonies were checked for the presence of the plasmid containing the insert by colony PCR reaction.

4.4.9 Preparation and transformation of electrocompetent *M. xanthus* cells

M. xanthus cells were grown overnight with shaking at 230 rpm at 32 °C to an OD_{550} of 0.5 – 0.9. Cells were harvested at 13 000 rpm for 1 min and the pellet was washed twice in 1 ml sterile ddH_2O and resuspended in 30 µl H_2O. The cell resupspension was immiediately used for electroporation. 1 µg plasmid DNA was added to 30 µl cells and the mixture was transferred into an electroporation cuvette (Bio-Rad, Munchen) and pulsed with 0.65 kV, 25 µF and 400 Ω. 1 ml of CTT media was added and mixed with cells, the cell suspension was transferred to a 25 ml Erlenmyer flask containing 1 ml of CTT media and incubated with shaking at 230 rpm at 32 °C for 6 h. Then, 2 ml (for

plasmid integrating at the endogenous site) and 100 µl (for plasmids integrating at the Mx8 site and Mxan 18-19 site) were mixed with 3.5 ml of soft agar and plated on CTT agar plates supplemented with appropriate antibiotics. The plates were incubated for 5 – 10 days at 32 °C in the dark. Grown colonies were transferred to fresh agar plates. Plasmid integration was verified by colony PCR.

4.5 Biochemical methods

4.5.1 SDS-polyacrylamide gel electrophoresis (SDS-PAGE)

To separate proteins by size under denaturing conditions SDS polyacrylamide gel electrophoresis (Laemmli, 1970) was performed with SDS gels with 10% to 16% polyacrylamide concentration. To denature proteins, samples were mixed with loading buffer (10% (v/v) glycerol, 60 mM Tris-HCl pH 6.8, 2% (w/v) SDS, 100 mM DTT, 3 mM EDTA, 0.005% (w/v) bromophenol blue) and boiled at 95 °C for 10 min before loading on the gel. Gel electrophoresis was made in Bio-Rad electrophoresis chamber (Bio-Rad, München) at 80-140 V in 1x Tris Glycin SDS (TGS) running buffer (Bio-Rad, München). To determine size of the proteins, the PageRuler Prestained Protein Ladder (Fermentas) was used for comparison.

4.5.2 Determination of total protein concentration in cell extracts

To determine protein concentration in a lysate of *M. xanthus* the Bio-Rad proteins assay kit was used accordingly to the manufacturer's manual. In order to make standard curve of protein concentration Pre-Diluted Protein Assay Standards: Bovine Serum Albumin (BSA) set (Thermo Scientific, Dreieich) was used. Standards were diluted in three volumes of H_2O and one volume of 5 x SDS sample buffer to get 10 µg/µl, 5 µg/µl, 2.5 µg/µl, 1.25 µg/µl and 0.625 µg/µl concentrations. These resulting dillutions were diluted again 25 times in H_2O and 20 µl of these samples were mixed with 980 µ 1:5 diluted Bradford reagent. After 5 min incubation at room temperature and in the dark, absorbane was measured at 595 nm with Ultrospec 2100 pro spectrophotometer (GE Healthcare Europe GmbH, Freiburg). To prepare *M. xanthus* cell lysate a pellet of cells were dissolved in 1 x SDS sample buffer and heated at 95 °C for 10 min. Lysate were diluted 1:25 in H_2O and 20 µl was mixed with 980 µl of 1:5 diluted Bradford reagent and incubated 5 minutes in the dark. Absorbance was measured ass described before. Protein concentration was calculated from the standard curve.

To determine protein concentration of the purified proteins the Bradford reagent (Bio-Rad) was used accordingly to yhe manufacturer's manual. The protein standard

curve was generated using Pre-Diluted Protein Assay Standards: Bovine Serum Albumin (BSA). The reaction samples were prepared in duplicates 1 ml reaction volume. After 5 min incubation at room temperature and in the dark, absorbane was measured at 595 nm with Ultrospec 2100 pro spectrophotometer (GE Healthcare Europe GmbH, Freiburg). Protein concentrations were determined based on the linear slope of the standard curve.

4.5.3 Immunoblot analysis

Proteins from cell extracts were separated in the gel by SDS-PAGE and transferred to a nitrocellulose membrane using "TransBlot® TurboTM Transfer System" from Bio-RaD at 1.3 A (0.0208/cm^2), 25 V for 7 min with transfer buffer (300 mM Tris, 300 mM Glycin, 0.05% SDS, pH 9.0) or using Hoefer^{TM} TE77 from Amersham at 50 mA (0.8 mA/cm^2) for 1h with anode transfer buffer (25 mM TriS, 192 mM Glycin, 0.01% SDS, 25% Methanol) and cathode transfer buffer (50 mM Tris, 384 mM Glycin, 0.2% SDS. 10% Methanol). After transfer, the membrane was blocked in 5% non-fat milk powder (w/v) in TBST (20 mM Tris-HCl, 137 mM NaCl, 0.05% (v/v) Tween 20, pH 7.0) for 1 h or overnight at 4 ^{o}C shaking. After blocking, the membrane was washing with TBST buffer. After washing, the primary antibody was added at the dilution listed in Table 12 in TBST buffer supplemented with 2% non-fat milk powder and incubated overnight at 4 ^{o}C shaking. After washing with TBST buffer, the membrane was incubated with secondary anti-rabbit immunoglobulin G peroxidase conjugate (Sigma) in a dilution 1:15 000 or with secondary anti-mouse immunoglobulin G, horseradish peroxidase lined whole antibody (GE Healthcare) in a dilution 1:2 000 for 1h at 4 ^{o}C shaking. After washing with TBST buffer the membrane was developed with the luminescent image analyzer LAS-4000 (Fujifilm).

Table 12. Dilutions of primary antibodies used for immunoblots analysis

antibody	dilution
α-MglA	1:2000
α-MglB	1:2000
α-RomR	1:5000
α-RomX	1:2000
α-RomY	1:5000
α-PilC	1:5000
α-GFP	1:2000
α-mCherry	1:1000

4.5.4 Proteins purification

Purification of MalE-RomR

To purify the proteins, *E. coli* Rosseta 2 (DE3)/pLysS strain (Novagen) was transformed with relevant plasmids. The culture were grown in 1.0l or 2.0l of LB with 0.5 % glucose and supplemented with appropriate antibiotics and 0.5% glucose when necessary at 30 °C to an OD_{600} of 0.5-0.7. The protein expression was induced by addition of IPTG to a final concentration of 0.5 mM. Then, cells were growing overnight at 18 °C.

The cells were harvested by centrifugation at 6 000 x g, 20 min at 4 °C and washed in wash buffer (50 mM Tris pH 7.5, 150 mM NaCl, 1 mM EDTA, 1mM DTT) and resuspended in 50ml Lysis buffer (50 ml of the wash buffer supplemented with PMSF 100 µg/ml, DNase 1 10U/ml and protease inhibitors – Complete Protease Inhibitor Cocktail Tablet from Roche). Next, cells were sonicated and centrifuged at 4 700 x rpm for 30 min at 4 °C to pellet the cellular debris. Cleared supernatant was loaded onto 5 ml MBPTrapHP (GE Healthcare) column equilibrated with wash buffer. Proteins were eluted with elution buffer (50 mM Tris pH 7.5, 150 NaCl, 1mM EDTA, 1mM DTT, 5% glycerol, 10 mM maltose). Eluted fractions containing MalE-RomR were loaded onto 5 ml HiTrap Q HP column (GE Healthcare) equilibrated with buffer A (50 mM Tris pH 7.5, 50 mM NaCl. 5 mM $MgCl_2$, 1 mM DTT, 5% glycerol. Proteins were eluted with buffer A along a gradient of 20 columns volume (CV) from 50 mM to 500 mM NaCl. Next, fractions containing MalE-RomR were loaded onto HiLoad 16/600 Superdex 200 pg (GE Healthcare) column that was equilibrated with Gefi buffer (50 mM Tris pH 7.5, 150 mM NaCl, 5 mM $MgCl_2$, 1 mM DTT, 5 % glycerol). Fractions with MalE-RomR were pooled, span-frozen in liquid nitrogen and stored at -80 °C.

Purification of MglA-His_6

To purify the proteins, *E. coli* Rosseta 2 (DE3)/pLysS strain (Novagen) was transformed with relevant plasmid. The culture were grown in 1.0 l or 2.0 l of LB with 0.5% glucose and supplemented with appropriate antibiotics and 0.5% glucose when necessary at 30 °C to an OD_{600} of 0.5-0.7. The protein expression was induced by addition of IPTG to a final concentration of 0.5 mM. Then, cells were growing overnight at 18 °C.

The cells were harvested by centrifugation at 6 000 x g, 20 min at 4 °C and washed in wash buffer (50 mM Tris pH 7.5, 150 mM NaCl, 10 mM imidazole, 5% glycerol, 5mM $MgCl_2$) and resuspended in Lysis buffer (50 ml of wash buffer supplemented with 1 mM DTT, 100 µg/ml PMSF, 10 U/ml DNase 1 and protease inhibitors – Complete Protease Inhibitor Cocktail Tablet from Roche). Next, cells were sonicated and centrifuged at 4 700 x rpm for 30 min at 4 °C to pellet the cellular debris. Cleared supernatant was filter with 0.45 µm sterile filter (Millipore Merck, Schwalbach). To purify MglA-His_6 only soluble fraction was used. Clear soluble fraction was loaded onto 5 ml HITrap Chelating

HP (GE Healthcare) column, preloaded with $NiSO_4$ and equilibrated with Wash buffer. Proteins was eluted with Elution buffer (50 mM Tris pH 7.5, 150 mM NaCl, 5% glycerol, 5 mM $MgCl_2$, 500 mM imidazole) along a gradient of 16 CV. Elution fractions containing MglA-His_6 were loaded onto HiLoad 16/600 Superdex 75 pg (GE Healthcare) column that was equilibrated with Gefi buffer (50 mM Tris pH 7.5, 150 mM NaCl, 5 mM $MgCl_2$, 1 mM DTT, 5 % glycerol). Fractions with MglA-His_6 were pooled, span-frozen in liquid nitrogen and stored at -80 ^oC.

Purification of His_6-MglB

To purify the proteins, *E. coli* Rosseta 2 (DE3)/pLysS strain (Novagen) was transformed with relevant plasmid. The culture were grown in 1.0l or 2.0l of LB with 0.5% glucose and supplemented with appropriate antibiotics and 0.5% glucose when necessary at 30 ^oC to an OD_{600} of 0.5-0.7. The protein expression was induced by addition of IPTG to a final concentration of 0.5 mM. Then, cells were growing overnight at 18 ^oC.

The cells were harvested by centrifugation at 6 000 x g, 20 min at 4 ^oC and washed in wash buffer (50 mM Tris pH 7.5, 150 mM NaCl, 10 mM imidazole, 5% glycerol, 5mM $MgCl_2$) and resuspended in Lysis buffer (50 ml of wash buffer supplemented with 1 mM DTT, 100 µg/ml PMSF, 10 U/ml DNase 1 and protease inhibitors – Complete Protease Inhibitor Cocktail Tablet from Roche). Next, cells were sonicated and centrifuged at 4 700 x rpm for 30 min at 4 ^oC to pellet the cellular debris. Cleared supernatant was filter with 0.45µ sterile filter (Millipore Merck, Schwalbach). To purify His_6-MglB only soluble fraction was used. Clear soluble fraction was loaded onto 5 ml HITrap Chelating HP (GE Healthcare) column, preloaded with $NiSO_4$ and equilibrated with Wash buffer. Proteins was eluted with Elution buffer (50 mM Tris pH 7.5, 150 mM NaCl, 5% glycerol, 5 mM $MgCl_2$, 500 mM imidazole) along a gradient of 16 CV. Elution fractions containing His_6-MglB were loaded onto HiLoad 16/600 Superdex 75 pg (GE Healthcare) column that was equilibrated with Gefi buffer (50 mM Tris pH 7.5, 150 mM NaCl, 5 mM $MgCl_2$, 1 mM DTT, 5% glycerol). Fractions with His_6-MglB were pooled, span-frozen in liquid nitrogen and stored at -80 ^oC.

Purification of His_6-RomX

To purify the proteins, *E. coli* Rosseta 2 (DE3)/pLysS strain (Novagen) was transformed with relevant plasmid. The culture were grown in 1.0 l or 2.0 l of LB with 0.5% glucose and supplemented with appropriate antibiotics and 0.5% glucose when necessary at 37 ^oC to an OD_{600} of 0.5-0.7. The protein expression was induced by addition of IPTG to a final concentration of 1.0 mM. Then, cells were growing for 3 hours at 37 ^oC.

The cells were harvested by centrifugation at 6 000 x g, 20 min at 4 °C and washed in wash buffer (50 mM Tris pH 7.5, 150 mM NaCl, 10 mM imidazole, 5% glycerol, 5mM $MgCl_2$) and resuspended in Lysis buffer (50 ml of wash buffer supplemented with 1 mM DTT, 100 µg/ml PMSF, 10 U/ml DNase 1 and protease inhibitors – Complete Protease Inhibitor Cocktail Tablet from Roche). Next, cells were sonicated and centrifuged at 4 700 x rpm for 30 min at 4 °C to pellet the cellular debris. Cleared supernatant was filter with 0.45µ sterile filter (Millipore Merck, Schwalbach). To purify His_6-RomX only soluble fraction was used. Clear soluble fraction was loaded onto 5 ml HITrap Chelating HP (GE Healthcare) column, preloaded with $NiSO_4$ and equilibrated with Wash buffer. Proteins was eluted with Elution buffer (50 mM Tris pH 7.5, 150 mM NaCl, 5% glycerol, 5 mM $MgCl_2$, 500 mM imidazole) along a gradient of 16 CV. Elution fractions containing His_6-RomX were loaded onto HiL0ad 16/600 Superdex 75 pg (GE Healthcare) column that was equilibrated with Gefi buffer (50 mM Tris pH 7.5, 150 mM NaCl, 5 mM $MgCl_2$, 1 mM DTT, 5 % glycerol). Fractions with His_6-RomX were pooled, span-frozen in liquid nitrogen and stored at -80 °C.

Purification of Strep-RomX

To purify the proteins, *E. coli* Rosseta 2 (DE3)/pLysS strain (Novagen) was transformed with relevant plasmid. The culture were grown in 1.0 l or 2.0 l of 2xYT with 0.5% glucose and supplemented with appropriate antibiotics and 0.5% glucose when necessary at 37 °C to an OD_{600} of 0.5-0.7. The protein expression was induced by addition of anhydrotetracycline to a final concentration of 200 µg/l. Then, cells were growing for ON at 18 °C.

The cells were harvested by centrifugation at 6 000 x g, 20 min at 4 °C and washed in wash buffer (100 mM Tris pH 8.0, 150 mM NaCl, 1 mM EDTA, 1 mM DTT) and resuspended in Lysis buffer (50 ml of wash buffer supplemented with 100 µg/ml PMSF, 10 U/ml DNase 1 and protease inhibitors – Complete Protease Inhibitor Cocktail Tablet from Roche). Next, cells were sonicated and centrifuged at 10000 x rpm for 20 min at 4 °C to pellet the cellular debris. Cleared supernatant was filter with 0.45 µm sterile filter (Millipore Merck, Schwalbach). To purify Strep-RomX only soluble fraction was used. Clear soluble fraction was loaded onto 5 ml Strep Traap HP (GE Healthcare) column, equilibrated with wash buffer. Proteins was eluted with Elution buffer (150 mM Tris pH 8.0, 150 mM NaCl, 1 mM EDTA, 2.5 mM Desthiobiotin). Elution fractions containing Strep-RomX were loaded onto HiL0ad 16/600 Superdex 75 pg (GE Healthcare) column that was equilibrated with Gefi buffer (50 mM Tris pH 7.5, 150 mM NaCl, 5 mM $MgCl_2$,

1 mM DTT, 5 % glycerol). Fractions with Strep-RomX were pooled, span-frozen in liquid nitrogen and stored at -80 °C.

4.5.5 GTPase assay

GTP-hydrolysis by MglA-His_6 was measured in an enzyme coupled spectrophotometric assay as reported in (Ingerman & Nunnari, 2005). For the assay, MglA-His_6 was preincubated for 30 min with 100 times molar excess of GTP in the room temperature. In parallel, equimolar combinations of His_6-MglB, RomX-His_6 and MalE-RomR were preincubated for 10 min before starting reaction. Eventually, RomX-His_6 and MalE-RomR were preincubated for 10min with MglA-His_6-GTP in a molar ratio 2:1. Reactions were started by adding His_6-MglB, His_6-RomX and/or MalE-RomR to the MglA-His_6/GTP or to MglA-His_6/GTP/ His_6-RomX and/or MalE-RomR mixtures. Final concentration in the reactions: MglA-His_6 3 µM, His_6-MglB 6 µM, His_6-RomX 6 µM and MalE-RomR 6 µM. GTPase assay was performed in the reaction buffer (50 mM Tris pH 7.5, 150 mM NaCl, 5% glycerol, 1 mM DTT, 5 mM $MgCl_2$). Absorption at 340 nm was followed for 60 min in one minute intervals at 37 °C. Absorbance versus time was plotted. In order to decrease noise, we did not utilize data from early time points. Only absorbance data that is liner with respect to time was used. By using the "add trendline" function of Microsoft Excel, data from each experiment was fitted. The slope of this line was multiplied by 60 and divided by the molar absorbitivity of NADH (6220 $M^{-1}cm^{-1}$) and by previously determined path length (0.23 cm) and by concentration of MglA-His_6. That processed data showed amount of hydrolyzed GTP per hour per molecule of MglA.

4.5.6 Pull down experiment

To test direct protein-protein interactions, 128 µg MalE-RomR, 58 µg His_6-RomX, 64 µg MalE, 48 µg MglA-His_6 were used. For the experiments to test affinity of MalE-RomR and His_6-RomX to the amylose resin, interactions between MalE-RomR and His_6-RomX and between MalE and His_6-RomX proteins were applied to 200 µL Amylose Resin previously equilibrated with buffer 1 (50 mM Tris pH 7.5, 150 mM NaCl, 5% glycerol, 1 mM DTT, 5 mM $MgCl_2$). Then, samples were incubated for 30 min at the room temperature. Next, resin was loaded into the column and washed 3 times 1 ml with buffer 1. Proteins were eluted with 2 times 200 µl of buffer 2 (buffer 1 suplemented with 10 mM maltose). Fractions were analyzed by the SDS-PAGE.

To test interactions between MglA-His_6 and Strep-RomX 27 µg of Strep-RomX (final concentration 10 µM) was mixed with 46 µg MglA-His_6 (final concentration 10 µM). MglA-His_6 was preincubated with GTP or GDP (final concentration 40 µM) for 30

min at RT. After 30 min incubation of Strep-RomX with MglA-His_6-GDP/GTP at RT proteins were incubated with 10 µl of strep-tactin XT MagStrep 'type3' XT Beads (IBA GmbH) for 30 min at RT. Than beads were washed 10x with 1 ml wash buffer (50 mM Tris pH 7.5, 150 mM NaCl, 5% glycerol, 1 mM DTT, 5 mM $MgCl_2$) supplemented with GDP or GTP, respectively. Proteins were eluted with 2x 100µl elution buffer (100 mM Tris pH 8.0, 150 mM NaCl, 1 mM EDTA, 50 mM Biotin). Fractions were analyzed by the SDS-PAGE

To test interactions between MglA-His_6 and MalE-RomR and MalE-RomR/His_6-RomX complex, MglA-His_6 was preincubated with 4 times molar excess of GTP or GDP for 30 min at the room temperature. Next, MglA-His_6 GTP/GDP was applied to an amylose resin with prebound MalE-RomR or MalE-RomR/ His_6-RomX for 30 min incubation at the room temperature. Proteins were prebounded to the resin and washed as described before. Next, resin was loaded into the column and washed with 3 times 1 ml of buffer 1 supplemented with 40 µM GTP or GDP respectively. Proteins were eluted from the column with 2 times 200 µl of buffer 2. Fractions were analyzed by the SDS-PAGE.

4.5.7 Nucleotide exchange experiments

Experiment of the release of mGDP from MglA was done as described in (Lenzen *et al.*, 1995) with modifications. Briefly, MglA-His_6 (2.016 µM) was preloaded with mGDP (403.226 nM) for 300 s at 25 °C in the presence or absence of His_6-RomX (4.032 µM) and/or MalE-RomR (4.032 µM) or BSA (8.064 µM). Loading was observed real time with monitoring fluorescence of mant (excitation 336, emission 450) on a temperature controlled ISS PC1 spectrofluorometer. Next, GTP was added to the final concentration of 2 µM. Reaction was performed in the exchange buffer (20 mM Tris pH 7.5, 200 mM NaCl, 10% glycerol, 1 mM DTT) at 25 °C and fluorescence was measured every second. Reaction was followed from this point for 800 s. Obtained data was standardized, time point after addition of GTP, when fluorescence signal was stabilized, was set up as time point zero and fluorescence arbitrary units 1.

For the experiment with binding of mGTP to MglA, MglA-His_6 (26.61 µM) was preloaded with GDP (106.48 µM) for 30 min at the room temperature. Subsequently, the MglA-His_6/GDP mix was added to a reaction cuvette with mGTP (524.62 nM). After signal stabilization, His_6-RomX and/or MalE-RomR or BSA were added. Final concentrations: MglA-His_6 2 µM, 8 µM GDP, mGTP 400 nM, His6-RomX 8 µM, MalE-RomR 8 µM, BSA 16 µM. Reaction was performed in the exchange buffer (20 mM Tris

pH 7.5, 200 mM NaCl, 10% glycerol, 1 mM DTT) at 25 °C and mant fluorescence (exc 336, emi 450) was measure every second and followed for 1500s on a temperature controlled ISS PC1 spectrofluorometer. Obtained data was standardized, time point after addition of His_6RomX and/or MalE-RomR or BSA, when fluorescence signal was stabilized, was set up as time point zero and fluorescence arbitrary units at zero. For the experiments that tested concentration dependences of His_6RomX/MalE-RomR complex, conditions and concentration of MglA-His_6, GDP and mGTP were the same as previously described.

In the experiment that tested binding of His_6-RomX/MalE-RomR to MglA-His_6 GTP, MglA-His_6 was loaded with mGTP for the 150s, monitored real life with mant fluorescence (exc 336, emi 450) at 25 °C on a temperature controlled ISS PC1 spectrofluorometer. Subsequently, His_6-RomX and/or MalE-RomR or BSA were added. Final concentrations in the reactions: MglA-His_6 2 µM, mGTP 400 nM, His6-RomX 8 µM, MalE-RomR 8 µM, BSA 16 µM. Reaction was performed in the exchange buffer. After proteins addition, reaction was followed for 350 s with fluorescence read out every second. Data was standardized, time point after addition of His_6RomX and/or MalE-RomR or BSA, when fluorescence signal was stabilized was set up as time point zero and fluorescence arbitrary units at zero.

5. References

Alley, M.R., J.R. Maddock & L. Shapiro, (1992) Polar localization of a bacterial chemoreceptor. *Genes Dev* **6**: 825-836.

Aronheim, A., D. Engelberg, N. Li, N. al-Alawi, J. Schlessinger & M. Karin, (1994) Membrane targeting of the nucleotide exchange factor Sos is sufficient for activating the Ras signaling pathway. *Cell* **78**: 949-961.

Balagam, R., D.B. Litwin, F. Czerwinski, M. Sun, H.B. Kaplan, J.W. Shaevitz & O.A. Igoshin, (2014) Myxococcus xanthus gliding motors are elastically coupled to the substrate as predicted by the focal adhesion model of gliding motility. *PLoS computational biology* **10**: e1003619.

Bernadac, A., M. Gavioli, J.C. Lazzaroni, S. Raina & R. Lloubes, (1998) Escherichia coli tol-pal mutants form outer membrane vesicles. *J Bacteriol* **180**: 4872-4878.

Bi, E.F. & J. Lutkenhaus, (1991) FtsZ ring structure associated with division in Escherichia coli. *Nature* **354**: 161-164.

Bischof, L.F., C. Friedrich, A. Harms, L.Søgaard-Andersen & C. van der Does, (2016) The Type IV Pilus Assembly ATPase PilB of Myxococcus xanthus Interacts with the Inner Membrane Platform Protein PilC and the Nucleotide-binding Protein PilM. *The Journal of biological chemistry* **291**: 6946-6957.

Black, W.P., Q. Xu & Z. Yang, (2006) Type IV pili function upstream of the Dif chemotaxis pathway in Myxococcus xanthus EPS regulation. *Molecular microbiology* **61**: 447-456.

Blackhart, B.D. & D.R. Zusman, (1985) "Frizzy" genes of Myxococcus xanthus are involved in control of frequency of reversal of gliding motility. *Proc Natl Acad Sci U S A* **82**: 8767-8770.

Blumer, J., J. Rey, L. Dehmelt, T. Mazel, Y.W. Wu, P. Bastiaens, R.S. Goody & A. Itzen, (2013) RabGEFs are a major determinant for specific Rab membrane targeting. *The Journal of cell biology* **200**: 287-300.

Bos, J.L., H. Rehmann & A. Wittinghofer, (2007) GEFs and GAPs: critical elements in the control of small G proteins. *Cell* **129**: 865-877.

Bourne, H.R., D.A. Sanders & F. McCormick, (1991) The GTPase superfamily: conserved structure and molecular mechanism. *Nature* **349**: 117-127.

Bowman, G.R., L.R. Comolli, J. Zhu, M. Eckart, M. Koenig, K.H. Downing, W.E. Moerner, T. Earnest & L. Shapiro, (2008) A polymeric protein anchors the chromosomal origin/ParB complex at a bacterial cell pole. *Cell* **134**: 945-955.

Bramkamp, M., R. Emmins, L. Weston, C. Donovan, R.A. Daniel & J. Errington, (2008) A novel component of the division-site selection system of Bacillus subtilis and a new mode of action for the division inhibitor MinCD. *Molecular microbiology* **70**: 1556-1569.

Bulyha, I., S. Lindow, L. Lin, K. Bolte, K. Wuichet, J. Kahnt, C. van der Does, M. Thanbichler & L.Søgaard-Andersen, (2013) Two small GTPases act in concert with the bactofilin cytoskeleton to regulate dynamic bacterial cell polarity. *Developmental cell* **25**: 119-131.

Bulyha, I., C. Schmidt, P. Lenz, V. Jakovljevic, A. Hone, B. Maier, M. Hoppert & L.Søgaard-Andersen, (2009) Regulation of the type IV pili molecular machine by dynamic localization of two motor proteins. *Molecular microbiology* **74**: 691-706.

Bustamante, V.H., I. Martinez-Flores, H.C. Vlamakis & D.R. Zusman, (2004) Analysis of the Frz signal transduction system of Myxococcus xanthus shows the importance

of the conserved C-terminal region of the cytoplasmic chemoreceptor FrzCD in sensing signals. *Molecular microbiology* **53**: 1501-1513.

Cai, Y., H.F. Chin, D. Lazarova, S. Menon, C. Fu, H. Cai, A. Sclafani, D.W. Rodgers, E.M. De La Cruz, S. Ferro-Novick & K.M. Reinisch, (2008) The structural basis for activation of the Rab Ypt1p by the TRAPP membrane-tethering complexes. *Cell* **133**: 1202-1213.

Chang, Y.W., L.A. Rettberg, A. Treuner-Lange, J. Iwasa, L.Søgaard-Andersen & G.J. Jensen, (2016) Architecture of the type IVa pilus machine. *Science* **351**: aad2001.

Charest, P.G. & R.A. Firtel, (2007) Big roles for small GTPases in the control of directed cell movement. *The Biochemical journal* **401**: 377-390.

Chen, Z., F. Medina, M.Y. Liu, C. Thomas, S.R. Sprang & P.C. Sternweis, (2010) Activated RhoA binds to the pleckstrin homology (PH) domain of PDZ-RhoGEF, a potential site for autoregulation. *The Journal of biological chemistry* **285**: 21070-21081.

Cherfils, J. & M. Zeghouf, (2013) Regulation of small GTPases by GEFs, GAPs, and GDIs. *Physiological reviews* **93**: 269-309.

Chiou, J.G., M.K. Balasubramanian & D.J. Lew, (2017) Cell Polarity in Yeast. *Annual review of cell and developmental biology* **33**: 77-101.

Cohen, L.A., A. Honda, P. Varnai, F.D. Brown, T. Balla & J.G. Donaldson, (2007) Active Arf6 recruits ARNO/cytohesin GEFs to the PM by binding their PH domains. *Molecular biology of the cell* **18**: 2244-2253.

Correa, N.E., F. Peng & K.E. Klose, (2005) Roles of the regulatory proteins FlhF and FlhG in the Vibrio cholerae flagellar transcription hierarchy. *J Bacteriol* **187**: 6324-6332.

Craig, L. & J. Li, (2008) Type IV pili: paradoxes in form and function. *Current opinion in structural biology* **18**: 267-277.

de Chaumont, F., S. Dallongeville, N. Chenouard, N. Herve, S. Pop, T. Provoost, V. Meas-Yedid, P. Pankajakshan, T. Lecomte, Y. Le Montagner, T. Lagache, A. Dufour & J.C. Olivo-Marin, (2012) Icy: an open bioimage informatics platform for extended reproducible research. *Nature methods* **9**: 690-696.

Domian, I.J., K.C. Quon & L. Shapiro, (1997) Cell type-specific phosphorylation and proteolysis of a transcriptional regulator controls the G1-to-S transition in a bacterial cell cycle. *Cell* **90**: 415-424.

Dubnau, D., (1999) DNA uptake in bacteria. *Annual review of microbiology* **53**: 217-244.

Ducret, A., O. Theodoly & T. Mignot, (2013) Single cell microfluidic studies of bacterial motility. *Methods in molecular biology* **966**: 97-107.

Ducret, A., M.P. Valignat, F. Mouhamar, T. Mignot & O. Theodoly, (2012) Wet-surface-enhanced ellipsometric contrast microscopy identifies slime as a major adhesion factor during bacterial surface motility. *Proc Natl Acad Sci U S A* **109**: 10036-10041.

Ebersbach, G., A. Briegel, G.J. Jensen & C. Jacobs-Wagner, (2008) A self-associating protein critical for chromosome attachment, division, and polar organization in caulobacter. *Cell* **134**: 956-968.

Evans, K.J., C. Lambert & R.E. Sockett, (2007) Predation by Bdellovibrio bacteriovorus HD100 requires type IV pili. *J Bacteriol* **189**: 4850-4859.

Faure, L.M., J.B. Fiche, L. Espinosa, A. Ducret, V. Anantharaman, J. Luciano, S. Lhospice, S.T. Islam, J. Treguier, M. Sotes, E. Kuru, M.S. Van Nieuwenhze, Y.V. Brun, O. Theodoly, L. Aravind, M. Nollmann & T. Mignot, (2016) The mechanism of force transmission at bacterial focal adhesion complexes. *Nature* **539**: 530-535.

Fogel, M.A. & M.K. Waldor, (2006) A dynamic, mitotic-like mechanism for bacterial chromosome segregation. *Genes Dev* **20**: 3269-3282.

Friedrich, C., I. Bulyha & L.Søgaard-Andersen, (2014) Outside-in assembly pathway of the type IV pilus system in Myxococcus xanthus. *J Bacteriol* **196**: 378-390.

Fukuhara, S., H. Chikumi & J.S. Gutkind, (2001) RGS-containing RhoGEFs: the missing link between transforming G proteins and Rho? *Oncogene* **20**: 1661-1668.

Gregory, J.A., E.C. Becker & K. Pogliano, (2008) Bacillus subtilis MinC destabilizes FtsZ-rings at new cell poles and contributes to the timing of cell division. *Genes Dev* **22**: 3475-3488.

Guzzo, M., R. Agrebi, L. Espinosa, G. Baronian, V. Molle, E.M. Mauriello, C. Brochier-Armanet & T. Mignot, (2015) Evolution and Design Governing Signal Precision and Amplification in a Bacterial Chemosensory Pathway. *PLoS Genet* **11**: e1005460.

Hartzell, P. & D. Kaiser, (1991) Function of MglA, a 22-kilodalton protein essential for gliding in Myxococcus xanthus. *J Bacteriol* **173**: 7615-7624.

Heasman, S.J. & A.J. Ridley, (2008) Mammalian Rho GTPases: new insights into their functions from in vivo studies. *Nature reviews. Molecular cell biology* **9**: 690-701.

Hemsath, L., R. Dvorsky, D. Fiegen, M.F. Carlier & M.R. Ahmadian, (2005) An electrostatic steering mechanism of Cdc42 recognition by Wiskott-Aldrich syndrome proteins. *Molecular cell* **20**: 313-324.

Hodgkin, J. & D. Kaiser, (1977) Cell-to-cell stimulation of movement in nonmotile mutants of Myxococcus. *Proc Natl Acad Sci U S A* **74**: 2938-2942.

Hodgkin, J. & D. Kaiser, (1979) Genetics of Gliding Motility in Myxococcus-Xanthus (Myxobacterales) - 2 Gene Systems Control Movement. *Molecular & General Genetics* **171**: 177-191.

Hoiczyk, E. & W. Baumeister, (1998) The junctional pore complex, a prokaryotic secretion organelle, is the molecular motor underlying gliding motility in cyanobacteria. *Current biology : CB* **8**: 1161-1168.

Hu, W., M. Hossain, R. Lux, J. Wang, Z. Yang, Y. Li & W. Shi, (2011) Exopolysaccharide-independent social motility of Myxococcus xanthus. *PLoS One* **6**: e16102.

Iida, Y., L. Hobley, C. Lambert, A.K. Fenton, R.E. Sockett & S. Aizawa, (2009) Roles of multiple flagellins in flagellar formation and flagellar growth post bdelloplast lysis in Bdellovibrio bacteriovorus. *Journal of molecular biology* **394**: 1011-1021.

Inclan, Y.F., S. Laurent & D.R. Zusman, (2008) The receiver domain of FrzE, a CheA-CheY fusion protein, regulates the CheA histidine kinase activity and downstream signalling to the A- and S-motility systems of Myxococcus xanthus. *Molecular microbiology* **68**: 1328-1339.

Inclan, Y.F., H.C. Vlamakis & D.R. Zusman, (2007) FrzZ, a dual CheY-like response regulator, functions as an output for the Frz chemosensory pathway of Myxococcus xanthus. *Molecular microbiology* **65**: 90-102.

Ingerman, E. & J. Nunnari, (2005) A continuous, regenerative coupled GTPase assay for dynamin-related proteins. *Methods in enzymology* **404**: 611-619.

Iniesta, A.A., F. Garcia-Heras, J. Abellon-Ruiz, A. Gallego-Garcia & M. Elias-Arnanz, (2012) Two systems for conditional gene expression in Myxococcus xanthus inducible by isopropyl-beta-D-thiogalactopyranoside or vanillate. *J Bacteriol* **194**: 5875-5885.

Jaffe, A.B. & A. Hall, (2005) Rho GTPases: biochemistry and biology. *Annual review of cell and developmental biology* **21**: 247-269.

Jakobczak, B., D. Keilberg, K. Wuichet & L.Søgaard-Andersen, (2015) Contact- and Protein Transfer-Dependent Stimulation of Assembly of the Gliding Motility Machinery in Myxococcus xanthus. *PLoS Genet* **11**: e1005341.

Jakovljevic, V., S. Leonardy, M. Hoppert & L.Søgaard-Andersen, (2008) PilB and PilT are ATPases acting antagonistically in type IV pilus function in Myxococcus xanthus. *J Bacteriol* **190**: 2411-2421.

Jelsbak, L. & L.Søgaard-Andersen, (2002) Pattern formation by a cell surface-associated morphogen in Myxococcus xanthus. *Proc Natl Acad Sci U S A* **99**: 2032-2037.

Julien, B., A.D. Kaiser & A. Garza, (2000) Spatial control of cell differentiation in Myxococcus xanthus. *Proc Natl Acad Sci U S A* **97**: 9098-9103.

Kaimer, C. & D.R. Zusman, (2013) Phosphorylation-dependent localization of the response regulator FrzZ signals cell reversals in Myxococcus xanthus. *Molecular microbiology* **88**: 740-753.

Kaimer, C. & D.R. Zusman, (2016) Regulation of cell reversal frequency in Myxococcus xanthus requires the balanced activity of CheY-like domains in FrzE and FrzZ. *Molecular microbiology* **100**: 379-395.

Kaiser, D., (1979) Social Gliding Is Correlated with the Presence of Pili in Myxococcus-Xanthus. *P Natl Acad Sci USA* **76**: 5952-5956.

Karimova, G., N. Dautin & D. Ladant, (2005) Interaction network among Escherichia coli membrane proteins involved in cell division as revealed by bacterial two-hybrid analysis. *J Bacteriol* **187**: 2233-2243.

Kawai, F., M. Shoda, R. Harashima, Y. Sadaie, H. Hara & K. Matsumoto, (2004) Cardiolipin domains in Bacillus subtilis marburg membranes. *J Bacteriol* **186**: 1475-1483.

Keilberg, D., K. Wuichet, F. Drescher & L.Søgaard-Andersen, (2012) A response regulator interfaces between the Frz chemosensory system and the MglA/MglB GTPase/GAP module to regulate polarity in Myxococcus xanthus. *PLoS Genet* **8**: e1002951.

Koch, M.K., C.A. McHugh & E. Hoiczyk, (2011) BacM, an N-terminally processed bactofilin of Myxococcus xanthus, is crucial for proper cell shape. *Molecular microbiology* **80**: 1031-1051.

Kortholt, A. & P.J. van Haastert, (2008) Highlighting the role of Ras and Rap during Dictyostelium chemotaxis. *Cellular signalling* **20**: 1415-1422.

Kroos, L., P. Hartzell, K. Stephens & D. Kaiser, (1988) A Link between Cell-Movement and Gene-Expression Argues That Motility Is Required for Cell Cell Signaling during Fruiting Body Development. *Gene Dev* **2**: 1677-1685.

Kuhlmann, J., I. Macara & A. Wittinghofer, (1997) Dynamic and equilibrium studies on the interaction of Ran with its effector, RanBP1. *Biochemistry* **36**: 12027-12035.

Kuhn, J., A. Briegel, E. Morschel, J. Kahnt, K. Leser, S. Wick, G.J. Jensen & M. Thanbichler, (2010) Bactofilins, a ubiquitous class of cytoskeletal proteins mediating polar localization of a cell wall synthase in Caulobacter crescentus. *The EMBO journal* **29**: 327-339.

Laemmli, U.K., (1970) Cleavage of structural proteins during the assembly of the head of bacteriophage T4. *Nature* **227**: 680-685.

Lambert, C., A.K. Fenton, L. Hobley & R.E. Sockett, (2011) Predatory Bdellovibrio bacteria use gliding motility to scout for prey on surfaces. *J Bacteriol* **193**: 3139-3141.

Lenarcic, R., S. Halbedel, L. Visser, M. Shaw, L.J. Wu, J. Errington, D. Marenduzzo & L.W. Hamoen, (2009) Localisation of DivIVA by targeting to negatively curved membranes. *The EMBO journal* **28**: 2272-2282.

Lenzen, C., R.H. Cool & A. Wittinghofer, (1995) Analysis of intrinsic and CDC25-stimulated guanine nucleotide exchange of p21ras-nucleotide complexes by fluorescence measurements. *Methods in enzymology* **255**: 95-109.

Leonard, D.A., R. Lin, R.A. Cerione & D. Manor, (1998) Biochemical studies of the mechanism of action of the Cdc42-GTPase-activating protein. *The Journal of biological chemistry* **273**: 16210-16215.

Leonardy, S., G. Freymark, S. Hebener, E. Ellehauge & L.Søgaard-Andersen, (2007) Coupling of protein localization and cell movements by a dynamically localized response regulator in Myxococcus xanthus. *The EMBO journal* **26**: 4433-4444.

Leonardy, S., M. Miertzschke, I. Bulyha, E. Sperling, A. Wittinghofer & L.Søgaard-Andersen, (2010) Regulation of dynamic polarity switching in bacteria by a Ras-like G-protein and its cognate GAP. *The EMBO journal* **29**: 2276-2289.

Li, Y., H. Sun, X. Ma, A. Lu, R. Lux, D. Zusman & W. Shi, (2003) Extracellular polysaccharides mediate pilus retraction during social motility of Myxococcus xanthus. *Proc Natl Acad Sci U S A* **100**: 5443-5448.

Lin, Q., W. Yang, D. Baird, Q. Feng & R.A. Cerione, (2006) Identification of a DOCK180-related guanine nucleotide exchange factor that is capable of mediating a positive feedback activation of Cdc42. *The Journal of biological chemistry* **281**: 35253-35262.

Lu, A., K. Cho, W.P. Black, X.Y. Duan, R. Lux, Z. Yang, H.B. Kaplan, D.R. Zusman & W. Shi, (2005) Exopolysaccharide biosynthesis genes required for social motility in Myxococcus xanthus. *Molecular microbiology* **55**: 206-220.

Luciano, J., R. Agrebi, A.V. Le Gall, M. Wartel, F. Fiegna, A. Ducret, C. Brochier-Armanet & T. Mignot, (2011) Emergence and modular evolution of a novel motility machinery in bacteria. *PLoS Genet* **7**: e1002268.

Maddock, J.R. & L. Shapiro, (1993) Polar location of the chemoreceptor complex in the Escherichia coli cell. *Science* **259**: 1717-1723.

Marchler-Bauer, A., Y. Bo, L. Han, J. He, C.J. Lanczycki, S. Lu, F. Chitsaz, M.K. Derbyshire, R.C. Geer, N.R. Gonzales, M. Gwadz, D.I. Hurwitz, F. Lu, G.H. Marchler, J.S. Song, N. Thanki, Z. Wang, R.A. Yamashita, D. Zhang, C. Zheng, L.Y. Geer & S.H. Bryant, (2017) CDD/SPARCLE: functional classification of proteins via subfamily domain architectures. *Nucleic acids research* **45**: D200-D203.

Margarit, S.M., H. Sondermann, B.E. Hall, B. Nagar, A. Hoelz, M. Pirruccello, D. Bar-Sagi & J. Kuriyan, (2003) Structural evidence for feedback activation by Ras.GTP of the Ras-specific nucleotide exchange factor SOS. *Cell* **112**: 685-695.

Mauriello, E.M., T. Mignot, Z. Yang & D.R. Zusman, (2010a) Gliding motility revisited: how do the myxobacteria move without flagella? *Microbiology and molecular biology reviews : MMBR* **74**: 229-249.

Mauriello, E.M., F. Mouhamar, B. Nan, A. Ducret, D. Dai, D.R. Zusman & T. Mignot, (2010b) Bacterial motility complexes require the actin-like protein, MreB and the Ras homologue, MglA. *The EMBO journal* **29**: 315-326.

McBride, M.J., T. Kohler & D.R. Zusman, (1992) Methylation of FrzCD, a methyl-accepting taxis protein of Myxococcus xanthus, is correlated with factors affecting cell behavior. *J Bacteriol* **174**: 4246-4257.

McBride, M.J., R.A. Weinberg & D.R. Zusman, (1989) "Frizzy" aggregation genes of the gliding bacterium Myxococcus xanthus show sequence similarities to the chemotaxis genes of enteric bacteria. *Proc Natl Acad Sci U S A* **86**: 424-428.

McLoon, A.L., K. Wuichet, M. Hasler, D. Keilberg, D. Szadkowski & L.Søgaard-Andersen, (2015) MglC, a Paralog of Myxococcus xanthus GTPase-Activating Protein MglB, Plays a Divergent Role in Motility Regulation. *J Bacteriol* **198**: 510-520.

Menetrey, J., M. Perderiset, J. Cicolari, T. Dubois, N. Elkhatib, F. El Khadali, M. Franco, P. Chavrier & A. Houdusse, (2007) Structural basis for ARF1-mediated recruitment of ARHGAP21 to Golgi membranes. *The EMBO journal* **26**: 1953-1962.

Merz, A.J., M. So & M.P. Sheetz, (2000) Pilus retraction powers bacterial twitching motility. *Nature* **407**: 98-102.

Miertzschke, M., C. Koerner, I.R. Vetter, D. Keilberg, E. Hot, S. Leonardy, L.Søgaard-Andersen & A. Wittinghofer, (2011) Structural analysis of the Ras-like G protein MglA and its cognate GAP MglB and implications for bacterial polarity. *The EMBO journal* **30**: 4185-4197.

Mignot, T., J.P. Merlie, Jr. & D.R. Zusman, (2005) Regulated pole-to-pole oscillations of a bacterial gliding motility protein. *Science* **310**: 855-857.

Mignot, T., J.W. Shaevitz, P.L. Hartzell & D.R. Zusman, (2007) Evidence that focal adhesion complexes power bacterial gliding motility. *Science* **315**: 853-856.

Mileykovskaya, E. & W. Dowhan, (2000) Visualization of phospholipid domains in Escherichia coli by using the cardiolipin-specific fluorescent dye 10-N-nonyl acridine orange. *J Bacteriol* **182**: 1172-1175.

Milner, D.S., R. Till, I. Cadby, A.L. Lovering, S.M. Basford, E.B. Saxon, S. Liddell, L.E. Williams & R.E. Sockett, (2014) Ras GTPase-like protein MglA, a controller of bacterial social-motility in Myxobacteria, has evolved to control bacterial predation by Bdellovibrio. *PLoS Genet* **10**: e1004253.

Nan, B., J.N. Bandaria, A. Moghtaderi, I.H. Sun, A. Yildiz & D.R. Zusman, (2013) Flagella stator homologs function as motors for myxobacterial gliding motility by moving in helical trajectories. *Proc Natl Acad Sci U S A* **110**: E1508-1513.

Nan, B., J. Chen, J.C. Neu, R.M. Berry, G. Oster & D.R. Zusman, (2011) Myxobacteria gliding motility requires cytoskeleton rotation powered by proton motive force. *Proc Natl Acad Sci U S A* **108**: 2498-2503.

Nan, B., E.M. Mauriello, I.H. Sun, A. Wong & D.R. Zusman, (2010) A multi-protein complex from Myxococcus xanthus required for bacterial gliding motility. *Molecular microbiology* **76**: 1539-1554.

Nudleman, E., D. Wall & D. Kaiser, (2006) Polar assembly of the type IV pilus secretin in Myxococcus xanthus. *Molecular microbiology* **60**: 16-29.

O'Toole, G.A. & R. Kolter, (1998) Flagellar and twitching motility are necessary for Pseudomonas aeruginosa biofilm development. *Molecular microbiology* **30**: 295-304.

Paintdakhi, A., B. Parry, M. Campos, I. Irnov, J. Elf, I. Surovtsev & C. Jacobs-Wagner, (2016) Oufti: an integrated software package for high-accuracy, high-throughput quantitative microscopy analysis. *Molecular microbiology* **99**: 767-777.

Patrick, J.E. & D.B. Kearns, (2008) MinJ (YvjD) is a topological determinant of cell division in Bacillus subtilis. *Molecular microbiology* **70**: 1166-1179.

Patryn, J., K. Allen, K. Dziewanowska, R. Otto & P.L. Hartzell, (2010) Localization of MglA, an essential gliding motility protein in Myxococcus xanthus. *Cytoskeleton* **67**: 322-337.

Postle, K., (2007) TonB system, in vivo assays and characterization. *Methods in enzymology* **422**: 245-269.

Ramamurthi, K.S., S. Lecuyer, H.A. Stone & R. Losick, (2009) Geometric cue for protein localization in a bacterium. *Science* **323**: 1354-1357.

Ramamurthi, K.S. & R. Losick, (2009) Negative membrane curvature as a cue for subcellular localization of a bacterial protein. *Proc Natl Acad Sci U S A* **106**: 13541-13545.

Richardson, B.C., C.M. McDonold & J.C. Fromme, (2012) The Sec7 Arf-GEF is recruited to the trans-Golgi network by positive feedback. *Developmental cell* **22**: 799-810.

Rittinger, K., P.A. Walker, J.F. Eccleston, S.J. Smerdon & S.J. Gamblin, (1997) Structure at 1.65 A of RhoA and its GTPase-activating protein in complex with a transition-state analogue. *Nature* **389**: 758-762.

Romantsov, T., A.R. Battle, J.L. Hendel, B. Martinac & J.M. Wood, (2010) Protein localization in Escherichia coli cells: comparison of the cytoplasmic membrane proteins ProP, LacY, ProW, AqpZ, MscS, and MscL. *J Bacteriol* **192**: 912-924.

Scheffzek, K., M.R. Ahmadian, W. Kabsch, L. Wiesmuller, A. Lautwein, F. Schmitz & A. Wittinghofer, (1997) The Ras-RasGAP complex: structural basis for GTPase activation and its loss in oncogenic Ras mutants. *Science* **277**: 333-338.

Schumacher, D. & L.Søgaard-Andersen, (2017) Regulation of Cell Polarity in Motility and Cell Division in Myxococcus xanthus. *Annual review of microbiology* **71**: 61-78.

Scott, A.E., E. Simon, S.K. Park, P. Andrews & D.R. Zusman, (2008) Site-specific receptor methylation of FrzCD in Myxococcus xanthus is controlled by a tetra-trico peptide repeat (TPR) containing regulatory domain of the FrzF methyltransferase. *Molecular microbiology* **69**: 724-735.

Sei, S., J.K. Mussio, Q.E. Yang, K. Nagashima, R.E. Parchment, M.C. Coffey, R.H. Shoemaker & J.E. Tomaszewski, (2009) Synergistic antitumor activity of oncolytic reovirus and chemotherapeutic agents in non-small cell lung cancer cells. *Molecular cancer* **8**: 47.

Shapiro, L., H.H. McAdams & R. Losick, (2009) Why and how bacteria localize proteins. *Science* **326**: 1225-1228.

Shi, W. & D.R. Zusman, (1993) The two motility systems of Myxococcus xanthus show different selective advantages on various surfaces. *Proc Natl Acad Sci U S A* **90**: 3378-3382.

Shi, X., S. Wegener-Feldbrugge, S. Huntley, N. Hamann, R. Hedderich & L.Søgaard-Andersen, (2008) Bioinformatics and experimental analysis of proteins of two-component systems in Myxococcus xanthus. *J Bacteriol* **190**: 613-624.

Simões, S., B. Denholm, D. Azevedo, S. Sotillos, P. Martin, H. Skaer, J.C. Hombria & A. Jacinto, (2006) Compartmentalisation of Rho regulators directs cell invagination during tissue morphogenesis. *Development* **133**: 4257-4267.

Skerker, J.M. & H.C. Berg, (2001) Direct observation of extension and retraction of type IV pili. *Proc Natl Acad Sci U S A* **98**: 6901-6904.

Sogaard-Andersen, L. & D. Kaiser, (1996) C factor, a cell-surface-associated intercellular signaling protein, stimulates the cytoplasmic Frz signal transduction system in Myxococcus xanthus. *Proc Natl Acad Sci U S A* **93**: 2675-2679.

Stock, A.M., V.L. Robinson & P.N. Goudreau, (2000) Two-component signal transduction. *Annual review of biochemistry* **69**: 183-215.

Sun, H., Z. Yang & W. Shi, (1999) Effect of cellular filamentation on adventurous and social gliding motility of Myxococcus xanthus. *Proc Natl Acad Sci U S A* **96**: 15178-15183.

Sun, M., M. Wartel, E. Cascales, J.W. Shaevitz & T. Mignot, (2011) Motor-driven intracellular transport powers bacterial gliding motility. *Proc Natl Acad Sci U S A* **108**: 7559-7564.

Treuner-Lange, A., E. Macia, M. Guzzo, E. Hot, L.M. Faure, B. Jakobczak, L. Espinosa, D. Alcor, A. Ducret, D. Keilberg, J.P. Castaing, S. Lacas Gervais, M. Franco, L.Søgaard-Andersen & T. Mignot, (2015) The small G-protein MglA connects to the MreB actin cytoskeleton at bacterial focal adhesions. *The Journal of cell biology* **210**: 243-256.

Treuner-Lange, A. & L.Søgaard-Andersen, (2014) Regulation of cell polarity in bacteria. *The Journal of cell biology* **206**: 7-17.

Trudeau, K.G., M.J. Ward & D.R. Zusman, (1996) Identification and characterization of FrzZ, a novel response regulator necessary for swarming and fruiting-body formation in Myxococcus xanthus. *Molecular microbiology* **20**: 645-655.

Vetter, I.R. & A. Wittinghofer, (2001) The guanine nucleotide-binding switch in three dimensions. *Science* **294**: 1299-1304.

Wall, D. & D. Kaiser, (1999) Type IV pili and cell motility. *Molecular microbiology* **32**: 1-10.

Wu, S.S. & D. Kaiser, (1996) Markerless deletions of pil genes in Myxococcus xanthus generated by counterselection with the Bacillus subtilis sacB gene. *J Bacteriol* **178**: 5817-5821.

Wu, S.S., J. Wu & D. Kaiser, (1997) The Myxococcus xanthus pilT locus is required for social gliding motility although pili are still produced. *Molecular microbiology* **23**: 109-121.

Wuichet, K. & L.Søgaard-Andersen, (2014) Evolution and diversity of the Ras superfamily of small GTPases in prokaryotes. *Genome biology and evolution* **7**: 57-70.

Yamaichi, Y., R. Bruckner, S. Ringgaard, A. Moll, D.E. Cameron, A. Briegel, G.J. Jensen, B.M. Davis & M.K. Waldor, (2012) A multidomain hub anchors the chromosome segregation and chemotactic machinery to the bacterial pole. *Genes Dev* **26**: 2348-2360.

Yang, R., S. Bartle, R. Otto, A. Stassinopoulos, M. Rogers, L. Plamann & P. Hartzell, (2004) AglZ is a filament-forming coiled-coil protein required for adventurous gliding motility of Myxococcus xanthus. *J Bacteriol* **186**: 6168-6178.

Yang, Z., X. Ma, L. Tong, H.B. Kaplan, L.J. Shimkets & W. Shi, (2000) Myxococcus xanthus dif genes are required for biogenesis of cell surface fibrils essential for social gliding motility. *J Bacteriol* **182**: 5793-5798.

Youderian, P., N. Burke, D.J. White & P.L. Hartzell, (2003) Identification of genes required for adventurous gliding motility in Myxococcus xanthus with the transposable element mariner. *Molecular microbiology* **49**: 555-570.

Zhang, Y., M. Franco, A. Ducret & T. Mignot, (2010) A bacterial Ras-like small GTP-binding protein and its cognate GAP establish a dynamic spatial polarity axis to control directed motility. *PLoS biology* **8**: e1000430.

Zhang, Y., M. Guzzo, A. Ducret, Y.Z. Li & T. Mignot, (2012) A dynamic response regulator protein modulates G-protein-dependent polarity in the bacterium Myxococcus xanthus. *PLoS Genet* **8**: e1002872.

Zhou, T. & B. Nan, (2017) Exopolysaccharides promote Myxococcus xanthus social motility by inhibiting cellular reversals. *Molecular microbiology* **103**: 729-743.

Acknowledgements

First of all I would like to thank my mentor, Prof. MD, PhD Lotte Søgaard-Andersen for giving me opportunity to work with fascinating world of regulation of motility in *M. xanthus*, for advices and ideas. Thanks to this challenging project and under her supervision, I could develop scientific skills and critical thinking.

Furthermore, I would like to thank my IMPRS and thesis committee, specifically: Prof. Dr. Martin Thanbichler, Prof. Dr. Gert Bange, Prof. Dr. Victor Sourjik and Dr. Simon Ringgaard. I would also like to thank Dr. Dorota Skotnicka and Dr. Magdalena Połatynska for all the help in writing and proof reading of this work.

I am very thankful to the collaborators, Prof. Dr. Ulrich Gerland and Manon Wigbers for great help with developing tools and procedures for fluorescent images analysis. Furthermore, I would like to thank Andrea Harms for all the work with proteins purification and biochemical analysis, without her help this work would lack conclusions. For founding, I would like to thank International Max Planck Research School for Environmental, Cellular and Molecular Microbiology and the German-Israeli Project Cooperation “Spatial and Temporal Regulation of Macromolecular Complex Formation in Bacteria”.

I would also like to thank members of “motility lab”, Anna and Luis for great working atmosphere. I could always ask them for help and resources and could count on a good word on the bad day. It was a great pleasure to work with you.

I am happy that I meet so many nice people in the lab. I really appreciate time spent with former and current members of the lab: Bene, Monika, Tobi, Dorotka, Magdziszka, Anna, Soficzka, Maria, Nuria, Luis, Deepak and all the others. I would also like to thank Steffi for all the help. Starting a life in Germany is not easy and I really appreciate her support in everyday life.

Finally, I would never accomplish all this without love and support of my family. They have never lost the faith that I can finish this work and thanks to this, I stayed strong and kept thinking positively.

Curriculum Vitae

Personal data

Name:	Dobromir Szadkowski
Date of birth:	05.10.1989
Place:	Nowy Dwor Mazowiecki, Poland

Education:

09/2008 - 06/2011	Secondary School No.1 Lowicz, Poland
10/2008 – 07/2011	Bachelor of Science, Univerity of Wroclaw, Poland Supervisor: Dr. Anna Krasowska
10/2011 - 07/2013	Master of Science Univerity of Wrocław, Poland Supervisor: Prof. Dr. Jolanta Zakrzewska-Czerwinska
From 08/2013	PhD program (Dr. rer. nat) Philipps-Universität Marburg Max-Planck-Institute for Terrestrial Microbiology, Marburg Supervisor: Prof.Dr. Lotte Søgaard-Andersen

List of publications

MglC, a Paralog of *Myxococcus xanthus* GTPase-Activating Protein MglB, Plays a Divergent Role in Motility Regulation,
McLoon AL, Wuichet K, Hasler M, Keilberg D, **Szadkowski D,** Søgaard-Andersen L. J Bacteriol 2015 Nov;198(3):510-20

The RomX/RomR MglA GEF complex establishes front-rear polarity for efficient motility in *M. xanthus*
Szadkowski D, Carreira L, Harms A, Wuichet K, Wigbers M, Potapova A, Keilberg D, Gerland U & Søgaard-Andersen L. (in preparation)

Erklärung

Hiermit versichere ich, dass ich die vorliegende Dissertation mit dem Titel„Identification and characterization of RomX and RomY, two novel motility regulators in *Myxococcus xanthus*“ selbstständig verfasst, keineanderen als die im Text angegebenen Hilfsmittel verwendet und sämtliche Stellen, dieim Wortlaut oder dem Sinn nach anderen Werken entnommen sind, mit Quellenangaben kenntlich gemacht habe.

Die Dissertation wurde in der jetzigen oder einer ähnlichen Form noch bei keiner anderen Hochschule eingereicht und hat noch keinen sonstigen Prüfungszwecken gedient.

Marburg, den____.____.____

_____

Dobromir Szadkowski

Einverständniserklärung

Hiermit erkläre ich mich einverstanden, dass die vorliegende Dissertation mit dem Titel

“Identification and characterization of RomX and RomY, two novel motility regulators in *Myxococcus xanthus*”

in Bibliotheken zugänglich gemacht wird. Dazu gehört, dass sie

von der Bibliothek der Einrichtung, in der meine Dissertation angefertigt wurde, zur Benutzung in ihren Räumen bereitgehalten wird;

in konventionellen und maschinenlesbaren Katalogen, Verzeichnissen und Datenbanken verzeichnet wird;

im Rahmen der urheberrechtlichen Bestimmungen für Kopierzwecke benutzt werden kann.

Marburg, den____.____.____

_____

Dobromir Szadkowski

_____

Prof. Dr. MD Lotte Søgaard-Andersen